UNIVERSIDADE DE TRÁS-OS-MONTES E ALTO DOURO

ESCOLA DE CIÊNCIAS E TECNOLOGIA

DETECTION AND MONITORING OF ACTIVE FIRES IN AFRICA AND EUROPE USING MSG-SEVIRI IMAGERY

Doutoramento em Física

Malik Amraoui

Vila Real, 2010

UNIVERSIDADE DE TRÁS-OS-MONTES E ALTO DOURO

ESCOLA DE CIÊNCIAS E TECNOLOGIA

DETECTION AND MONITORING OF ACTIVE FIRES IN AFRICA AND EUROPE USING MSG-SEVIRI IMAGERY

"Tese apresentada nesta Universidade para obtenção do grau de doutor"

Orientador: Professor Doutor Carlos do Carmo de Portugal e Castro da Camara, professor associado da Faculdade de Ciências da Universidade de Lisboa

Co-orientador: Professor Doutor José Miguel Oliveira Cardoso Pereira, professor catedrático do Instituto Superior de Agronomia da Universidade Técnica de Lisboa

Doutoramento em Física

Malik Amraoui

Vila Real, 2010

Dedicated to my loving daughter *Yasmine*

DETECÇÃO E MONITORIZAÇÃO DE FOGOS ACTIVOS EM ÁFRICA E NA EUROPA UTILIZANDO IMAGENS DO MSG-SEVIRI

RESUMO

A queima de biomassa é extremamente importante às escalas global, continental, regional e local, tendo um impacto dramático aos níveis atmosférico, climático, ambiental e socio-económico. O lançamento do Meteosat-8/SEVIRI constitui uma oportunidade única para detectar e monitorizar fogos de vegetação em África e na Europa, em tempo quase real, na medida em que são fornecidas imagens com intervalos de 15 minutos. A severidade dos problemas relacionados com os fogos de vegetação, conjuntamente com as solicitações expressas pela comunidade ligada à monitorização ambiental e à gestão de riscos, bem como por um número crescente de utilizadores de aplicações agrícolas e florestais, motivaram a presente investigação com vista ao desenvolvimento, no âmbito da *Satellite Application Facility on Land Surface Analysis* da EUMETSAT, de duas linhas de aplicação com vista a explorar a capacidade do Meteosat-8/SEVIRI de detectar e monitorizar: (i) fogos activos em África e na Europa, com o objectivo de proceder à disseminação operacional do produto *Fire Detection and Monitoring* (FD&M) e; (ii) sinais de stress da vegetação e de risco meteorológico de ocorrência de fogos, com o objectivo de proceder à disseminação operacional do produto *Fire Risk Map* (FRM).

Apresenta-se um procedimento operacional que permite detectar fogos activos com base em informação do Meteosat-8/SEVIRI em África e na Europa. A metodologia baseia-se em algoritmos contextuais, anteriormente projectados para instrumentos polares, síncrono solares, nomeadamente o NOAA/AVHRR e o TERRA-AQUA/MODIS. A informação acerca da actividade dos fogos, obtida a partir de um algoritmo desenvolvido para o efeito, é então utilizada: (i) para analisar as distribuições espacial e temporal dos fogos activos em África e na Europa em relação com os diferentes tipos de coberto vegetal e para caracterizar os ciclos diários de actividade de fogos em África; (ii) avaliar o potencial das imagens do Meteosat-8 para investigar o papel dos factores meteorológicos na actividade dos fogos na Europa Mediterrânica, nomeadamente através da análise de dois eventos extremos que atingiram a Itália e a Península Balcânica durante o Verão de 2007 e; (iii) calibrar um índice de risco de incêndio na Europa Mediterrânica com o objectivo de gerar operacionalmente cartas de risco de incêndio na Europa Mediterrânica.

Palavras-chave: Meteosat-8/SEVIRI, fogos activos em África e Europa, algoritmo contextual, LSA SAF, produto FD&M, factores meteorológicos, índice de risco de incêndio, produto FRM.

Contacto: malik@utad.pt

DETECTION AND MONITORING OF ACTIVE FIRES IN AFRICA AND EUROPE USING MSG-SEVIRI IMAGERY

ABSTRACT

Biomass burning is extremely important at the global, the continental, the regional and the local scales, and has dramatic impacts at the atmospheric, the climatic, the environmental and the socio-economical levels. The launch of Meteosat-8/SEVIRI provides a unique opportunity to detect and monitor wildfires, over Africa and Europe, in near-real-time by providing images at 15 minutes interval. The severity of wildfire-related problems, together with the demands from environment monitoring and risk management and a growing number of users in agricultural and forestry applications has led the present research to the development, within the framework of EUMETSAT Satellite Application Facility on Land Surface Analysis, of two lines of applications aiming to explore the capability of Meteosat-8/SEVIRI to detect and monitor: (i) active fires over Africa and Europe, leading to the operational dissemination of the Fire Detection and Monitoring (FD&M) product and; (ii) signals of vegetation stress and the meteorological risk of fire, leading to the operational dissemination of the Fire Risk Map (FRM) product.

An operational procedure is presented that allows detecting active fires based on information from Meteosat-8/SEVIRI over Africa and Europe. The methodology is based on heritage from contextual algorithms designed for polar, sun-synchronous instruments, namely NOAA/AVHRR and TERRA-AQUA/MODIS. Information about fire activity obtained by the developed algorithm is then used; (i) to analyze the spatial and temporal distribution of active fires over Africa and Europe related to different land cover types and to characterize the daily cycle of fire activity over Africa; (ii) to assess the potential of Meteosat-8 imagery to investigate the role of meteorological factors on fire activity in Mediterranean Europe, namely by analysing two extreme fire events that stroke Italy and the Balkan Peninsula during summer 2007 and; (iii) to calibrate a fire risk index over Mediterranean Europe with the aim of operationally generating maps of fire risk over Mediterranean Europe.

Keywords: Meteosat-8/SEVIRI, active fires over Africa and Europe, contextual algorithm, LSA SAF, FD&M product, meteorological factors, fire risk index, FRM product.

Contact: malik@utad.pt

Table of Contents

Acknowledgements

This dissertation has greatly benefited from the help, interest and support of many people from many parts of Portugal. My sincere apologies are due to anyone who in the following has been inadvertently omitted.

I am most grateful to my primary supervisor Prof. Carlos do Carmo de Portugal e Castro da Camara for his continuous guidance, encouragement and patience from the beginning of this research work until the production of all papers and this thesis. I have gained a lot of scientific knowledge from him, and I shall always remember and be grateful for his contribution in this research work.

Many tanks to my secondary supervisor Prof. José Miguel Cardoso Pereira for his support, patience and critical guidance during developing phase of research and during paper writing.

My appreciation goes to the Portuguese Foundation of Science and Technology (FCT) and to the European Social Fund (European Commission) for supporting the performed research (Grant No. SFRH/BD/36964/2007). My gratitude goes to the framework of the Project Satellite Application Facility on Land Surface Analysis (LSA SAF), an R&D and operational Project supported by EUMETSAT, where the research was partly performed.

I would like to thank Sandra Freitas, Carla Barroso and Pedro Diegues from *Instituto de Meteorologia* (Portugal) for their readiness in helping me to understand the used remote sensing data and its acquisition from the LSA SAF.

Very spatial and warmest thanks to my family, especially to my parents for their blessings, and to closest friends for their great support and encouragement, particularly during the last months.

List of Figures

Chapter 1

Chapter 2

Chapter 3

Chapter 4

List of Tables

Chapter 2

Chapter 3

Chapter 4

Acronyms and Symbols

A^2	Anderson-Darling test
AVHRR	Advanced Very High Resolution Radiometer
AWiFS	Advanced Wide Field Sensor
B	Intercept coefficient
B	Bias
BIA	Bureau of Indian Affairs
BLM	Bureau of Land Management
BUI	Build-Up Index
CFFDRS	Canadian Forest Fire Danger Rating System
CFFWIS	Canadian Forest Fire Weather Index System
CH_4	Methane
CO	Carbon monoxide
CO_2	Carbon dioxide
DC	Drought Code
DMC	Duff Moisture Code
DG JRC	Directorate-General Joint Research Center
DSR	Daily Severity Rating
ECMWF	European Centre for Medium-Range Weather Forecasts Reanalysis
ECT	Escola de Ciências e Tecnologia
EFFIS	European Forest Fire Information System
ESA	European Space Agency
EUMETSAT	European Organisation for the Exploitation of Meteorological Satellites
FD&M	Fire Detection and Monitoring product
FFBT	Forest Fire Behaviour Tables
FFDI	Forest Fire Danger Index
FFMC	Fine Fuel Moisture Code
FiDAlgo	Fire Detection Algorithm
FRM	Fire Risk Map product
FWI	Fire Weather Index
GBA2000	Global Burnt Area — 2000 initiative
GLC2000	Global Land Cover 2000
GOES	Geostationary Operational Environmental Satellites
GP	Generalized Pareto
GPCC	Global Precipitation Climatology Centre
Gpm	Geopotential metre
HRV	High Resolution Visible
IDL	Instituto Dom Luiz
IPCC	Intergovernmental Panel on Climate Change
IR	Infrared
IR3.9	Infrared SEVIRI channel centred at 3.92 μm
IR10.8	Infrared SEVIRI channel centred at 10.8 μm
ISI	Initial Spread Index
IR12.0	Infrared SEVIRI channel centred at 12.0 μm
JRC	Joint Research Centre
K	Tail index (shape) parameter of the generalized Pareto distributions

Kt	Knot, unit of speed equal to one nautical mile per hour (1.852 km/h)
L	Maximum likelihood function of the model with no-covariate
L'	Maximum likelihood function of the new model
LSA SAF	Land Surface Analysis of Satellite Application Facility
M	Slope coefficient
Meteosat	Meteorological Satellites
MIR	Middle Infrared
MODIS	Moderate Resolution Imaging Spectrometer
MSG	Meteosat Second Generation
NAfr	Northern Africa
NGP	Normalized Geostationary Projection
NO	Nitrous oxide
NO_2	Nitrogen dioxide
NOAA	National Oceanographic and Atmospheric Administration
NPS	National Park Service
NWP	Numerical Weather Prediction
O_3	Ozone
Pdfs	probability distribution functions
PF	Potential Fire pixel
P24	24 hours accumulated precipitation
R	Risk of fire
R(0.6)	Reflectance of VIS0.6
R(0.8)	Reflectance of VIS0.8
RETRO	Reanalysis of the Tropospheric chemical composition project
RH850	Relative humidity at 850 hPa
RMSE	Root Mean Square Error
S	Standard deviation
S^2	Variance
SAF	Satellite Application Facility
SAfr	Southern Africa
SEVIRI	Spinning Enhanced Visible and Infrared Imager
SLP	Sea Level Pressure
SSP	Sub-Satellite Point
SZA	Solar Zenith Angle
Tb(3.9)	IR3.9 brightness temperature
$\overline{Tb}(3.9)$	Mean IR3.9 brightness temperature of valid background pixels
$Tb_i(3.9)$	IR3.9 brightness temperature for a given pixel in 5×5 pixels grid
$Tb_{PF}(3.9)$	IR3.9 brightness temperature of potential fire pixel
Tb(10.8)	IR10.8 brightness temperature
Tb(12.0)	IR12.0 brightness temperature
Td2	Dew point temperature at 2 meters height
TOA	Top Of the Atmosphere
T2	Air temperature at 2 meters height
T850	Temperature at 850 hPa
USFS	U.S. Department of Agriculture's Forest Service
UTAD	Universidade de Trás-os-Montes e Alto Douro
UTC	Coordinated Universal Time
U10	Zonal and meridional wind components at 10 metres
U250	Wind speed at 205 hPa
VIRS	Visible and Infrared Scanner

VIS0.6	Visible SEVIRI channel centred at 0.635 μm
VIS0.8	Visible SEVIRI channel centred at 0.810 μm
Z250	250 hPa Geopotential height
Z500	500 hPa Geopotential height
Z850	850 hPa Geopotential height
α	Tail index (shape) parameter of the generalized Pareto distributions
$\delta(3.9)$	Mean absolute deviation of Tb(3.9)
$\delta(\Delta T)$	Mean absolute deviation of ΔT
θ	Location parameter of the generalized Pareto distributions
Λ	Likelihood ratio statistic - standard likelihood ratio test
ΔT	Difference between brightness temperatures of IR3.9 and IR10.8
$\overline{\Delta T}$	Mean difference between brightness temperatures of IR3.9 and IR10.8
ΔT_i	ΔT for a given valid pixel in 5×5 pixels grid
ΔT_{PF}	ΔT of potential fire pixel
ρ	Correlation coefficient
ρ^2	Coefficient of determination
σ	Scale parameter of the generalized Pareto distributions

CHAPTER 1: Introduction

1.1 Wildfires in the Earth system

Fire is a worldwide phenomenon that already appears in the geological record soon after the emergence of terrestrial plants (Bowman *et al.*, 2009), during the Devonian geologic period, about 350-400 million years ago (Pyne, 2001). In the following Carboniferous period (360-300 million years ago) there is a record of extensive charcoal deposits, mainly preserved in near-shore clastic sediments, which provide evidence of significant and widespread wildfires (Scott, 2000). The latter geologic period coincides with the colonization of the terrestrial biosphere, the evolution of tree species, and the increasing concentration of atmospheric oxygen, leading, up till the present, to the existence of the three ingredients required for the occurrence of most fires, *i.e.* to the so-called "combustion triangle": Oxygen, Fuel (vegetation) and Heat (ignition sources as lightning and volcanoes).

Fires have a local nature in what respects to their occurrence but their impacts are at the global scale making fire an integral part of the Earth's biosphere. For instance, the global and local impacts of fire result from both the fire itself and from substances emitted during burning (Csiszar *et al.*, 2005) and therefore the multi-scale effects make the study of fire crucial in understanding the Earth system (Andreae, 1991).

The regional and local impacts of vegetation fire are varied. The smoke and particulate matter associated with fires have negative effects on human health by irritating eyes, lungs and even skin (Galanter *et al.*, 2000). Fire may also destroy valuable timber and infrastructures and plays a key role in the functioning of terrestrial ecosystems. As a disturbing agent, the pattern of vegetation fire (namely the spatial distribution, the fire return interval and the severity of burning) directly controls plant community development by promoting regeneration of ecosystems, recycling the nutrients and maintaining biological diversity (Levine *et al.*, 1999). Fire further favours those plants and tree species which have developed adaptations to fire (*e.g.* vegetative reproduction and fire-resistant seeds and cones) and eliminates those species which are less resistant to fire (Justice *et al.*, 2006). Many ecosystems would not be sustainable without the occurrence of fires. Most forests would evolve towards mono-species stands of low productivity, encouraging other disturbances such as widespread diseases. Savannas are also dependent on the frequent occurrence of fires to avoid their evolution into forests.

Beyond the above-mentioned direct impact on vegetation distribution and composition, fire indirectly affects plant community development in a variety of ways. The combustion process and heat pulse modify various properties of soils, such as porosity, and temporarily reduce the soil fauna. In some circumstances, vegetation fires may lead to the depletion of plant nutrients through surface runoff or increased soil leaching (Justice *et al.*, 2006). The amount and availability of nutrients generally increase after a fire due to the abrupt release of the elements stored in the vegetation, and supports the regeneration of ecosystems. With the removal of the vegetation cover together with the

blackening of the surface by charcoal, surface albedo tends to decrease substantially and therefore soils receive and intercept more sunlight radiation. The decrease in albedo may affect local biochemical processes (Brown, 1983) and regional atmospheric circulations and associated rainfall regimes (Govaerts *at al.*, 2002).

The impacts of fire at the global scale are primarily due to fire emissions that release various gases and particulate matters in the atmosphere, with important implications (Levine, 1991). Vegetation is essentially composed by carbon, hydrogen and oxygen that recombine during combustion and emitted gases depend on the type of vegetation burned, its moisture content, the local supply of oxygen and the type of fire. In a perfectly efficient combustion process (flaming phase of fire) water vapour, carbon dioxide (CO_2) and energy (heat and light) are emitted in large quantities. However, the combustion of biomass in wildland fires is not fully efficient, due to high fuel moisture, insufficient oxygenation of the reaction zone and inefficient heat transfer among other factors. Under these circumstances, the flaming combustion coexists with less efficient smouldering combustion (Pereira and Govaerts, 2001), that produces other greenhouse gases, contributing to global warming, like carbon monoxide (CO), methane (CH_4) and nitrous oxide (NO).

A secondary product of fire is tropospheric ozone (O_3), whose formation is due to the oxidation of CH_4 and CO in the presence of NO and nitrogen dioxide (NO_2), all products of fire (Csiszar *et al.*, 2005). In addition to its highly reactive chemical properties O_3 is responsible for damaging plants and is prejudicial to the human health (Galanter *et al.*, 2000).

Particulate matters are also emitted as a result of vegetation combustion and may act as cloud condensation nuclei (McCollum *et al.*, 2000). The resulting increase in cloud cover may have a cooling or warming effect depending on the type of clouds formed (Csiszar *et al.*, 2005). Gases and particulate matters, emitted by fire, also referred to as aerosols, rise in the lowest portion of the atmosphere (troposphere) and may be transported at cross-continental scale (Chatfield *et al.*, 1998; Damoah *et al.*, 2004). In particular, the vertical convection movements associated to the Inter Tropical Convergence Zone and storms, or generated by intense wildfires (pyro-convection) distribute aerosols up to the lower stratosphere.

Fire is widely recognized as a critical component of the Earth system, with a strong influence on carbon and energy balances, climate change and ecosystem dynamics over multiple temporal and spatial scales (Bowman *et al.*, 2009; Flannigan *et al.*, 2009). In fact, an increase in fire severity, results in deforestation and ecosystem degradation that lead to a decrease of total long-term carbon storage and to an increasing of CO, CO_2, and CH_4 concentrations in the atmosphere. The resulting perturbation in global carbon balance enhances the greenhouse effect associated to the above mentioned radiatively active gases, which are the major drivers of climate change. On the other hand, there is a long-term increase in both the extent and severity of wildfires which is generally attributed on the one hand to the demographic and socio-economic changes which have

affected land use and land cover, and on the other hand to climate change that has increased the likelihood of occurrence of weather patterns favouring the onset and spread of wildfires (Trigo *et al.*, 2006).

1.2 Fire triangles and regimes

Disturbance regimes are generally described by means of their type, frequency, predictability, extent, magnitude, synergism with other disturbances, and seasonality (White and Pickett, 1985; Agee, 1993; Baker, 2009). As a disturbance agent, the concept of fire regime integrates the characteristics associated with occurrence of fires and its role in a particular ecosystem. Fire regimes also describe the type of fuel consumed (soil, ground, crown fires), the size of fires, their intensity (the energy released), severity (the ecological disturbance), frequency and seasonality (Bond and Keeley, 2005).

A suite of climate, fuel, and landscape variables is required for fire to occur and spread, although their relative importance changes across scales. Fire triangles are a common frame for conceptualizing the interaction of these variables, and the elements of the triangles are nested and, together, they define a range of conditions, from those that start fires at the local scale to those that consider fire as an Earth system process, *i.e.* at the global scale (Whitlock *et al.*, 2010). As a descriptor of the drivers of fire at the smallest scales, the fire-fundamentals triangle links oxygen, heat, and fuel at hourly-to-annual time scales, whereas the fire-event triangle links weather, fuels, and topography as factors that influence ignition probability, rate-of-fire spread, and fire intensity at the seasonal-to-annual time scales (Rothermel, 1972; Pyne, 1996). On the decadal-to-millennial time scales, the fire-regime triangle includes variables that determine the characteristic pattern, frequency, and intensity of fire at the landscape and larger spatial scales (Whitlock *et al.*, 2010). It may be noted that the fire-regime triangle defines the linkages between vegetation, which is a determinant of broad-scale fuel characteristics, climate conditions that support fire weather, and ignition sources, either human or natural (Moritz *et al.*, 2005; Parisien and Moritz, 2009).

Although the fire-triangle concept, the conceptualization of fire triangles places the greatest human influence in shaping the fire-regime triangle, human effects are present at all scales (Dantonio and Vitousek, 1992). Management objectives focused on ecosystem sustainability require information from the fire-regime triangle, and these human-vegetation-climate linkages have gained wider attention regarding to projected future climate change (Whitlock *et al.*, 2010).

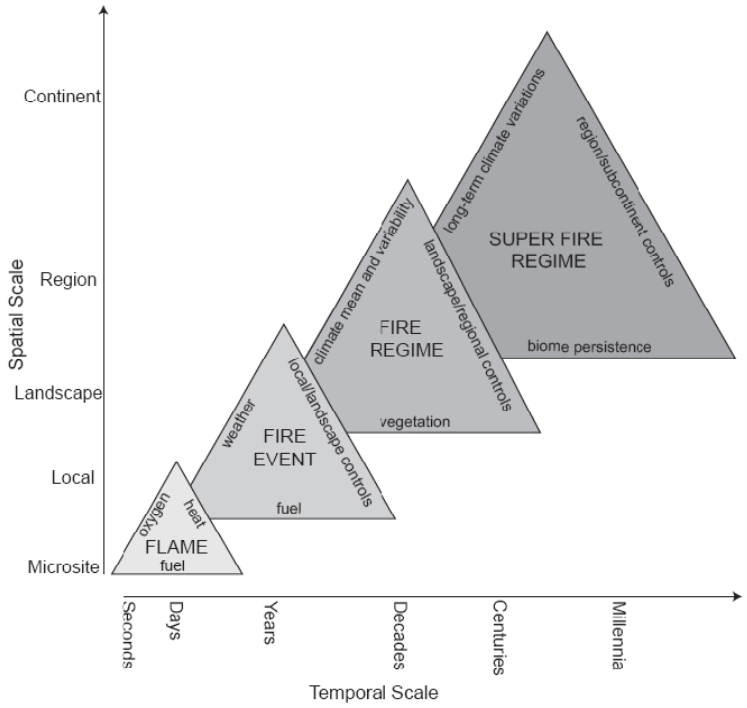

Figure 1.1. Controls of fire at multiple temporal and spatial scales conceptualized as fire triangles. The side of each triangle indicates the dominant drivers at different temporal and spatial scales, and the overlap of triangles reminds their nested nature. The long temporal perspective offered by paleoecological data suggests the need for a broader conceptualization of fire regimes and even for the introduction of a super-fire regime triangle that considers the variability of fire characteristics over the lifespan and spatial extent of a biome (from Whitlock *et al.*, 2010).

In what respects to the fire-regime triangle, it may be noted that vegetation is considered the fuel of fires encompassing live vegetation individuals (*e.g.* grass, shrub, trees), aboveground vegetation residues (*e.g.* leaf litter, fallen branches), and bellow ground partially decayed biomass (*e.g.* peats). Weather and climate, the second element of the fire-regime triangle, have in turn a profound influence on wildland fire ignition, fire behaviour, and fire severity. For instance, at the regional scale and at the seasonal or inter-annual time scales, severe droughts at the beginning of the fire season (late spring and early summer) inevitably lead to high levels of vegetation stress increasing the flammability of live and dead fuels. At the local and daily scales, extreme weather conditions, including wind, atmospheric stability, fuel moisture, and relative humidity during the fire season promote the ignition and spread of wildfires. Finally, one cannot ignore that fire regimes are largely influenced by the anthropogenic use of fires for agriculture activities, land management practices, as a clearing tool for ecosystem conversion (*e.g.* deforestation), and even for criminal purposes. In fact, the natural occurrence of fires is greatly biased by anthropogenic activities, the third element of the fire-regime triangle, either towards an increase as a land management tool, or a decrease

as a result of fire suppression strategies (fire fighting and preventive fires) (Velben *et al.*, 2000).

As mentioned above, the three factors that constitute the fire-regime triangle have specific influence of their own, but it is worth stressing that their interaction is the final determinant of fire regimes. On the long term, climate patterns shape the global distribution of the vegetation and, in addition, the anthropogenic factor plays a major role through the conversion/management of natural ecosystems associated to agricultural expansion and other activities, and through human-induced climate change. At inter-annual timescales, climate variability may also modify local to regional vegetation characteristics, especially in arid and semi-arid ecosystems. Down to the seasonal scale, the fuel moisture cycle is the result of the interaction between climate and the vegetation.

1.3 Remote sensing of active fires

Earth system science has an interdisciplinary character and is strongly coupled to remote sensing. In fact, satellite observations are often the only way to obtain the required information to understand the processes of individual systems as well as those linking the different systems. Great progress has been made in the last two decades with the advent of the space program and associated Earth observations (Kafatos *et al.*, 1998). The number of remote sensing images that are being collected every day from satellites, aerial sensors, telescopes and other sensor platforms is extremely large and plans of new missions are building up every day. On the other hand, remotely sensed data, combined with additional data from ecosystem models, offer an unprecedented opportunity for predicting and understanding the behaviour of the Earth's ecosystem (Tan *et al.*, 2002).

The present concern for the environment is also increasing the interest in monitoring and predicting ecosystem changes (Muzy *et al.*, 2002). Vegetation fires are one such phenomenon that is widely predicted, detected, monitored and assessed based on information from remote sensing satellites. As an indicator of the relevance of fire, reports from various sources estimate fires to affect on average 3.5 million squared kilometres of vegetation in recent years, the size of India, with ensuing carbon emissions equivalent to a third of fossil fuel combustion, and further characterised by important year to year variability (Ito and Penner, 2004; Tansay *et al.*, 2004a,b; van der Werf *et al.*, 2006; Le Page *et al.*, 2008). In this respect, it may be noted that Africa is often referred to as "the burning continent" because it has the largest share mostly located in sub-saharan savannas and Miombo woodlands.

Satellite remote sensing of active fires is limited by the detection capabilities of the instruments and there is also the possibility of errors as a result of sampling

inconsistencies (Csiszar *et al.*, 2005). Despite the limitations of such systems, observations from Earth-orbiting remote sensing satellites may be considered the key to a better characterization of the extent and influence of vegetation fires since they provide a rather uniform measurement of fires over the entire Earth's surface and they offer the means for developing a consistent long-term record of fires at the local, regional, continental and global scales (Justice and Korontzi, 2001).

The burning of biomass is accompanied by a wide variety of characteristic spectral signature changes that can be detected by remote sensing (Roberts and Wooster, 2008). Such signatures include those related to pre-fire indicators, to the intense thermal emissions from combustion, to the albedo and spectral reflectance of newly burned surfaces, and to the presence of smoke plumes containing trace gases and aerosols in highly elevated concentrations. In fact, satellite observations have been giving new insights about the atmospheric impacts of fires. Emissions stemming from the combustion process may also be estimated based on the area burnt and the characteristics of vegetation, as well as on emission factors specific to the compound considered.

Detection of fire activity has long been identified as a task with great potential to be derived either from polar-orbiters and from geostationary satellites and, since the last decade of the 20th century, more and more sophisticated fire detection algorithms have been successively developed. However, one of the major constraints in monitoring the vegetation fires over Europe and Africa has been the lack of high frequency observations combined with high or coarse spatial resolution data. In fact, geostationary meteorological satellite systems provide much higher frequency of observation of the land surface than sun-synchronous systems but, until recently, their spatial and spectral resolutions were sub-optimal for vegetation fire monitoring. The launch in 2002, by the European Space Agency (ESA) in cooperation with the European Organization for the Exploitation of Meteorological Satellites (EUMETSAT), of Meteosat-8, the first geostationary satellite of the Meteosat Second Generation (MSG) opened up new perspectives in active fire monitoring in the above mentioned continents, thanks to the improved characteristics in the temporal (one image every 15 minutes), the spatial (a sampling distance of 3 km at the sub-satellite point) and the spectral (12 channels) domains provided by the Spinning Enhanced Visible and Infrared Imager (SEVIRI), the main payload of the MSG series.

In short, apart from Meteosat-8, there are no existing satellites that could be used for continuous monitoring of fire activities over Europe and Africa. Furthermore the high temporal resolution of MSG could help in characterizing the dynamic nature of vegetation fires. The research to be undertaken within the framework of the present thesis may be viewed as an example of such rationale and will explore the potential of MSG system for detecting and monitoring vegetation fires over Europe and Africa.

1.4 Research objectives

Vegetation fires are a disturbance agent and a dynamic phenomenon capable of burning the accumulated biomass on hourly or even sub-hourly basis, depending on the combination of the main factors belonging to the fire triangles. On the other hand, the improved temporal, spatial and spectral characteristics of the MSG series render its satellites particularly adequate for Earth surface observation, and namely for fire detection and monitoring. In this context, the first objective of the present research is to exploit the potentials of MSG by developing a contextual algorithm for detecting active fires over Africa and Europe. The algorithm will be hereafter referred to as *Fi*re *D*etection *Algo*rithm (FiDAlgo) and the underlying method is based on heritage from contextual algorithms designed for polar, sun-synchronous instruments, namely the National Oceanographic and Atmospheric Administration/Advanced Very High Resolution Radiometer (NOAA/AVHRR) and the TERRA-AQUA/Moderate Resolution Imaging Spectrometer (TERRA-AQUA/ MODIS). The procedure is closely related with one of the activities developed within the framework of EUMETSAT's Satellite Application Facility on Land Surface Analysis (LSA SAF), the so-called Fire Detection and Monitoring (FD&M) product.

The LSA SAF project is part of the Satellite Application Facility (SAF) Network, a set of specialised development and processing centres, serving as the EUMETSAT distributed Applications Ground Segment (Schmetz *et al.*, 2002). The SAF network complements the product-oriented activities at the EUMETSAT Central Facility in Darmstadt. The scope of the LSA SAF is to take full advantage of remotely sensed data to support land, land-atmosphere interactions and biosphere applications; a strong emphasis is put on developing and implementing algorithms that will allow an operational use of data from EUMETSAT satellites (Trigo *et al.*, 2010). The LSA SAF products are relevant to a wide range of applications and, since the beginning of its scientific and technical activities, particular attention has been devoted to the end-user community (Tavares and DaCamara, 1999). Although the Numerical Weather Prediction (NWP) community has been identified as having the greatest potential to fully exploit the LSA SAF products and was therefore assigned the highest priority during the Development Phase (DaCamara and Tavares, 2001), the LSA SAF addresses a much broader community (Tavares and DaCamara, 2002), including amongst others agricultural and forestry applications and natural hazard management. Whereas agricultural and forestry applications require information on soil and vegetation properties, natural hazard management requires frequent observations of terrestrial surfaces in both the solar and thermal bands together with merged information from NWP models and surface characteristics (DaCamara, 2006).

FiDAlgo is a universal algorithm and appears as an especially adequate tool to monitor fire activity over Africa and Europe, though with different purposes. Over Africa, the magnitude of wildfires is important and the importance of the impact of fire events on

climatic, atmospheric and ecological processes has been recognised by the scientific community. Thus, detection and monitoring of burning activity, using MSG imagery at the maximum temporal resolution, is the key to characterize vegetation fires at the higher frequency cycles, *e.g.* daily or even weekly. Increasing the temporal resolution of vegetation fire data to hourly or even sub-hourly intervals may also contribute towards improving models of environmental processes affected by biomass burning (*e.g.* regional and continental scale greenhouse gas emissions, regional ecological impacts and land-use and land-cover dynamics).

Southern Europe climates are predominantly Mediterranean, *i.e.* characterized by cool wet winters followed by hot dry summers that make the region especially prone to the occurrence of a large number of fire events. The fire season burns hundreds of thousands of hectares of forests, shrublands and grasslands every year, causing extensive economical and ecological losses and often human casualties (Pyne, 2006; Ventura and Vasconcelos, 2006). Accordingly, fire detection and monitoring over Mediterranean Europe is particularly useful to quantify the severity of fire episodes, which in turn allow having a better understanding of regional trends and variability of fire occurrences as well as having a deeper insight into the associated weather and climate regimes, vegetation cover and landscape structure. High frequency fire information from FiDAlgo is also relevant for civil protection and forest protection activities.

Finally, it is worth noting that weather and climate have a profound influence on wildland fire ignition, fire behaviour, and fire severity (Benson *et al.*, 2009). For instance, and as already mentioned, at the regional scale and at the seasonal or inter-annual time scales, severe droughts at the beginning of the fire season inevitably lead to high levels of vegetation stress increasing the flammability of live and dead fuels. At the local and daily scales, extreme weather conditions, including wind, atmospheric stability, fuel moisture, and relative humidity during the fire season promote the ignition and spread of wildfires (Pereira *et al.*, 2005; Trigo *et al.*, 2006; Rasilla *et al.*, 2010). In this context, the second objective of this research is to assess the potential of Meteosat-8 imagery to assess the role of meteorological factors on fire activity in Mediterranean Europe. Finally, the third objective of this research is to demonstrate how high frequency observations of occurrences of active fires as detected by FiDAlgo may be used to calibrate a fire risk index over Mediterranean Europe, which results from an integrated use of meteorological information from the European Centre for Medium-Range Weather Forecasts Reanalysis (ECMWF) forecasts and vegetation land cover map from the Global Land Cover (GLC2000).

1.5 Structure of the thesis

This thesis is organized based on three publications (one published, one accepted and one submitted). Chronologically, they reflect the progressive fulfilment of the objectives in light of the findings achieved and new hypotheses formulated throughout the investigation.

Chapter 2 presents the operational algorithm (FiDAlgo) that allows detecting active fires based on information from Meteosat-8/SEVIRI over Africa. An overview is provided of results obtained for January and July 2007, respectively over Northern and Southern Africa, paying special attention to the spatial and temporal distribution of active fires. An assessment of the robustness of the algorithm, consistency of results and added value of the product is made by studying the daily cycle of fire activity over two regions located in northern and southern hemisphere Africa and by means of systematic comparisons against fire incidence reported in previous works and against hot spots extracted from the global daily active fire product developed by the MODIS Fire Team.

The work developed in Chapter 3 makes use of FiDAlgo to detect and monitor active fires over Europe based on information from Meteosat-8/SEVIRI. An analysis is performed on the spatial and temporal distributions of fire events during the period of July and August 2007-2009 related to the types of land cover affected. Special attention is devoted to two extreme events of fire activity, respectively on July 24-25 and August 22-27, 2007 that stroke Italy and the Balkan Peninsula. The role of meteorological factors in the two periods is investigated by analysing composites of meteorological fields as well as vertical profiles of meteorological variables. Finally, the impact of long- and short-term meteorological components is assessed by analysing the fields of three weather-based indices, namely the Build-Up Index, the Initial Spread Index and the Fire Weather Index that are part of the Canadian Forest Fire Weather Index System.

A procedure is presented in Chapter 4 that allows operationally generating daily maps of fire risk over three regions of Mediterranean Europe (the Iberian Peninsula, Italy and Greece) which are very prone to the occurrence of large fire events. The rationale of the developed methodology is to provide the user community with information on meteorological risk that will allow adopting the adequate measures to mitigate fire damage. The generated maps of fire risk are based on an integrated use of meteorological information from ECMWF forecasts, on vegetation land cover from GLC2000 and on occurrences of active fires as detected by MSG-SEVIRI. The obtained levels of fire danger are associated to probabilities of occurrence of fires exceeding specified magnitudes. It is shown that statistical models based on two-parameter Generalized Pareto (GP) distributions adequately fit the observed samples of duration of active fires and that these models are significantly improved when the Fire Weather Index (FWI) is used as a covariate to model both the shape and scale parameters of the GP distributions. A set of five coherent classes of fire risk is then derived by defining a "reference value" of active fire duration associated to the geographical location and the vegetation type and by analysing the risk departure from the "background" due to meteorological factors. Validation of results is performed in the period of July-August 2007-2009 and it is shown that all three regions present an overall similar behaviour,

with a virtual absence of fire occurrences of large duration in the classes of very low and low risk of fire. On the other hand, fires of small duration concentrate in the classes of moderate, high and very high risk and there is a displacement of the modal class towards classes of higher risk with increasing duration.

Finally, in Chapter 5, an overall review is given of the research performed and some final comments are given about the capability of Meteosat8-SEVIRI to detect and monitor fires in Africa and Europe.

CHAPTER 2: Detection and monitoring of African vegetation fires using MSG-SEVIRI imagery

M. Amraoui [a,b],C.C. DaCamara [b], J.M.C. Pereira [c]

[a] Physics Department, School of Sciences and Technology, University of Trás-os-Montes e Alto Douro (ECT-UTAD), Vila Real, Portugal

[b] University of Lisbon, Instituto Dom Luiz (IDL), Lisbon, Portugal

[c] School of Agronomy, Technical University of Lisbon, Lisbon, Portugal

This Chapter was published in Remote Sensing of Environment in February 2010:

Amraoui, M. *et al.* (2010). Detection and monitoring of African vegetation fires using MSG-SEVIRI imagery. *Remote Sensing of Environment*, 114, 1038-1052.

Abstract

An operational procedure is presented that allows detecting active fires based on information from Meteosat-8/SEVIRI over Africa. The procedure takes advantage of the temporal resolution of SEVIRI (one image every 15 minutes), and relies on information from SEVIRI channels (namely 0.6, 0.8, 3.9, 10.8 and 12.0 μm) together with information on illumination angles. The method is based on heritage from contextual algorithms designed for polar, sun-synchronous instruments, namely NOAA/AVHRR and MODIS/TERRA-AQUA. A potential fire pixel is compared with the neighbouring ones and the decision is made based on relative thresholds as derived from the pixels in the neighbourhood.

An overview is provided of results obtained for January and July 2007, respectively over Northern Africa (NAfr) and Southern Africa (SAfr), paying special attention to the spatial and temporal distribution of active fires. In both NAfr and SAfr, two types of vegetation clearly dominate in terms of fire activity, namely tree-covered areas, containing 40 % of total fires observed, and shrub-covered areas, with 25 % (19%) of total fires in NAfr (SAfr). However, marked differences were also be found between the two regions; more than two-thirds (70%) of fires in SAfr were observed in land cover classes dominated by trees but the proportion is much lower (40%) in the case of NAfr. The duration of active fires in both regions tends to follow two-parameter generalized Pareto distributions, with both the scale and the shape parameters presenting very similar values for NAfr and SAfr.

An assessment of the robustness of the algorithm, consistency of results and added value of the product was made by studying the daily cycle of fire activity over two regions located in northern and southern hemisphere Africa and by means of systematic comparisons against fire incidence reported in previous works and against hot spots extracted from the global daily active fire product developed by the MODIS Fire Team. The observed fire incidence by land cover class compares well with the results reported in previous works and it is shown that there is an overall coherence between results obtained from SEVIRI and MODIS when adequate spatial and temporal scales are chosen when performing the comparison. Data from MODIS and SEVIRI may be viewed as complementary, the latter having the added value of providing a much finer temporal resolution that allows uncovering certain aspects of fire behaviour, namely the characterization of daily fire cycles.

Keywords: Fire detection, Contextual algorithm, Meteosat-8/SEVIRI, African vegetation fires, Spatial and temporal distribution of active fires.

I. Introduction

Fires are an important and highly variable source of air pollution in many regions of the world and they constitute a significant, if not dominant, factor controlling the interannual variability of the atmospheric composition (Schultz *et al.*, 2008). In this respect, African vegetation fires play a central role in tropical and subtropical atmospheric chemistry and, according to Lacaux *et al.* (1993), account for 57% of all tropical burning (49% from savanna fires and 8% from forest burns). Savanna fires are responsible for over 90% of the biomass burnt in Africa, in contrast to what happens in South America and Southeast Asia, where forest fires are more important (Delmas *et al.*, 1991). Using data from Global Burnt Area — 2000 initiative (GBA2000) and relying on satellite remote sensing techniques and procedures of Grégoire *et al.* (2003), Ito and Penner (2004) estimated that the African areas burned correspond to 217 Mha/year; 72% for grasslands, 16% for woodlands and 12% for forests. Using data for the period 1960–2000, Schultz *et al.* (2008) give an average African burned area, including tropical deforestation, of 269 Mha/year, with 136 Mha/year for northern Africa and 133 Mha/year for southern Africa.

Estimates of global direct carbon emissions from wildland fires range from 1428 Tg C/a as estimated by Ito and Penner (2004) to 2771 Tg C/a as calculated by Galanter *et al.* (2000). According to the 41-year inventory of vegetation fire emissions constructed for the Reanalysis of the Tropospheric chemical composition over the past 40 years project (RETRO), the global total direct carbon emission flux from wildland fire emissions amounts to 2078 Tg C/a (Schultz *et al.*, 2008), the African continent contributing to about one half of the global vegetation fire emissions; 24.75% for northern Africa and 23.49% for southern Africa. However, as pointed out by the authors, future versions of the inventory will benefit from ongoing analyses of burned areas based on satellite data.

Several studies have used remotely sensed data to characterize the seasonality of vegetation fires at the continental and global scales (Barbosa *et al.*, 1999; Cahoon *et al.*, 1992; Csiszar *et al.*, 2005; Dwyer *et al.*, 1999; Dwyer, Grégoire, *et al.*, 2000; Dwyer, Pinnock, *et al.*, 2000; Generoso *et al.*, 2003; Giglio *et al.*, 2006; Le Page *et al.*, 2008; Schultz, 2002; Silva *et al.*, 2003; Tansey, Grégoire, Stroppiana, *et al.*, 2004; Tansey, Grégoire, Binaghi, *et al.*, 2004). All of these analyses relied on satellite systems with a frequency of overpass ranging from a minimum of every 3–4 days to a maximum of 4 times per day. This is adequate to depict seasonal patterns extending over a period of a few months, but of limited utility to analyse higher frequency periodicities, such as daily, or even weekly fire cycles. Nevertheless, a few authors (Abuelgasim & Fraser, 2002; Ji, 2005; Prins & Menzel, 1994) have addressed these higher temporal frequencies, under the constraints imposed by the temporal resolution of the satellite systems used, and found clear evidence of daily cycles, in contrast with an earlier report by Cahoon *et al.* (1992), who claimed that African vegetation fires displayed no strong daily cyclical pattern.

In a recent work, Giglio (2007) characterized the average diurnal fire cycle in 15 regions of the tropics and subtropics using seven years of observations made with the Visible and Infrared Scanner (VIRS) and the Moderate Resolution Imaging Spectrometer (MODIS) instruments. The author noted that the diurnal cycle was prominent in all these regions, with a maximum of activity in the early-to late afternoon and typically little or no burning between 00:00 and 08:00 local time. Giglio (2007) further reported that the distribution of fire activity is generally skewed, with a somewhat longer tail after the peak, as burning continues into the evening. Although a single peak in fire activity is generally observed throughout the day, a secondary morning peak in fire activity was also found by the author in the eastern Sahel and northern Australia regions.

Quantitative characterization of daily fire cycles is important for several reasons; i) the chemical composition of pyrogenic emissions is affected by dead fuel moisture content (Andreae & Merlet, 2001; Hoffer *et al.*, 2006), which tracks the daily cycle of atmospheric relative humidity, with timelags that are a function of fuel particle size; ii) higher nocturnal atmospheric stability, and especially low level inversions, may lead to decreased injection heights, thus restricting long-distance dispersal of combustion products (Garstang & Tyson, 1997); iii) the optical depth of biomass burning smoke aerosol displays a strong daily cycle (Smirnov *et al.*, 2002; Eck *et al.*, 2003) and generates radiative impacts that disturb cloud formation and convective rainfall patterns in the tropics (Rosenfeld, 1999; Smirnov *et al.*, 2002; Andreae *et al.*, 2004). Increasing the temporal resolution of vegetation fire data to hourly or even sub-hourly intervals may therefore contribute towards improving models of environmental processes affected by biomass burning. High frequency fire information is also relevant for civil protection and forest protection activities (Pereira & Govaerts, 2001).

Geostationary meteorological satellite systems provide much higher frequency of observation of the land surface than sun-synchronous systems but, until recently, their spatial and spectral resolutions were sub-optimal for vegetation fire monitoring. Nevertheless, various authors demonstrated the capability of earlier geostationary satellites to detect active fires (Prins & Menzel, 1992, 1994; Prins & Schmetz, 2000) and to estimate burned areas (Boschetti *et al.*, 2003). New possibilities were opened up with the launch in 2002, by the European Space Agency (ESA) in cooperation with the European Organisation for the Exploitation of Meteorological Satellites (EUMETSAT), of Meteosat-8, the first satellite of the Meteosat Second Generation (MSG). Temporal, spatial and spectral characteristics of the MSG series were substantially improved (Schmetz *et al.*, 2002), rendering its satellites very adequate for Earth surface observation, and namely for fire monitoring (Cihlar *et al.*, 1999; Pereira & Govaerts, 2001). The potential of MSG was promptly explored, namely by expanding the scope of previous fire applications of geostationary systems with the goal of quantifying fire intensity and biomass consumption (Roberts *et al.*, 2005; Roberts & Wooster, 2008).

The aim of the present study is to develop a contextual algorithm for detecting active fires, using information provided by MSG at the maximum temporal resolution. The

developed algorithm, hereafter referred to as Fire Detection Algorithm (FiDAlgo), will be applied and tested during January 2007 over northern Africa and during July 2007 over southern Africa, *i.e.* during one month within the respective dry seasons. Maps of active fires as derived from FiDAlgo will then be produced every 15-min and results will be compared against independent data, namely those from the MODIS Fire Team.

A description of used data and of the study area is provided in Section 2. Section 3 gives a brief survey of the state of the art followed by a detailed description of FiDAlgo. Section 4 presents the results obtained when applying the algorithm over northern and southern Africa, respectively during January and July 2007. Special attention is devoted to the spatial distribution and the temporal organization of fire activity and an assessment is made on the robustness of the algorithm, consistency of results and added value of the product. Some concluding remarks are given in Section 5.

II. Data and study area

The main payload of the MSG satellites is the Spinning Enhanced Visible and Infrared Imager (SEVIRI). From its vantage point approximately 36000 km above the equator, at 0° longitude, the SEVIRI radiometer on board Meteosat-8 scans the Earth's full disc in 15-minute repeat cycles using 12 spectral channels: three in the visible, eight in the infrared part of the electromagnetic spectrum and one High Resolution Visible (HRV). With the exception of the 1-km HRV, all channels have a spatial resolution of 4.8 km and a sampling distance of 3 km at the sub-satellite point (SSP), and thus have a nominal oversampling factor of 1.6. Further details about MSG channels may be found in Schmetz *et al.* (2002).

As part of EUMETSAT's Satellite Application Facility (SAF) Network, the SAF on Land Surface Analysis (LSA SAF) is a specialised development and processing centre whose aim is to take full advantage of remotely sensed data, particularly those available from EUMETSAT sensors, to describe/derive land surface properties/variables (DaCamara, 2006). In March 2007, the LSA SAF Team initiated a line of research related with fire applications.

The present work is closely related with one of the activities within the new line of research, namely the development of the so-called Fire Detection and Monitoring (FD&M) product (DaCamara *et al.*, 2007; Amraoui *et al.*, 2008) that is running in the parallel chain of the LSA SAF System. FiDAlgo is operationally being applied and tested over Africa, where large regions are affected by widespread wildfires. Subject every year to a long dry season, these regions broadly coincide with the distribution of savannas, shrublands and grasslands, a relationship which is not accidental since the existence of a fire-prone climate is a major determinant of the distribution of that type of vegetation (van Wilgen & Scholes, 1997). The dominant plant species in these areas

concentrate most of their aboveground biomass in fine leaves and branches, which burn easily when dry, and support the rapid spread of wildfires (Scholes, 1997; Frost, 1999).

Fire frequency depends on fuel availability, which is controlled by mean annual precipitation, soil fertility, and herbivory (Desanker *et al.*, 1997). Natural fires in most African ecosystems occur due to lightning ignitions generated by convective thunderstorms, which are frequent at the end of the dry season. Nowadays, however, human activity is responsible for the vast majority of fires in Africa. In northern Africa fires burn primarily during the period November–March, progressing from the edge of the Sahara in the north to the fringes of the central African rainforest, in the south. Most fires in southern Africa occur during May to October, moving approximately north-west (northern Angola and southern Democratic Republic of Congo) in June–July to south-east (Tanzania and Mozambique) in September–October (Kendall *et al.*, 1997; Barbosa *et al.*, 1999; Dwyer, Pinnock, *et al.*, 2000).

The present study is based on imagery from two fixed windows defined in the Meteosat disk which cover the African continent. Figure 2.1 depicts the two windows, respectively denoted as NAfr and SAfr. Fig. 1 also presents the land cover associated to each pixel, which was obtained by degrading GLC2000 (Bartholomé & Belward, 2005) to the Meteosat disk resolution. The percentage of land pixels over the two windows for GLC2000 classes is given in Table 2.1.

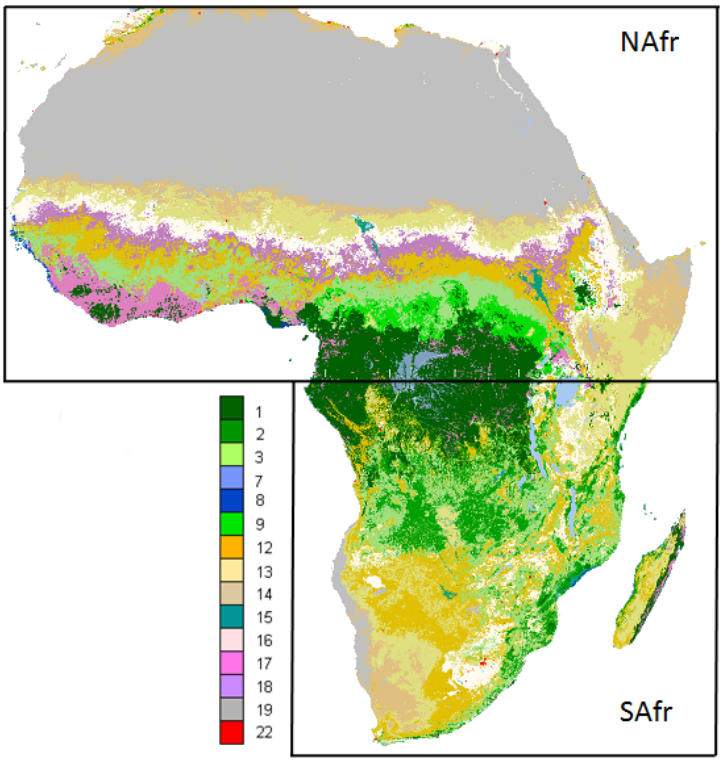

Figure 2.1. Land cover types over the NAfr and SAfr windows as obtained by degrading GLC2000 to the MSG disk. Numbers in the colour bar refer to the land cover types of Table 2.1.

Land cover information from GLC2000 was used to generate a desert and water mask with the aim of; i) eliminating hot and/or highly reflective surfaces (*e.g.* bare soils, urban zones, coastline regions and inland water bodies including rivers and lakes) where burning is not likely to occur; and ii) reducing computing time by eliminating image processing over masked pixels. A mask of volcanoes was also added using data from the Global Volcanism Program (http://www.volcano.si.edu).

Remotely-sensed information from the NAfr and SAfr windows, respectively covers the periods of January and July 2007. NAfr (SAfr) images consist of 1151 rows×2211 columns (1191 rows×1211 columns) for a total number of 1745872 (810698) land pixels and consist of top of the atmosphere (TOA) radiances of SEVIRI/Meteosat-8 at the maximal temporal resolution (*i.e.* every 15min) for the following bands; visible channels centred at 0.635 μm (VIS0.6) and 0.81 μm (VIS0.8) and infrared channels centred at 3.92 μm (IR3.9), 10.8 μm(IR10.8) and 12.0 μm(IR12.0). TOA visible radiances from VIS0.6 and VIS0.8 were converted into reflectances, respectively referred to hereafter as R(0.6) and R(0.8). TOA infrared radiances from channels IR3.9, IR10.8 and IR12.0 were in turn converted into brightness temperatures, respectively denoted hereafter as Tb(3.9), Tb(10.8) and Tb(12.0).

Table 2.1. Representativeness of GLC2000 land cover classes over NAfr and SAfr windows.

		Percentage of land pixels	
C	Land cover type	NAfr	SAfr
1	Tree cover, broadleaved, evergreen	6,3	14,9
2	Tree cover, broadleaved, closed	0,1	13,9
3	Tree cover, broadleaved, deciduous, open	6,6	18,1
7	Tree cover, regularly flooded, fresh water	0,4	0,7
8	Tree cover, regularly flooded, saline water	0,1	0,1
9	Mosaic: tree cover/other natural vegetation	2,6	0,1
12	Shrub cover, closed-open, deciduous	7,2	22,1
13	Herbaceous cover, closed-open	7,8	14,7
14	Sparse herbaceous or sparse shrub cover	6,3	3,3
15	Regularly flooded shrub and/or herbaceous cover	0,3	0,5
16	Cultivated and managed areas	7,4	8,4
17	Mosaic: cropland/tree cover/other natural vegetation	3,5	1,0
18	Mosaic: cropland/shrub or grass cover	4,9	0,0
19	Bare areas	46,4	2,1
22	Artificial surfaces and associated areas	0,1	0,1

III. Rationale

III.1. Background

Depending on whether they are smouldering or flaming, most fires burn at temperatures between 500 and 1200 K (Dwyer, Pinnock, *et al.*, 2000) but even higher temperatures (>1400 K) may occur in forested areas (Giglio *et al.*, 1999). At these temperatures and in accordance with Planck's theory of blackbody radiation, there is a very strong emission in the middle-infrared (MIR) at wavelengths of 3–5 μm, as opposed to the background where the peaks of emission are located in the long-wave infrared (IR) at wavelengths on the order of 10 μm.

Most of the existing operational fire detection algorithms were developed for regional, continental and global applications and have been tuned accordingly. Generally speaking, the techniques utilize similar processing steps and input data (predominantly short- and long-wave IR bands) and the algorithms may be placed in two broad categories: fixed-threshold techniques and spatial analysis (or contextual) techniques (Justice & Dowty, 1994). Earlier fire detection algorithms relied on static thresholds that were applied to the values recorded in MIR and IR channels. Appropriate values for the thresholds were computed empirically, depending on vegetation type, region and time of year (Li & Giglio, 2000).

More recent methods use contextual algorithms where values of thresholds are dynamically derived using appropriate statistics obtained from neighbouring pixels. As pointed out by Flasse and Ceccato (1996), the main difference between contextual and fixed threshold algorithms is that a decision is made on a relative basis rather than on an absolute one; if the contrast between a given pixel and its surroundings is high enough, then the pixel is flagged as containing an active fire.

Contextual algorithms were first explored by Prins and Menzel (1992), using the Geostationary Operational Environmental Satellites (GOES) data, and by Justice *et al.* (1993), using the Advanced Very High Resolution Radiometer (AVHRR) data. The approach was also adopted for global and regional fire monitoring (Justice & Malingreau, 1996; Eva & Flasse, 1996; Dwyer *et al.*, 1998; Stroppiana *et al.*, 2000), and for the World Fire Web initiative (Grégoire *et al.*, 2000). More recently, the contextual approach was used by the MODIS Fire Team to develop a global daily active fire product from MODIS data (Justice *et al.*, 2002; Giglio, Descloitres, *et al.*, 2003).

III.2. Description of FiDAlgo

FiDAlgo builds upon the above-mentioned contextual algorithms for AVHRR and MODIS. For each pixel and time-step, FiDAlgo uses the solar zenith angle, SEVIRI reflectances R(0.6) and R(0.8), and brightness temperatures Tb(3.9), Tb(10.8) and Tb(12.0). Table 2.2 summarises the channels used and the respective purposes.

As schematically shown in Figure 2.2, the method consists of the following four main steps; 1) Pre-processing, 2) Selection of potential fire pixels, 3) Detection of contaminated pixels and 4) Confirmation of active fire pixels.

Table 2.2. SEVIRI channels used in FiDAlgo.

Channel	Purpose
R(0.6)	Cloud detection
R(0.8)	Cloud detection, bright surface and sunglint detection
Tb(3.9)	Active fire detection
Tb(10.8)	Active fire detection
Tb(12.0)	Cloud detection

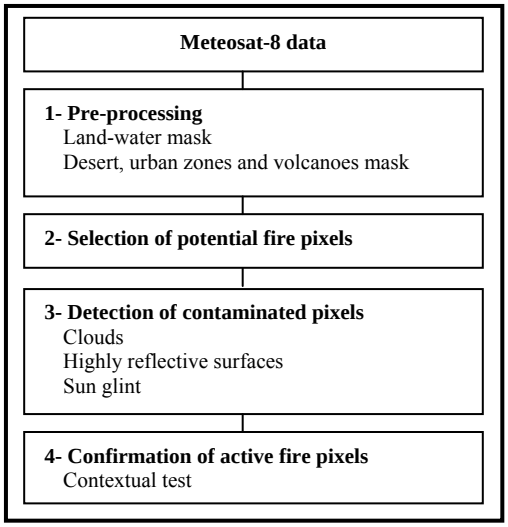

Figure 2.2. Schematic overview of the processing stages of FiDAlgo.

III.2.1. Step 1- pre-processing

Surfaces such as exposed soil and rock are highly reflective at 3.9 μm, and may be the source of false fire detections. For instance, the algorithm by Arino *et al.* (1993) systematically identified large desert regions as very extensive burning areas, spanning thousands of pixels (Giglio *et al.*, 1999; Mota *et al.*, 2006). In order to mitigate false alarms, pixels classified in the above-described land mask as bare soils, inland water, volcanoes and urban zones were not considered for further analysis.

III.2.2. Step 2- selection of potential fire pixels

Selection of pixels likely to contain an active fire (Figure 2.3) may be achieved by simply applying appropriate thresholds to MIR and to differences between MIR and IR channels, on a pixel-by-pixel basis (*e.g.*, Arino *et al.*, 1993; Flasse & Ceccato, 1996; Stroppiana *et al.*, 2000; Justice *et al.*, 2002; Giglio, Descloitres, *et al.*, 2003; Giglio, Kendall, *et al.*, 2003).

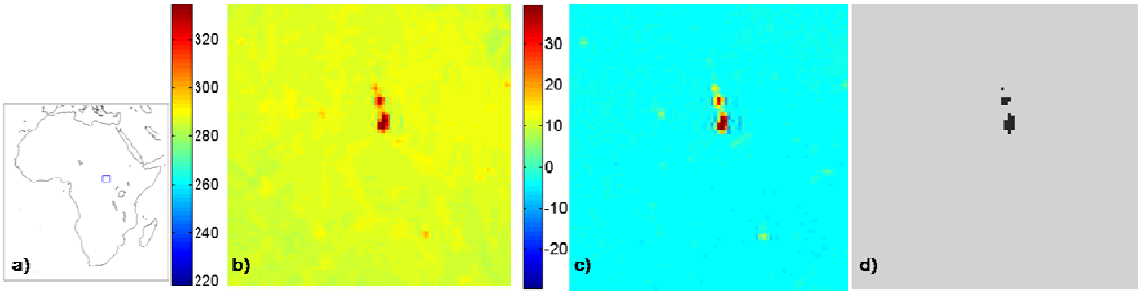

Figure 2.3. An example of fire pixels as identified over a selected region in the African continent using information from Meteosat image obtained by SEVIRI at 23:00 UTC OF 23/01/2007. A) map of Africa where the location of the region is identified by the small rectangular frame; B) values (in K) of Tb(3.9) according to the colour bar on the left; C) values (in K) of ΔT=Tb(3.9)−Tb(10.8) according to the colour bar on the left; D) location of confirmed vegetation fires (pixels in black) by FiDAlgo (see Step 4 of the algorithm).

Since the reflected MIR component increases with decreasing solar zenith angle, near solar noon a stronger reflected component may boost Tb(3.9) above the prescribed threshold leading to the detection of spurious fires. On the other hand, as the solar component drops off with increasing solar zenith angle, some small fires may not pass the threshold test (Giglio *et al.*, 1999). With the aim of mitigating commission (omission) errors for low (high) solar zenith angles (SZA), during day time (*i.e.* for SZA<85°) thresholds imposed by FiDAlgo both on Tb(3.9) and on differences ΔT=Tb(3.9)−Tb(10.8) vary throughout the day. A number of situations where omission and commission errors have occurred was visually inspected and, based on such experience, a pixel is considered as containing a potential fire if one of the following conditions is fulfilled:

$$\begin{aligned}
&\mathrm{Tb}(3.9) \geq 315\mathrm{K} \text{ and } \Delta T \geq 10\mathrm{K} \text{ for } \mathrm{SZA} < 70^\circ \\
&\mathrm{Tb}(3.9) \geq 313\mathrm{K} \text{ and } \Delta T \geq 9\mathrm{K} \text{ for } 70^\circ \leq \mathrm{SZA} < 73^\circ \\
&\mathrm{Tb}(3.9) \geq 311\mathrm{K} \text{ and } \Delta T \geq 7\mathrm{K} \text{ for } 73^\circ \leq \mathrm{SZA} < 76^\circ \qquad (2.1a) \\
&\mathrm{Tb}(3.9) \geq 309\mathrm{K} \text{ and } \Delta T \geq 5\mathrm{K} \text{ for } 76^\circ \leq \mathrm{SZA} < 79^\circ
\end{aligned}$$

$$\mathrm{Tb}(3.9) \geq 307\mathrm{K} \text{ and } \Delta\mathrm{T} \geq 4\mathrm{K} \text{ for } 79° \leq \mathrm{SZA} < 82°$$

$$\mathrm{Tb}(3.9) \geq 306\mathrm{K} \text{ and } \Delta\mathrm{T} \geq 3\mathrm{K} \text{ for } 82° \leq \mathrm{SZA} < 85°$$

During night time (*i.e.* for SZA ≥ 85°), a potential fire is attributed to a given pixel if the following condition holds:

$$\mathrm{Tb}(3.9) \geq 305\mathrm{K} \text{ and } \Delta\mathrm{T} \geq 3\mathrm{K} \text{ for } \mathrm{SZA} \geq 85° \qquad (2.1b)$$

III.2.3. Step 3- detection of contaminated pixels

Contamination of channel 3.9 μm by clouds is the most commonly occurring source of false alarms during daytime. When illuminated by sunlight, clouds typically appear as regions of elevated Tb(3.9) (due to reflected sunlight) and of reduced Tb(10.8) (due to their cooler temperatures), leading to a net increase in ΔT that may give rise to an erroneous detection of pixels affected by active fires.

Several cloud identification techniques may be employed, ranging in quality from simple (*e.g.* spatially fixed thresholds) to highly sophisticated (interactive analyst-controlled). The following two extreme situations may result; (1) excessive cloud detection, which inadvertently masks fires, smoke and large cloud-free areas; (2) failure to mask most small and some large clouds, causing many false alarms (Giglio *et al.*, 1999).

Cloud detection by FiDAlgo is based on a simplified version of the Saunders and Kriebel (1988) algorithm. A given day time pixel is considered as cloud or contaminated by clouds, and therefore eliminated, if one of the following three conditions is met:

$$\mathrm{R}(0.6) + \mathrm{R}(0.8) > 1.2$$

or

$$\mathrm{Tb}(12.0) < 265\mathrm{K} \qquad (2.2a)$$

or

$$\mathrm{R}(0.6) + \mathrm{R}(0.8) > 0.8 \text{ and } \mathrm{Tb}(12.0) < 285\mathrm{K}$$

During night time, pixels are flagged as cloud if the following condition is satisfied:

$$\mathrm{Tb}(12.0) < 265\mathrm{K} \qquad (2.2b)$$

Since SEVIRI channel IR3.9 covers parts of both the solar and thermal ranges of the electromagnetic spectrum, it is crucial to reject those pixels whose values in the IR3.9 channel would be too high (or even saturate) due to high reflection, rather than high temperature (Flasse & Ceccato, 1996).

Accordingly, a given pixel is considered as representing a highly reflective surface, and therefore eliminated if the following condition (Giglio *et al.*, 1999) is fulfilled during daytime:

$$\mathrm{R}(0.8) > 0.25 \qquad (2.3)$$

For certain sun–earth-satellite configurations false fire detections may occur due to specular reflexion of sunlight by water bodies, wet soils, cirrus clouds, cloud edges and, in rare instances, by bare soils (Stroppiana *et al.*, 2000; Giglio, Descloitres, *et al.*, 2003).

A given pixel is considered contaminated by sunglint, and therefore eliminated, if i) its neighbouring pixels are water bodies, sparsely vegetated or bare soils or contaminated by clouds and 2) the following condition is fulfilled during daytime:

$$\mathrm{SZA} > 40° \text{ and } \mathrm{R}(0.8) > 0.20 \qquad (2.4)$$

Figure 2.4 shows examples of detection of contaminated pixels (clouds, highly reflective surfaces and areas of sunglint).

III.2.4. Step 4- confirmation of active fire pixels

A potential fire pixel is confirmed as a pixel containing an active fire by comparing its spectral signature against the radiative properties of the respective background (Kaufman *et al.*, 1998). The background is defined as a 5×5 pixels grid centred at the

potential fire pixel and valid background pixels are all those that were neither masked in step 3 nor identified as potential fire pixels in step 2.

Valid background pixels are then used to compute a set of statistics that characterise the background (Giglio *et al.*, 1999), namely the mean and the mean absolute deviation of Tb(3.9), respectively denoted as $\overline{\mathrm{Tb}}(3.9)$ and $\delta(3.9)$:

$$\overline{\mathrm{Tb}}(3.9) = \frac{1}{N}\sum_{i=1}^{N} \mathrm{Tb}_i(3.9) \qquad (2.5a)$$

$$\delta(3.9) = \frac{1}{N}\sum_{i=1}^{N} \left|\mathrm{Tb}_i(3.9) - \overline{\mathrm{Tb}}(3.9)\right| \qquad (2.5b)$$

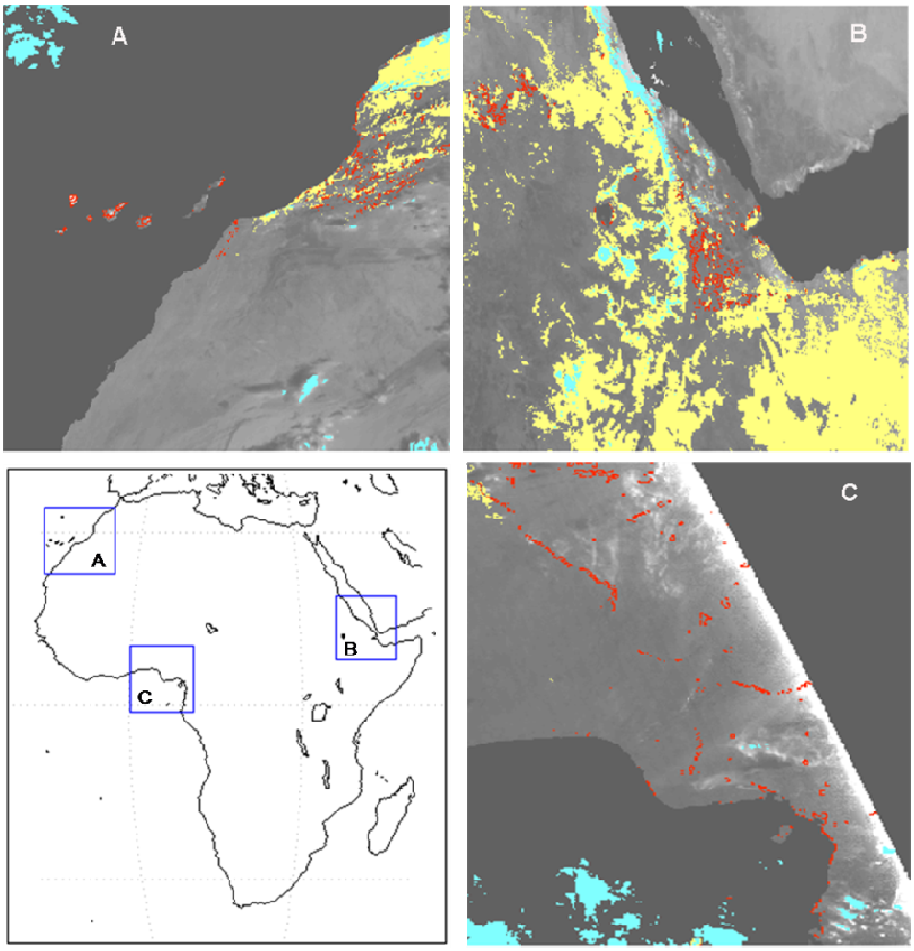

Figure 2.4. Examples of contaminated pixels as identified in three selected regions in the African continent whose locations are given by the rectangular frames in the map of Africa (lower left panel). Images correspond to SEVIRI R(0.8) as obtained at 08:00 UTC of 23/01/2007 (A), 11:15 UTC of 22/01/2007 (B) and 17:15 UTC of 23/01/2007 (C). Cyan, yellow, and red pixels respectively indicate clouds, highly reflective surfaces and areas of sunglint.

as well as the mean and mean absolute deviation of ΔT, respectively denoted as ΔT and δ(ΔT):

$$\overline{\Delta T} = \frac{1}{N}\sum_{i=1}^{N} \Delta T_i \qquad (2.6a)$$

$$\delta(\Delta T) = \frac{1}{N}\sum_{i=1}^{N} |\Delta T_i - \overline{\Delta T}| \qquad (2.6b)$$

The number of valid neighbouring pixels in the grid must be at least three, *i.e.* $N \geq 3$. If there is an insufficient number of valid surrounding pixels, statistics are not computed and the pixel is kept classified as potentially containing a fire.

A potential fire pixel is finally confirmed as a pixel containing an active fire when one of the two following conditions is met (Giglio *et al.*, 1999):

$$Tb_{PF}(3.9) > \overline{Tb}(3.9) + \delta(3.9) - 3$$

and (2.7a)

$$\Delta T_{PF} > \overline{\Delta T} + \max(2.5 * \delta(\Delta T), 4)$$

during daytime or:

$$\Delta T_{PF} > \overline{\Delta T} + \max(2.5 * \delta(\Delta T), 4) \qquad (2.7b)$$

during night time. The subscript PF in the previous expressions indicates values corresponding to the potential fire pixel.

IV. Results

IV.1. Spatial and temporal distribution of fire activity

FiDAlgo was applied over NAfr and SAfr windows using the maximum temporal resolution of the SEVIRI radiometer (*i.e.*, one image every 15min). The procedure allowed identifying both active fires (*i.e.* occurrences in a given pixel of a given image) and fire pixels (*i.e.* pixels where at least one active fire was detected, throughout the study period). Identified fire pixels were further classified into the following three categories;

Single occurrence fires, defined as active fires that are isolated events in space and time, *i.e.* having occurred only once in the entire period and with no active fires identified in the neighbouring pixels, neither in the same image nor in the previous and the following ones;

Fires over sparse herbaceous or sparse shrub cover, defined as active fires not included in the previous category and occurring over pixels classified as belonging to GLC2000 class 14 (Table 2.1 and Figure 2.1);

Vegetation fires, which include all active fires that do not belong to the previous categories.

As shown in Table 2.3, a grand total of 370239 (325923) active fires were detected, distributed over 73046 (73863) fire pixels within the NAfr (SAfr) window, during January (July) 2007. Single occurrences account for about 5% of active fires in both windows and fires over sparse herbaceous or sparse shrub cover represent about 2.5% in NAfr, being negligible in SAfr.

Table 2.3. Active fires and fire pixels over NAfr and SAfr windows during January and July 2007, respectively.

	NAfr	SAfr
Vegetation fires	341 801	310 771
Single occurrence	19 581	15 132
Sparse herb./shrub.	8 857	20
Active fires	370 239	325 923
Fire pixels	73 046	73 863

It is worth noting that the goal of this exercise is to check whether observed fire distribution for each region and time frame is consistent with those obtained in previous analyses, as a further means to assess algorithm performance. Our aim is not to derive overall conclusions on the biogeography of African vegetation fires, based only on two months of data analysis.

Figure 2.5 presents the spatial distribution of identified active fires and fire pixels. Most burning activity during January over NAfr may be found in the Sudanian region, especially in southern Chad, the Central African Republic, southern Sudan and in various regions of West Africa, with the exception of Nigeria, which displays lower fire density. Burning activity during July over SAfr is concentrated in northern Angola, the southern Democratic Republic of Congo and western Zambia.

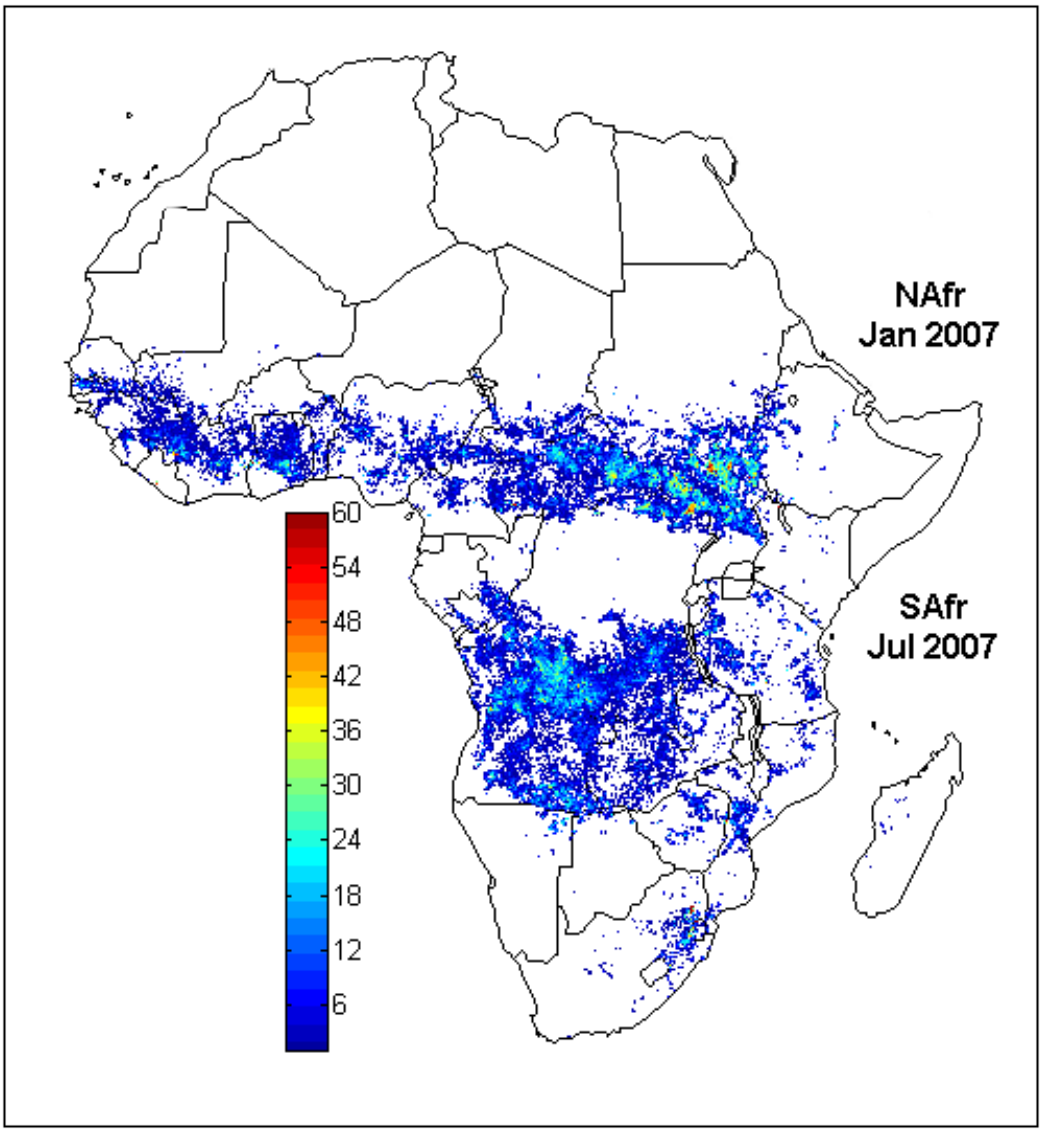

Figure 2.5. Fire pixels over NAfr and SAfr windows, respectively during January and July 2007. The colour bar indicates for each fire pixel the number of active fires identified.

Table 2.4 presents the distribution of vegetation fires among the different GLC2000 land cover classes. Three groups of vegetation cover may be considered, namely trees (*i.e.* classes 1, 2, 3 and 9), shrub/herbaceous (*i.e.* classes 12, 13 and 15) and cropland/shrub (*i.e.* classes 16, 17 and 18). The first group is characterised by large

proportions of fire pixels in both NAfr and SAfr windows, namely "Mosaic: tree cover/other natural vegetation" (class 9) with 70% of fire pixels in NAfr, "Tree cover, broadleaved, deciduous, open" (class 3) with 60% (44%) of fire pixels in NAfr (SAfr) and "Tree cover, broadleaved, closed" (class 2) with 34% in SAfr. The group of shrub/herbaceous is also associated to high fire activity in NAfr, where values of 47% and 33% may be observed respectively in the classes of "Regularly flooded shrub and/or herbaceous cover" (class 15) and "Shrub cover, closed-open, deciduous" (class 12). A marked contrast may be observed in this group between NAfr and SAfr windows. For instance, class 15 where the number of total pixels is of the same order of magnitude (respectively 5132 and 4042 in NAfr and SAfr) has a fraction of fire pixels that is almost six times larger in NAfr than in SAfr. On the other hand, in the case of class 12, although there are more pixels in SAfr than in NAfr (respectively 179,394 versus 115,495), there are more fire pixels in NAfr than in SAfr (respectively 40,924 versus 29,937) resulting in a fraction of fire pixels in NAfr that is almost the double than in SAfr. Finally the third group of cropland/shrub is virtually absent in SAfr and is characterised by low values of fraction of fire activity in NAfr.

Table 2.4. Distribution of active fires among the different GLC2000 land cover classes (see Table 2.1) for NAfr and SAfr windows, during January and July 2007, respectively. Fractions of active fire pixels larger than 33% are represented in bold.

C	NAfr (Jan 2007)			SAfr (Jul 2007)		
	Fire pixels	Total number of pixels	Fraction (%)	Fire pixels	Total number of pixels	Fraction (%)
1	2264	110519	2	7777	121290	6
2	0	948	0	38959	113021	**34**
3	68919	115495	**60**	64053	146928	**44**
9	31735	45466	**70**	68	548	12
12	40924	125819	**33**	29937	179394	17
13	3480	136240	3	13589	119271	11
15	2395	5132	**47**	306	4042	8
16	2258	129328	2	5040	68286	7
17	6476	60414	11	190	8472	2
18	12085	86238	14	0	20	0

Several authors (Malamud *et al.*, 1998; Reed & McKelvey, 2002) have pointed out that wildfire size distributions tend to follow power laws. The high temporal resolution of SEVIRI allows investigating whether the temporal organization also tends to follow a power-law distribution. Figure 2.6 presents histograms of duration of active fires as detected by FiDAlgo over NAfr and SAfr. The exponential-type decay and the long tail that may be observed in both histograms suggest fitting a power-law distribution to the two obtained samples. Figure 2.6 also shows the probability distribution functions (pdfs) of two-parameter generalized Pareto distributions as obtained from maximum likelihood estimates from the samples. The histograms for NAfr and SAfr have a similar behaviour and the same happens with the corresponding pdfs of the generalized Pareto distributions. This is further corroborated by the obtained values for the parameters of

the distributions, respectively 0.5169 (0.5164) in the case of the scale parameter, σ, for NAfr (SAfr) and 0.3790 (0.2762) in the case of the tail index (shape) parameter, k, for NAfr (SAfr). The similar statistical behaviour presented by both windows is another indicator of the consistency of results obtained, as well as of the robustness of the algorithm developed.

A deeper insight into the frequency distribution of active fire duration may be obtained by considering the probability, Pr(X>x), that the number of active fires, X, is greater than a given threshold x. In the present case, such probability is given by:

$$\Pr(X > x) = \left(1 + \kappa\frac{x}{\sigma}\right)^{-1/\kappa}, \; x \geq 0 \qquad (2.8)$$

and therefore the new variable Y=ln(1 + kx/σ) is exponentially distributed with expected value 1/k. This result is especially interesting since it suggests that the logarithm of the scaled number of active fire events over the African continent (*i.e.* over NAfr and SAfr) tends to occur with a constant probability per unit length of time.

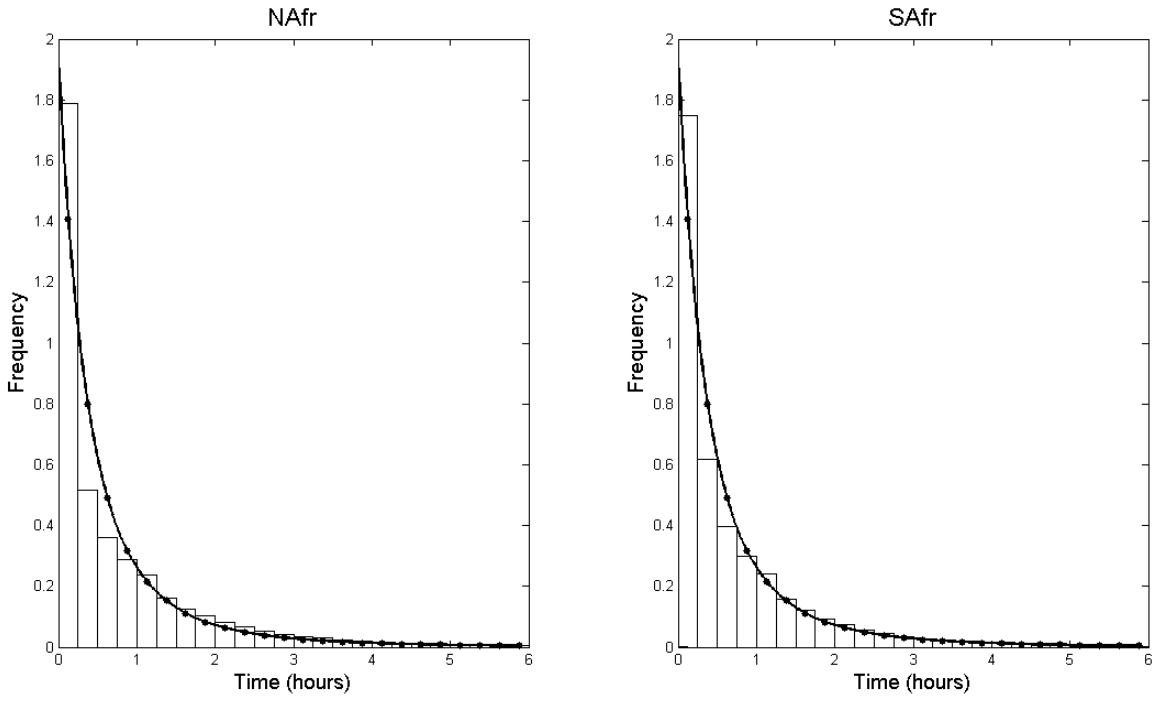

Figure 2.6. Frequency histograms of duration of active fires in NAfr (left panel) and SAfr (right panel) and the corresponding two-parameter generalized Pareto distribution using maximum likelihood estimates of the parameters.

IV.2. Consistency and added value of the developed product

Results obtained with FiDAlgo were compared against hot spots extracted from the global daily active fire product developed by the MODIS Fire Team (Justice *et al.*, 2002). In this respect, it may be noted that when comparing results derived from geostationary sensors, such as SEVIRI, with those from polar-orbit sensors, such as MODIS, the spatial and the temporal resolutions of the instruments are the two main factors that have to be accounted for. Moreover, when the comparison involves data from polar sensors with finer spatial resolution, the procedure is especially complex due to errors caused by data misregistration (Calle *et al.*, 2008).

The FiDAlgo algorithm is based on information from SEVIRI sensor on-board Meteosat-8. As already pointed out, SEVIRI provides a very high temporal resolution (*i.e.* images with a 15-minute repeat cycle) but the size of the sensor footprint is rather large (4.8 km at the SSP). Nevertheless, in what respects to sensitivity, SEVIRI is able to detect fires of less than 1 ha in size over the Iberian Peninsula, with a fire temperature higher than 600 K (Calle *et al.*, 2006). In what regards commission errors, it is worth emphasizing that FiDAlgo includes several tests aiming to detect and eliminate false alarms, as discussed in Section 3.

The MODIS active fire data consist of hot spots as detected by MODIS sensor on board the polar-orbiting Terra and Aqua platforms (http://maps.geog.umd.edu/firms/). The MODIS Fire detection is based on a contextual algorithm developed by Giglio, Descloitres, *et al.* (2003). Information is obtained from thermal channels at coarse spatial resolution (*i.e.* with a pixel size of the order of 1×1 km^2) and with a low temporal resolution consisting of four observations per day from the Terra AM (10:30 and 22:30) and Aqua PM (13:30 and 01:30) (Justice *et al.*, 2002) and corresponding to the maximum temporal resolution of the above mentioned radiometer. The MODIS active fire data is part of the MODIS Fire Products that include an identification of the occurrence of thermal anomalies, which in most cases consist of active fires, but are sometimes associated to volcanic eruptions or to flares from gas wells. The dataset also includes estimates of the total emitted power from fires and of the burned area (Justice *et al.*, 2006).

As shown in Figure 2.7, comparison of the FD&M product was performed in two regions of the African continent, both characterised by intense fire activity. Region 1 within NAfr window (extending from 3.48° to 8.82° N and from 22.57° to 29.07° E) encompasses the extreme south of the Republic of Sudan, eastern Central African Republic and the north of the Democratic Republic of the Congo. Region 2 within SAfr window (extending from 5.44° to 10.86° S and from 17.41° to 23.57° E) covers the north of the Republic of Angola and the south of the Democratic Republic of the Congo. The period of study spans one month in both selected regions, namely January and July 2007 for the regions within NAfr and SAfr, respectively.

Both regions selected have the same size (192×192 SEVIRI pixels), but differ on land cover types. Region 1, located in the NAfr window (left panel of the Figure 2.7), is mostly covered by three classes of GLC2000 that account for 88% of the area (*i.e.* "Tree cover, broadleaved, evergreen", "Tree cover, broadleaved, deciduous, open" and "Mosaic: tree cover/other natural vegetation"). The remainder 12% of pixels, in the North-East of the region, are covered by "Shrub cover, closed-open, deciduous". In the case of region 2, located in the SAfr window (right panel of the Figure 2.7), 87% of pixels is associated to three classes dominated by trees (*i.e.* "Tree cover, broadleaved, evergreen", "Tree cover, broadleaved, closed" and "Tree cover, broadleaved, deciduous, open"). The remainder 13% of pixels is covered by "Shrub cover, closed-open, deciduous", and "Herbaceous cover, closed-open" classes of the GLC2000.

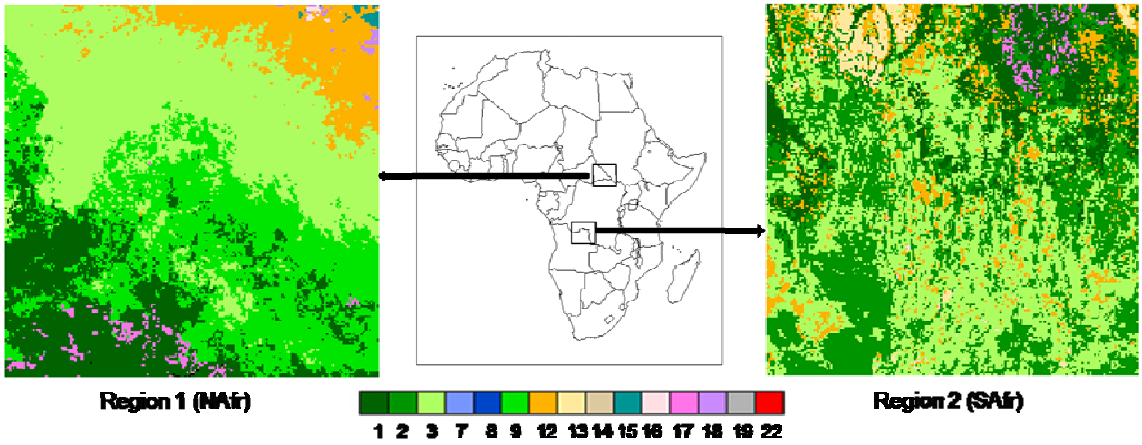

Figure 2.7. The two selected regions for the comparison analysis, and respective land cover based on GLC2000 classification. The two small rectangular regions in the map of Africa (central panel) indicate the geographical location of region 1 (region 2) within the NAfr (SAfr) window. Numbers in the colour bar refer to the land cover types in Table 2.1.

Figure 2.8 presents the two datasets used for the comparison analysis in the two selected regions. The upper (lower) panels correspond to the region 1 (region 2) within NAfr (SAfr) window and indicate the location of the fire pixels and the number of identified active fires, within fire pixels, obtained respectively from SEVIRI using FiDAlgo (left panels) and from the MODIS active fire data base (right panels). Table 2.5 provides a summary of the number of active fires and fire pixels identified by each sensor in the two considered regions. For both sensors the number of active fires is always much larger than the fire pixels. This feature is however due to different reasons; in the case of SEVIRI, the high temporal resolution allows counting as fire pixels the fire event(s) that take place in a given SEVIRI pixel during the entire life cycle(s), and this is further reinforced by the low spatial resolution that turns possible a given SEVIRI pixel to be flagged as containing active fires more than once during the month. On the other hand,

in the case of MODIS, the high number of active fires in a given SEVIRI pixel is due to the process of degrading from the spatial resolution of MODIS (*i.e.* 1×1 km^2) to the one of SEVIRI that allows counting as active fires all fire events in MODIS pixels contained in a given SEVIRI pixel. Nevertheless, results in Figure 2.8 and Table 2.5 point out the existence of large discrepancies between the two instruments and the two regions that deserve to be analysed.

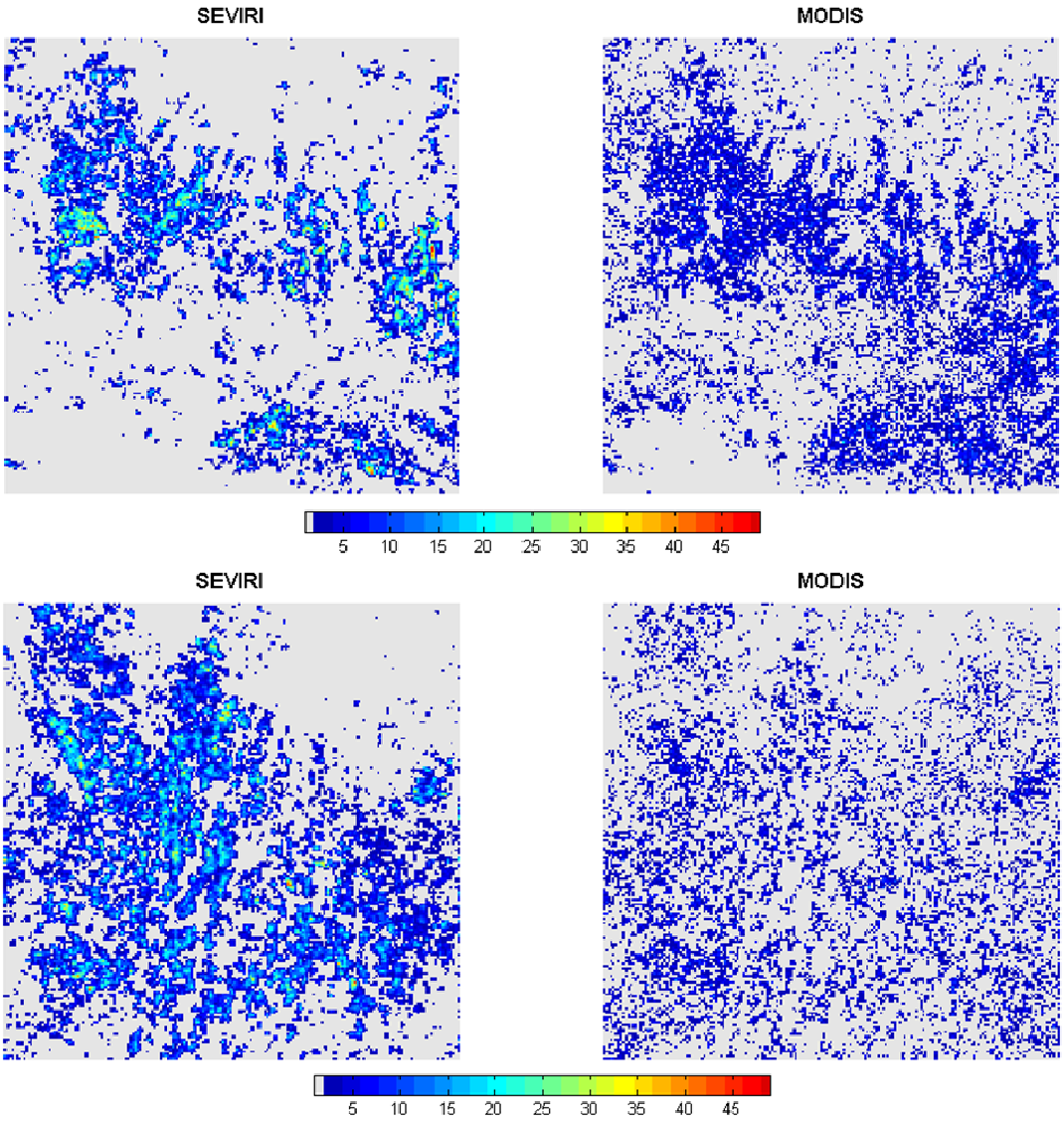

Figure 2.8. Fire pixels detected over the two selected regions of 192×192 pixels, region 1 within NAfr window (upper panels) and region 2 within SAfr window (lower panels) during January and July 2007, respectively. Left (right) panels display fire counts as obtained from SEVIRI using FiDAlgo (from the MODIS active fire data base). For each fire pixel, the colour bar indicates the number of active fires identified.

Figure 2.9 presents the daily cycles of the median of fire activity in regions 1 and 2 as derived from the collection of daily cycles identified, by FiDAlgo, each day of the considered periods. Figure 2.9 also presents the daily cycles of the first quartile, the median and the third quartile of the fraction of cloud-contaminated pixels in regions 1 and 2. As mentioned in previous studies (*e.g.* Amraoui *et al.*, 2008) both regions present a well defined peak located around 13:00. However the daily cycle of active fires in region 2 (lower panel) is more concentrated in turn of its maximum whereas in region 1 (upper panel) the daily cycle extends into the late afternoon as previously reported by Giglio (2007). In agreement with the findings by Roberts and Wooster (2007), the daily cycle of active fires presents a slightly asymmetric distribution in both regions, with a steeper increase before the maximum and a slower decrease during the afternoon, region 1 even presenting a secondary peak around 18:00. Nevertheless there is virtually no fire activity between midnight and 08:00.

Table 2.5. Number of active fire and fire pixels in the selected regions from FiDAlgo using SEVIRI data and from the MODIS active fire data base.

	Region 1 (NAfr window)		Region 2 (SAfr window)	
	SEVIRI	MODIS	SEVIRI	MODIS
Active fire	79 876	56 954	121 314	39 620
Fire pixels	12 603	18 268	19 609	16 556

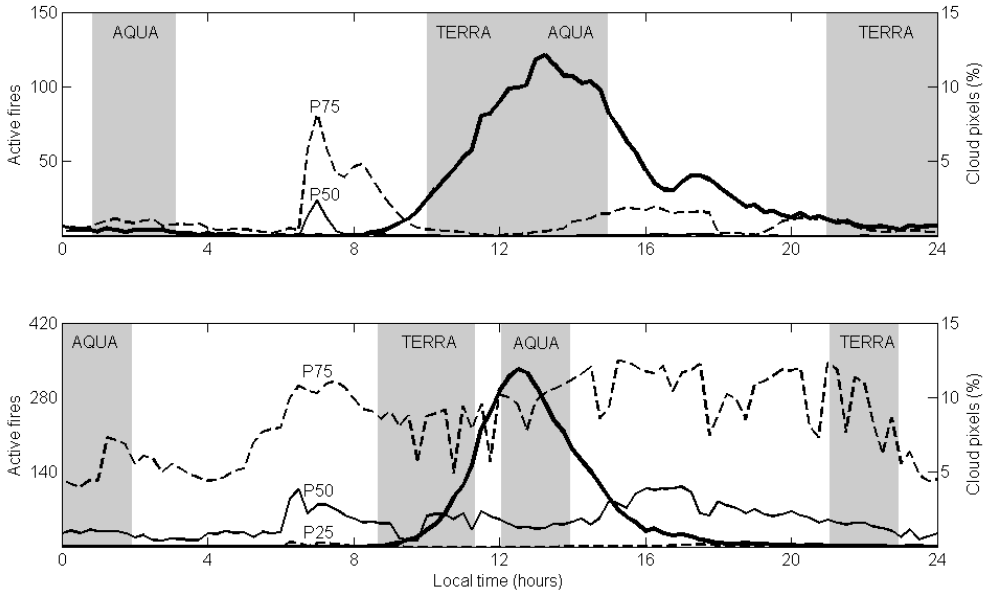

Figure 2.9. Daily cycles of fire activity and of fraction of cloud-contaminated pixels over region 1 within NAfr window (upper panel) and region 2 within SAfr window (lower panel) during January and July 2007, respectively. The thick curves represents the median of the daily cycles of active fires identified during the considered periods whereas the thin curves represent the first and the third quartiles (dashed lines), and the median (solid line) of the daily cycles of percentage of pixels identified as contaminated by clouds. Grey bars delimit the times of overpass of TERRA and AQUA during the considered periods.

Region 2 tends to be cloudier than region 1 and cloud cover tends to spread during the day in region 2 as opposed to region 1 where a conspicuous peak of cloudiness may be observed in the early morning that is attributable to radiative fog. An abrupt decrease in cloudiness around 18:00 is also noticeable in region 1 raising the possibility that the above-mentioned secondary peak in fire activity is an artefact due to changes in cloud cover.

The above-described characteristics of the daily cycle of fire activity point out both the added value brought by the fine temporal resolution of SEVIRI and the difficulties of characterising the daily cycle using information from polar-orbit sensors, such as MODIS. The grey bars in Figure 2.9 delimit the times of overpass of TERRA and AQUA during the considered periods of January 2007 in region 1 and July 2007 in region 2. It is worth noting that within each grey bar there will be generally one observation per day, in a total of four. This may lead to severe biases when characterising the daily cycle of fire activity, especially if the overpass misses the narrow time band in turn of the maximum or if there is obscuration by clouds.

The very different sampling of the diurnal cycles of active fires provided by SEVIRI and MODIS severely impairs any attempt to make a direct comparison (*e.g.* in a given pixel and at a given time) between information provided by the two sensors. This difficulty may be partly circumvented by relying on the study by Calle *et al.* (2008) who have developed an operational procedure that allows dealing with the problem posed by the different spatial and temporal scales of geostationary and polar orbiting instruments. Their study covered the region of Galicia (Spain) spanning a period of intense fire activity, from the 1st to the 20th of August 2006. The authors relied on remotely sensed data from three different sensors; SEVIRI, on-board Meteosat-8, MODIS, on-board Terra and Aqua, and AWiFS, on-board Resourcesat-1.

The procedure consists in dividing the region in squared blocks with length L × L and then fitting a linear model of active fire counts as obtained using SEVIRI in each block versus the counts obtained in the same block when using a different sensor. Calle *et al.*, 2008 have shown that the coefficient of determination, ρ^2, linearly increased with the logarithm of L, *i.e.* according to the law $\rho^2=\alpha + \beta \ln(L)$, where α and β are constants.

In the present study the procedure by Calle *et al.* (2008) is generalized to the time domain, *i.e.* the study area and period were subdivided in space-time blocks of N SEVIRI pixels × N SEVIRI pixels × T days, and linear models were derived that relate fire counts over each block as obtained from FiDAlgo with corresponding numbers from the MODIS active fire database. An extended law relating ρ^2 with ln(N) and ln(T) will also be investigated, *i.e.* the coefficient of determination is estimated according to the linear model:

$$\rho^2 = c + a \cdot \ln(N) + b \cdot \ln(T) \qquad (2.9a)$$

where a, b and c are parameters to be estimated.

It is worth noting that the above equation may be rewritten in the form of the following power law:

$$e^{\rho^2} = C \times N^a \times T^b \qquad (2.9b)$$

where $C = e^c$.

The different features of the results obtained with the FD&M and MODIS products suggest investigating the relationship between fire counts as obtained from MODIS and from SEVIRI, as well as the dependency of such relationship on the adopted spatial and temporal scales. The two selected areas were accordingly subdivided in blocks of N SEVIRI pixels × N SEVIRI pixels × T days for different combinations of N and T. Fire counts as obtained from FiDAlgo were then related with those obtained from MODIS by means of linear models and the respective coefficients of determination, ρ^2, were used as a measure of goodness-of-fit. Linear models of the type described by equations (2.9a) and (2.9b) were used to characterize the dependency of coefficients of determination on the spatial scale N and the temporal scale T. The two following linear models were obtained:

$$\rho^2 = 0.02 + 0.21 \cdot \ln(N) + 0.07 \cdot \ln(T) \qquad (2.10a)$$

for region 1, in NAfr, and

$$\rho^2 = -0.02 + 0.17 \cdot \ln(N) + 0.07 \cdot \ln(T) \qquad (2.10b)$$

for region 2, in SAfr. Both models are shown in Figure 2.10 and their adequacy to describe the dependency of ρ^2 on N and T is worth being noted, given the high values of the obtained correlation coefficients, respectively 0.95 and 0.96 for the linear models defined over the regions inside NAfr and SAfr.

The similarity between the coefficients of the models obtained for the two regions is striking, especially in what regards the dependency with ln(T), where the coefficient of

0.07 is the same in both models. The increase of ρ^2 with ln(N) is larger than the one with ln(T), being slightly greater in the case of the region 1. Possible reasons explaining the different statistical behaviour of regions 1 and 2 will be discussed below.

The results obtained show that a given explained variance may be achieved using models based on different pairs of N and T. Choice of specific values of explained variance ρ^2, spatial scale N and temporal scale T will then depend on the purpose of the study to be undertaken. Table 2.6 and Figure 2.11 present examples of the results obtained based on three different combinations of N and T, all of them leading to linear models characterized by values of $\rho^2 \approx 0.64$ for region 1 and $\rho^2 \approx 0.51$ for region 2.

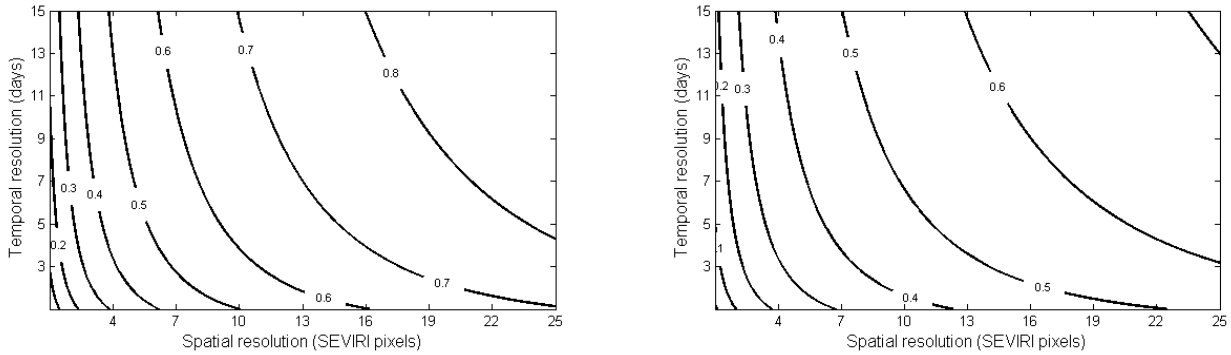

Figure 2.10. Dependency on spatial resolution (in SEVIRI pixels) and time resolution (in days) of the coefficient of determination (ρ^2) of linear models relating number of active fires obtained from the FD&M product versus those obtained from the MODIS active fire database, respectively over the selected regions of 192×192 SEVIRI pixels for region 1 within NAfr (left panel) and region 2 within SAfr (right panel).

Table 2.6. Examples of linear models defined over region 1 (in NAfr) and region 2 (in SAfr), relating the number of active fires as obtained from the MODIS active fire database (y_{MODIS}) with the number of active fires as obtained from the FD&M product (x_{SEVIRI}). m, b and ρ respectively denote the slope, intercept and correlation coefficient of each linear model, whereas B, S and RMSE respectively denote the bias, the standard deviation and the root mean square error, e (defined as $x_{SEVIRI} - y_{MODIS}$).

	NxN pixels – T days	Number of pixels	$Y_{MODIS} = m \times x_{SEVIRI} + b$			$e = x_{SEVIRI} - y_{MODIS}$		
			m	b	ρ	B	S	RMSE
Region 1 (NAfr)	6x6 pixels – 10 days	2 695	0.30	11.73	0.79	8.95	50.27	51.06
	8x8 pixels – 6 days	2 567	0.30	12.31	0.81	9.39	56.53	57.30
	12x12 pixels – 3 days	1 653	0.31	15.42	0.81	9.83	60.95	61.74
Region 2 (SAfr)	6x6 pixels – 10 days	1 939	0.14	6.21	0.72	29.46	52.10	59.86
	8x8 pixels – 6 days	1 626	0.14	6.55	0.72	31.67	55.36	63.78
	12x12 pixels – 3 days	1 981	0.15	8.91	0.71	33.70	58.66	67.64

The general characteristics of the models developed for the two regions are very similar. As clearly apparent in Figure 2.11, for blocks containing a small number of active fires the FD&M product will indicate lower values than the MODIS product. Besides being related to the very different sampling of the diurnal cycle between the two sensors this feature also reflects the different spatial and temporal resolutions provided by SEVIRI and MODIS. The positive values of the intercept and the low value (well below 1) of the slope (Table 2.6) are attributable to the low spatial resolution of the SEVIRI instrument. In the case of blocks containing a high number of active fires, the FD&M product will indicate much higher values than the MODIS product (Figure 2.11), a feature that may result from the much higher imaging frequency of the SEVIRI instrument and reflects on the positive values of bias B obtained (Table 2.6).

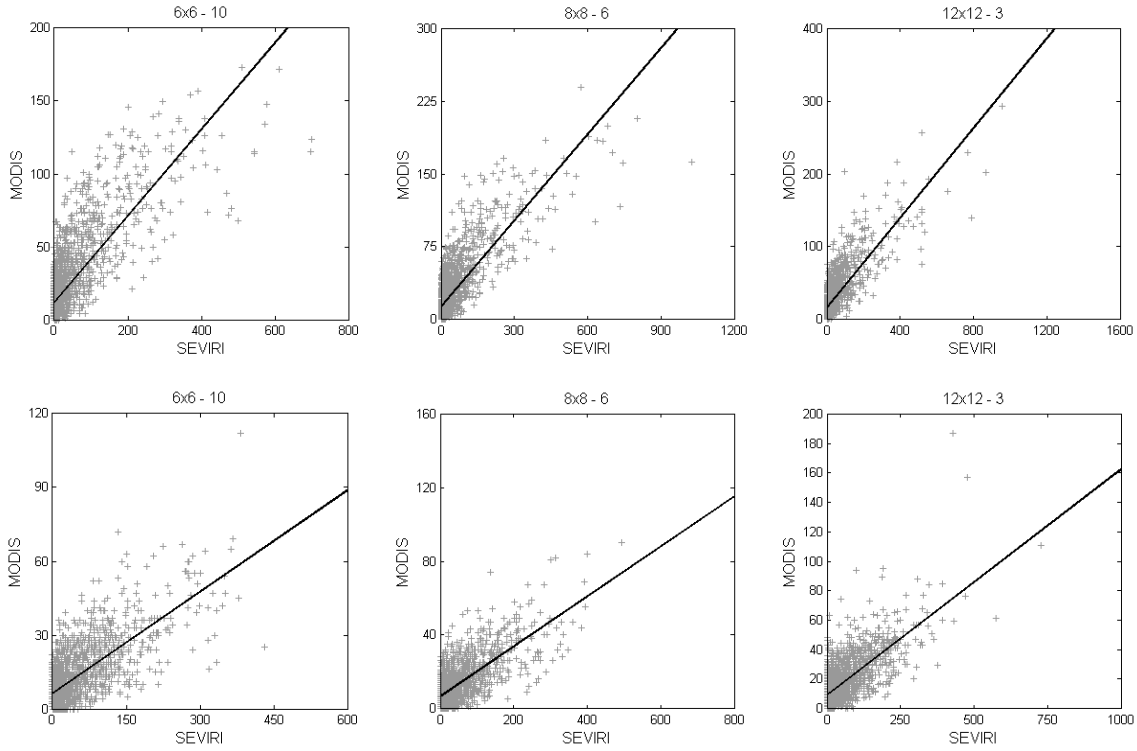

Figure 2.11. Scatterplots and regression lines for the three linear models described in Table 2.6, respectively for region 1 (upper panels) and region 2 (lower panels). Different scales (in both axes) were used in the figures.

However, there are some statistical differences in the models for regions 1 and 2 that deserve to be pointed out. As shown in Table 2.6, the slope and intercept of the linear models in region 1 are about twice as large as those in region 2. On the other hand, although the mean square error, $(RMSE)^2$, is by large due to random errors, the contribution of systematic errors is much larger in region 2, accounting for almost one fourth of the total error; in fact, the square of the bias, B^2, represents 3% (25%) of the mean square error in region 1 (region 2), the remaining 97% (75%) being explained by

the variance, S^2. The dissimilar behaviour of the models in the two regions may be attributed to differences in landscape structure and land cover, as well as to the number of fire pixels and active fires. The latter aspect is clearly revealed by the results presented in Table 2.5; whereas in region 1 the number of SEVIRI fire pixels is just slightly above two thirds of the MODIS fire pixels, such is not the case in region 2, where the number of SEVIRI fire pixels is even larger than the number detected with MODIS. The apparent increase in omission errors by MODIS may be attributed to the fact that the landscape in region 2 is much more fragmented than that of region 1.

V. Discussion and conclusions

An overall description was given of the Fire Detection and Monitoring (FD&M) product that allows identifying active fires using information provided by MSG at the maximum temporal resolution. The active fire detection algorithm developed (FiDAlgo) is based on the heritage from polar, sun-synchronous instruments. The fire incidence observed over Africa compares well with the results obtained by Barbosa *et al.* (1999), and Tansey, Grégoire, Stroppiana, *et al.* (2004), Tansey, Grégoire, Binaghi, *et al.* (2004). The former authors used White's Vegetation of Africa map (White, 1983), and found that over 50% of the area burned, detected during the period 1982–1991, was located in three vegetation types, designated "Undifferentiated Ethiopian, Sudanian, and North Zambezian woodland", "Sudanian woodland with abundant Isoberlinia", and "Mosaic of Guineo-Congolian Lowland Forest and Secondary Grassland". An additional 20% of area burned affected "Wetter Zambezian Woodland Miombo", "Somalia-Masai Acacia-Commiphora Deciduous Bushland and Thicket", and "Drier Zambezian Miombo Woodland". Therefore, areas of open tree cover (*i.e.*, woodlands) are also found to be the vegetation type most affected by fire. Plate 3 of Barbosa *et al.* (1999) shows the location of the six most fire-prone African vegetation types, confirming the good match with our findings. In their analysis of global area burned during the year 2000, Tansey, Grégoire, Stroppiana, *et al.* (2004), Tansey, Grégoire, Binaghi, *et al.* (2004) identified the Northern Hemisphere sub-tropical shrubland and wooded grassland belt in Africa (with the exception of Somalia and Nigeria) as the region with the greatest burning activity per surface area in the world. In southern hemisphere Africa, peaks of burned area density were found in northern Angola and the southern Democratic Republic of Congo, also concurring with our own results.

An analysis of the daily cycle of the median of fire activity was also performed in two regions, respectively located in northern and southern hemisphere Africa, respectively during January and July 2007. The added value brought by the increased temporal resolution of the SEVIRI sensor is well apparent, especially when compared with the poorer sampling by polar-orbit sensors such as MODIS that may lead to severe biases when characterising the daily cycle of fire activity. On the other hand the degradation in

the spatial resolution of SEVIRI with increasing view angle does not seem to be a crucial issue in what respects to the detection of active fires in the African continent if one takes into account the above-mentioned study by Calle *et al.*, 2006 that states the ability of SEVIRI to detect fires of less than 1 ha over the Iberian Peninsula.

The very different sampling of the diurnal cycles of active fires provided by SEVIRI and MODIS raises difficulties when attempting to make direct comparisons between information provided by the two sensors. A different approach was accordingly adopted which consisted in subdividing the study area and period in space-time blocks of N SEVIRI pixels×N SEVIRI pixels×T days, and then adjusting linear models that relate fire counts over each block as obtained from FiDAlgo with corresponding numbers from the MODIS active fire database. Results obtained with FiDAlgo matched well those from the MODIS fire product when adequate spatial and temporal scales are chosen. Despite the differences discussed above results from the comparison between the FD&M and the MODIS products reveal an overall coherence between the products when adequate spatial and temporal scales are chosen. The two products may be viewed as complementary, the FD&M product having the added value of a much finer temporal resolution, capable of detailing lesser studied patterns of fire behaviour, namely the characterization of daily and weekly fire cycles. This may prove useful for atmospheric emissions and transport studies, as well as for clarifying aspects of anthropogenic fire ignition behaviour, namely its variation among diverse climates and land use/land cover types. From a methodological perspective, use of both the spatial and temporal dimensions for product comparison is a novel aspect of this study, made relevant by the very high temporal resolution of SEVIRI data. To the best of our knowledge, this study was also the first to reveal that fire duration distributions follow power laws, of the kind previously identified for fire size distributions.

Acknowledgments

The Portuguese Foundation of Science and Technology (FCT) has supported the research performed by the first author (Grant No. SFRH/BD/36964/2007). The authors are indebted to Minnie Wong for her assistance in retrieving MODIS active fire data for Africa during January and July 2007. The authors also acknowledge the kind assistance of Sandra Freitas and Carla Barroso of Instituto de Meteorologia (Portugal) in the retrieval of Meteosat-8 data. The research was performed within the framework of the Project Satellite Application Facility on Land Surface Analysis (LSA SAF), an R&D and operational Project supported by EUMETSAT.

References

Abuelgasim, A.A., & Fraser, R.H. (2002). Day and night-time active fire detection over North America using NOAA-16 AVHRR data. *IEEE International Geoscience and Remote Sensing Symposium*, 3, 1489-1491, 24-28 June 2002, Toronto.

Amraoui, M., DaCamara, C.C., & Pereira, J.M.C. (2008). Fire detection and monitoring over Africa. *2008 EUMETSAT Meteorological Satellite Conference, Darmstadt, Germany, 08 - 12 September. EUMETSAT P.52*. 978-92-9110-082-8

Andreae, M.O., & Merlet, P. (2001). Emission of trace gases and aerosols from biomass burning. *Global Biogeochemical Cycles, 15*, 955-966. 2000GB001382

Andreae, M.O., Rosenfeld, D., Artaxo, P., Costa, A.A., Frank, G.P., Longo, K.M., & Silva-Dias, M.A.F. (2004). Smoking rain clouds over the Amazon. *Scie*nce, 303, 1337-1342.

Arino, O., Melinotte, J.-M., & Calabresi, G. (1993). Fire, cloud, land, water: the "Ionia" AVHRR CD-Browser of ESRIN. *EOQ 41*, *ESA*, *EST EC, Noordwijk, July 1993*.

Barbosa, P.M., Stroppiana, D., Grégoire, J.-M., & Pereira, J.M.C. (1999). An assessment of vegetation fire in Africa (1981-1991): burned areas, burned biomass, and atmospheric emissions. *Global Biogeochemical Cycles, 13*, 933-950.

Bartholomé, E., & Belward, A.S. (2005). GLC2000: A new approach to global land cover mapping from Earth observation data. *International Journal of Remote Sensing*, *26*, 1959-1977.

Boschetti, L., Brivio, P.A., & Gregoire, J.-M. (2003). The use of Meteosat and GMS imagery to detect burned areas in tropical environments. *Remote Sensing of Environment*, *85*, 78-91.

Cahoon, D.R., Stocks, B.J., Levine, J.S., Cofer, W.R., & O'Neill, K.P. (1992). Seasonal distribution of African savanna fires. *Nature*, *359*, 812-815.

Calle, A., Casanova, J.L., & Romo, A. (2006). Fire detection and monitoring using MSG Spinning Enhanced visible and Infrared Imager (SEVIRI) data. *Journal of Geophysical Research*, *111*, G04S06. doi: 10.1029/2005JG000116G04S06

Calle, A., Gonzalez-Alonso, F., & Merino de Miguel, S. (2008). Validation of active forest fires detected by MSG-SEVIRI by means of MODIS hot spots and AWiFS images. *International Journal of Remote Sensing*, *29*, 3407-3415.

Cihlar, J., Belward, A., & Govaerts, Y. (1999). Meteosat Second Generation opportunities for land surface research and applications. *EUMETSAT Scientific Publications EUM SP 01*.

Csiszar, I., Denis, L., Giglio, L., Justice, C.O., & Hewson, J. (2005). Global fire activity from two years of MODIS data. *International Journal of Wildland Fire*, *14*, 117-130. doi: 10.1071/WF03078

DaCamara, C.C. (2006). The Land Surface Analysis SAF: one year of pre-operational activity. *The 2006 EUMETSAT Meteorological Satellite Conference*, *Helsinki, Finland, 12-16 June 2006, EUMETSAT P.48* (8pp.), 92-9110-076-5 (available from http://www.eumetsat.int/Home/Main/Publications/index.htm).

DaCamara, C.C., Calado, T.J., Amraoui, M., &. Pereira, J.M.C (2007). The SAF for Land Surface Analysis: wildfire applications. *2007 EUMETSAT Meteorological Satellite Conference and the 15th Satellite Meteorology & Oceanography Conference of the American Meteorological Society, Amsterdam, Netherlands, 24 - 28 September*, *EUMETSAT P.50*. 92-9110-079-X

Delmas, R.A., Loudjani, P., Podaire, A., & Menaut, J.C. (1991). Biomass burning in Africa: an assessment of annually burned biomass. In J.S. Levine (Ed.), *Global Biomass Burning. Atmospheric, Climatic, and Biospheric Implication* (pp. 126-132). Cambridge, Massachusetts: MIT Press.

Desanker, P.V., Frost, P.G.H., Justice, C.O., & Scholes, R.J. (1997). The Miombo network: framework for a terrestrial transect study of land-use and land-cover change in Miombo ecosystems of Central Africa. *IGBP Report, Vol. 41,* Stockholm, Sweden: The International Geosphere-Biosphere Programme (IGBP), 190 pp.

Dwyer, E., Grégoire, J.-M., & Malingreau, J.P. (1998). A global analysis of vegetation fires using satellite images: spatial and temporal dynamics. *Ambio*, *27*, 175-181.

Dwyer, E., Pereira, J.M.C., Grégoire, J.-M., & DaCamara, C.C. (1999). Characterization of the spatio-temporal patterns of global fire activity using satellite imagery for the period April 1992 to March 1993, *Journal of Biogeography*, *27*, 57-69. doi: 10.1046/j.1365-2699.2000.00339.x

Dwyer, E., Grégoire, J.-M., & Pereira, J.M.C. (2000a). Climate and vegetation as driving factors in global fire activity. In J.L. Innes, M. Beniston and M.M. Verstraete (Ed.), *Biomass burning and its inter-relationships with the climate system* (pp. 171-191), New York: Springer.

Dwyer, E., Pinnock, S., Grégoire, J.-M., & Pereira, J.M.C. (2000b). Global spatial and temporal distribution of vegetation fire as determined from satellite observations. *International Journal of Remote Sensing*, *21*, 1289-1302.

Eck, T.F., Holben, B.N., Ward, D.E., Mukelabai, M.M, Dubovik, O., Smirnov, A., Schafer, J.S., Hsu, N.C., Piketh, S.J., Queface, A., Le Roux, J., Swap, R.J., & Slutsker, I. (2003). Variability of biomass burning aerosol optical characteristics in Southern Africa during the SAFARI 2000 dry season campaign and a comparison of single

scattering albedo estimates from radiometric measurements. *Journal of Geophysical Research*, *108*. doi:10.1029/2002JD002321

Eva, H., & Flasse, S. (1996). Contextual and multi-threshold algorithms for regional active fire detection with AVHRR data. *Remote Sensing Reviews*, *14*, 333-351.

Flasse, S.P., & Ceccato, P. (1996). A contextual algorithm for AVHRR fire detection. *International Journal of Remote Sensing*, *17*, 419-424.

Frost, P.G.H. (1999). Fire in Southern African woodlands origins, impacts, effects, and control. *Proceeding of an FAO Meeting on Public Policies Affecting Forest Fires, FAO Forestry Paper, 13*, (pp. 181-205).

Galanter, M., Levy II, H., & Carmichael, G.R. (2000). Impacts of biomass burning on tropospheric CO, NOx and O3. *Journal of Geophysical Research*, *105*, 6633-6653.

Garstang, M., & Tyson, P.D. (1997). Atmospheric circulation, vertical structure and transport over Southern Africa during the SAFARI-92 campaign. In B.W. van Wilgen, M.O. Andreae, J.G. Goldammer and J.A. Lindesay (Ed.), *Fire in Southern Africa Savannas: Ecological and Atmospheric Perspectives* (pp. 57-88). Johannesburg, South Africa: Witwatersrand University Press.

Generoso, S., Balkanski, F.-M., Boucher, O., & Schulz, M. (2003). Improving the seasonal cycle and interannual variations of biomass burning aerosol sources. *Atmospheric Chemistry and Physics*, *3*, 1211-1222.

Giglio, L., Kendall, J.D., & Justice, C.O. (1999). Evaluation of global fire detection algorithms using simulated AVHRR infrared data. *International Journal of Remote Sensing*, *20*, 1947-1985.

Giglio, L., Descloitres, J., Justice, C.O., & Kaufman, Y.J. (2003a). An enhanced contextual fire detection algorithm for MODIS. *Remote Sensing of Environment*, *87*, 273-282.

Giglio, L., Kendall, D., & Mack, R (2003b). A multi-year active fire dataset for the tropics derived from the TRMM VIRS. *International Journal of Remote Sensing*, *24*, 4505-4525.

Giglio, L., Csiszar, I., & Justice, C.O. (2006). Global distribution and seasonality of active fires as observed with the Terra and Aqua Moderate Resolution Imaging Spectroradiometer (MODIS) sensors. *Journal of Geophysical Research*, *111*, G02016. doi:10.1029/2005JG000142

Giglio, L. (2007). Characterization of the tropical diurnal fire cycle using VIRS and MODIS observations. *Remote Sensing of Environment*, *108*, 407-421.

Grégoire, J.-M., Cahoon, D.R., Stroppiana, D., Pinnock, S., Eva, H., Arino, O., Rosaz, J.M., & Csiszar, I. (2000). Forest fire monitoring and mapping for GOFC: current

products and information networks based on NOAA-AVHRR, ERS-ATSR and SPOT-VGT systems. *Forest Fire Monitoring and Mapping: A component of Global Observation of Forest Cover* (pp. 111-135), Ispra, Italy: Joint Research Centre.

Grégoire, J.-M., Tansey, K., & Silva, J.M.N. (2003). The GBA2000 initiative: Developing a global burned area database from SPOT-VEGETATION imagery. *International Journal of Remote Sensing, 24*, 1369-1376.

Hoffer, A., Gelencsér, A., Blazsó, M., Guyon, P., Artaxo, P., & Andreae, M.O. (2006). Diel and seasonal variations in the chemical composition of biomass burning aerosol. *Atmospheric Chemistry and Physics, 6*, 3505-3515.

Ito, A., & Penner, J.E. (2004). Global estimates of biomass burning emissions based on satellite imagery for the year 2000. *Journal of Geophysical Research, 109*, D14S05. doi:10.1029/2003JD004423

Ji, Y. (2005). Diurnal cycle and intra-seasonal variability of TRMM rainfall and fire products. *Geoscience and Remote Sensing Symposium, IGARSS '05, Proceeding 2005, IEEE International*, *Vol. 6.* (pp. 4127-4129).

Justice, C.O., Malingreau, J.P., & Setzer, A.W. (1993). Satellite remote sensing of fires: potential and limitations. In P.J. Crutzen and J.G. Goldammer (Ed.), *Fire in the Environment: the Ecological Atmospheric, and Climatic Importance of Vegetation Fires* (pp. 77-88). New York: J. Wiley & Sons.

Justice, C.O., & Dowty, P. (1994). The IGBP-DIS satellite fire detection algorithm workshop technical report. *IGBP-DIS Working Paper 9, NASA/GSFC, Greenbelt; Maryland; USA, February, 1993*.

Justice, C.O., & Malingreau, J.P. (1996). Report of the The IGBP-DIS fire algorithm workshop 2. *IGBP-DIS Working Paper 14, Ispra, Italy, October 1995*.

Justice, C.O., Giglio, L., Korontzi, S., Owens, J., Morisette, J.T., Roy, D., Descloitres, J., Alleaume, S., Petitcolin, F., & Kaufman, Y. (2002). The MODIS fire products. *Remote Sensing of Environment, 83*, 244-262.

Justice, C.O., Giglio, L., Boschetti, L., Toy, D., Csiszar, I., Morisette, J., & Kaufman, Y. (2006). MODIS fire products. *Algorithm Technical Background Document, Version 2.3, October 2006, EOS ID#2741* (pp. 34).

Kaufman, Y.L., Justice, C.O., Flynn, L., Kendall, J.D., Prins, E., Giglio, L., Ward, D.E, Menzel, W.P., & Setzer, A.W. (1998). Potential global fire monitoring from EOS-MODIS. *Journal of Geophysical Research, 103*, 215-238.

Kendall, J.D., Justice, C.O., Dowty, P.R., Elvidge, C.D., & Goldammer, J.G. (1997). Remote Sensing of Fires in Southern Africa During the SAFARI 1992 Campaign. In B. van Wilgen, M. Andreae, J. Goldammer and J.A. Lindesay (Ed.), *Fire in Southern African Savannas* (pp. 89-133). Johannesburg: Witwatersrand University Press.

Lacaux, J.-P., Cachier, H., & Delmas, R. (1993). Biomass burning in Africa: An overview of its impact on atmospheric chemistry. In P.J. Crutzen and J.G. Goldammer (Ed.), *Fire in the Environment: The Ecological, Atmospheric, and Climatic Importance of Vegetation Fires* (pp. 159-191). Chichester, England: J.Wiley & Sons.

Le Page, Y., Pereira, J.M.C., Trigo, R.M., DaCamara, C.C., Oom, D., & Mota, B. (2008). Global fire activity patterns (1996-2006) and climatic influence: an analysis using the World Fire Atlas. *Atmospheric Chemistry and Physics, 8*, 1911-1924.

Li., Z. and L. Giglio (2000) A review of AVHRR-based fire detection algorithms. In F. Ahern, J.-M. Grégoire, and C. Justice (Eds.), *Forest Fire Monitoring and Mapping: A Component of Global Observation of Forest Cover. European Commission EUR 19588*.

Malamud, B.D., Morein, G., & Turcotte, D. L. (1998). Forest fires: An example of selforganized critical behavior. *Science, 281*, 1840-1842.

Mota, B., Pereira, J.M.C., Oom, D., Vasconcelos, M.J.P., & Schultz, M. (2006). Screening the ESA ATSR-2 World Fire Atlas (1997-2002). *Atmospheric Chemistry and Physics, 6*, 1409-1424.

Pereira, J.M.C., & Govaerts, Y. (2001). Potential fire applications from MSG/SEVIRI observations. EUMETSAT Programme Development Department, Technical Memorandum No. 7.

Prins, E.M., & Menzel, W.P. (1992). Geostationary satellite detection of biomass burning in Southern America. *International Journal of Remote Sensing, 13*, 2783-2799.

Prins, E.M., & Menzel, W.P. (1994). Trends in South American biomass burning detected with the GOES VAS from 1983-1991. *Journal of Geophysical Research, 99*, 16719-16735.

Prins, E.M., & Schmetz, J. (2000). Diurnal active fire detection using a suite of international geostationary satellites. In F. Ahern, J.-M. Grégoire and C. Justice (ed.), *Forest Fire Monitoring and Mapping: A Component of Global Observation of Forest Cover European Commission Joint Research Centre*. (pp.139-148) EUR19588EN

Reed, W.J., & McKelvey, K. S. (2002). Power-law behavior and parametric models for the size-distribution of forest fires. *Ecological Modelling, 150*, 239-254.

Roberts, G., Wooster, M.J., Perry, G.L.W., Drake, N., Rebelo, L-M., & Dipotso, F. (2005). Retrieval of biomass combustion rates and totals from fire radiative power observations: application to southern Africa using geostationary SEVIRI Imagery. *Journal of Geophysical Research, 110*, D21111. doi: 10.1029/2005JD006018

Roberts, G., & Wooster, M.J. (2007). New perspectives on African biomass burning dynamics. *EOS, Transactions, American Geophysical Union, 88*, 369-370.

Roberts, G.J., & Wooster, M.J. (2008). Fire detection and fire characterization over Africa using Meteosat SEVIRI. *IEEE Transactions on Geoscience and Remote Sensing, 46*, 1200-1218.

Rosenfeld, D. (1999). TRMM observed first direct evidence of smoke from forest fires inhibiting rainfall. *Geophysical Research Letters, 26*, 3105-3108.

Saunders, R.W., & Kriebel, K.T. (1988). An improved method for detecting clear sky and cloud radiances from AVHRR data. *International Journal of Remote Sensing, 9*, 123-150.

Schmetz, J., Pili, P., Tjemkes, S., Just, D., Kerkmann, J., Rota, S., & Ratier, A. (2002). An introduction to Meteosat Second Generation (MSG). *Bulletin of the American Meteorological Society, 83*, 977–992. doi:10.1175/1520-0477(2002)083

Scholes, R.J. (1997). Savanna. In R.M. Cowling, D.M. Richardson and S.M. Pierce (Ed.), *Vegetation of Southern Africa* (pp. 258-277). Cambridge: Cambridge University Press.

Schultz, M.G. (2002). On the use of ATSR fire count data to estimate the seasonal and interannual variability of vegetation fire emissions. *Atmospheric Chemistry and Physics, 2*, 387-395.

Schultz, M.G., Heil, A., Hoelzemann, J.J., Spessa, A., Thonicke, K., Goldammer, J.G., Held, A.C., Pereira, J.M.C., & Bolscher, M. van het (2008). Global wildland fire emissions from 1960 to 2000. *Global Biogeochemical Cycles, 22*, GB2002. doi:10.1029/2007GB003031

Silva, J.M.N., Pereira, J.M.C., Cabral, A.I., Sá, A.C.L., Vasconcelos, M.J.P., Mota, B., & Grégoire, J.-M. (2003). An estimate of area burned in Southern Africa during the 2000 dry season using SPOT-VEGETATION satellite data. *Journal of Geophysical Research, 108*. doi:10.1029/2002JD002320

Smirnov, A., Holben, B.N., Eck, T.F., Slutsker, I., Chatenet, B., & Pinker, R.T. (2002). Diurnal variability of aerosol optical depth observed at AERONET (Aerosol Robotic Network) sites. *Geophysical Research Letters, 29*. doi:10.1029/2002GL016305

Stroppiana, D., Pinnock, S., & Grégoire, J.-M. (2000). The global fire product: daily fire occurrence from April 1992 to December 1993 derived from NOAA AVHRR data. *International Journal of Remote Sensing, 21*, 1279-1288.

Tansey, K.J., Grégoire, J.-M., Stroppiana, D., Sousa, A., Silva, J., Pereira, J.M.C., Boschetti, L., Maggi, M., Brivio, P., Fraser, R., Flasse, S., Ershov, D., Binaghi, E., Graetz, D., & Peduzzi, P. (2004a). Vegetation burning in the year 2000: global burned area estimates from SPOT VEGETATION data. *Journal of Geophysical Research, - Atmospheres, 109*. doi:10.1029/2003JD003598

Tansey, K., Grégoire, J-M., Binaghi, E., Boschetti, L., Brivio, P.A., Ershov, D., Flasse, S., Fraser, R., Graetz, D., Maggi, M., Peduzzi, P., Pereira, J.M.C., Silva, J., Sousa, A., & Stroppiana, D. (2004b). A global inventory of burned areas at 1 km resolution for the year 2000 derived from SPOT VEGETATION data. *Climatic Change, 67*, 345–377.

van Wilgen, B.W., & Scholes, R.J. (1997). The vegetation and fire regimes of Southern-hemisphere Africa. In BW van Wilgen, MO Andreae, JG Goldammer, and JA Lindesay (Ed.), *Fire in Southern African Savannas: Ecological and Atmospheric Perspectives* (pp. 27-46). Johannesburg, South Africa: Witwatersrand University Press.

White, F. (1983). The vegetation of Africa, a descriptive memoir to accompany the UNESCO/AETFAT/UNSO vegetation map of Africa. *Natural resources research Report XX*. UNESCO 356 pp.

CHAPTER 3: Using Meteosat-8 imagery to investigate the role of meteorological factors on fire activity in Mediterranean Europe

Malik Amraoui[a,b], Margarida L.R. Liberato[a,b], Teresa J. Calado[b,c], Carlos C. DaCamara[b], Luís Pinto Coelho[c] and Ricardo M. Trigo[b]

[a] School of Sciences and Technology, University of Trás-os-Montes e Alto Douro (UTAD), Vila Real, Portugal

[b] University of Lisbon, Instituto Dom Luiz (IDL), Lisbon, Portugal

[c] Instituto de Meteorologia, Lisbon, Portugal.

This Chapter has been submitted to Agricultural and Forest Meteorology in July 2010.

Abstract

Mediterranean regions are some of the most affected by wildfires and information about fire activity, as provided by the SEVIRI instrument on-board Meteosat-8, appears especially appealing to monitor and investigate fire activity. An analysis is accordingly performed on the spatial distribution of fire events during the period of July and August 2007-2009. Around half of fire pixels were detected in croplands, the remaining half being evenly distributed between forest and shrub as opposed to the distribution of persistent fire events (more than 10 h of duration) where 90% occurred in forests and shrublands, evenly distributed among these two classes. With almost half of the fire events and the most severe episodes, the year of 2007 is the most serious, allowing an assessment of the role of meteorological conditions on large fire events by studying two extreme events, respectively on July 24-25 and August 22-27. Structural similarities were found between the two episodes and a conceptual model is proposed for meteorological conditions strongly favouring the occurrence of severe wildfire episodes in Italy and the Balkan Peninsula. On the one hand there is, at the surface, strong northerly advection of very hot and very dry air over the region, as steered by the presence of a ridge over central Europe together with a thermal depression over southwest Asia. On the other hand, the advected air is further heated by adiabatic compression associated to strong subsidence from around 700 up to 250 hPa, associated to the presence of a ridge over the Eastern Mediterranean and to the anomalous displacement of the jet streak towards the northwest. The importance of both short- and long-term atmospheric conditions on meteorological fire risk is also put into evidence by analysing the fields of three weather-based indices, namely the Build-Up Index, the Initial Spread Index and the Fire Weather Index that are part of the Canadian Forest Fire Weather Index System. The uncovered relationships of fire activity and fire persistence with landcover types as well as with atmospheric circulation and meteorological risk strongly suggest using Meteosat-8/SEVIRI data on fire activity to generate statistically calibrated maps of fire risk in Mediterranean Europe.

Keywords: Fire activity, Mediterranean Europe, Fire Meteorology, FWI, Meteosat-8, Fire risk.

I. Introduction

Fire is a prominent global phenomenon (Le Page *et al.*, 2008) and wildfires are critical elements in the Earth system, linking climate, human activity, and vegetation (Ichoku *et al.*, 2003). With 200-500 Mha burnt annually, fire disturbs a larger area over a wider variety of biomes across the globe than any other natural disturbance to land-based eco-systems (Lavorel, *et al.*, 2007; Ichoku *et al.*, 2008).

At the regional level, Southern Europe occupies a prominent position, given the occurrence of devastating summertime wildfires that burn hundreds of thousands of hectares of forests, shrublands and grasslands every year, causing extensive economical and ecological losses and often human casualties (Pereira, 1999). The Mediterranean basin is also considered a "hot spot" for climate change studies, not only because of its high sensitivity to changes in recent decades (IPCC, 2007) but also for the reason that according to the majority of models the most likely evolution of this region is towards a hotter and drier climate, with a significant higher risk of intense heatwave episodes (Fisher and Schär 2010).

The rainy and mild winters followed by warm and dry summers make the region especially prone to the occurrence of a large number of fire events and to the onset of extreme episodes that determine per se the total amount of burned area in a whole fire season (Pereira *et al.*, 2005; Pyne, 2006; Ventura and Vasconcelos, 2006). It is therefore not surprising that the largest numbers of fires and amounts of burnt area in Europe are found in southern European countries, namely in Portugal, Spain, France, Italy, Greece and Croatia (Pereira *et al.*, 2006; Barbosa *et al.*, 2007). Besides, it is worth stressing that the relevance of wildfires as an environmental crisis in Mediterranean countries arises from a combination of natural factors (*e.g.* vegetation stress, topography, weather and climate) with a long history of human management practices in natural environments that favour anthropogenic ignitions (Chuvieco *et al.*, 1997; Viegas *et al.*, 1999; Trigo *et al.*, 2006; Benson *et al.*, 2009; Rasilla *et al.*, 2010). For instance, in the Mediterranean and South-eastern European countries, the recent structural and demographic changes have led to an increase of fire hazard, resulting in about 300,000 to 500,000 ha of forests and other wooded land burnt every year in the region (DG JRC 2006; Dimitrakopulos and Mitsopoulos, 2006; Nikolov, 2006).

Weather and climate have nevertheless a profound influence on wildland fire ignition, fire behaviour, and fire severity (Benson *et al.*, 2009). The vast majority of burned area in Southern Europe is in fact concentrated into a reduced number of extreme events that occur during a short period of time, and are associated to several atmospheric mechanisms, working at different temporal and spatial scales (Pereira *et al.*, 2005). For instance, at the regional scale and at the seasonal or inter-annual time scales, severe droughts at the beginning of the fire season (late spring and early summer) inevitably lead to high levels of vegetation stress increasing the flammability of live and dead

fuels. At the local and daily scales, extreme weather conditions, including wind, atmospheric stability, fuel moisture, and relative humidity during the fire season promote the ignition and spread of wildfires (Pereira *et al.*, 2005; Trigo *et al.*, 2006; Rasilla *et al.*, 2010).

In the last forty years, a great deal of effort has been spent by the scientific community to investigate the potential linkages between synoptic-, meso-, and local-scale weather and wildfire activity. Brotak and Reifsnyder (1977) studied the upper air conditions associated to 52 major wildland fires in the eastern United States from 1963 to 1973 and found the fires occurred to be related to frontal passages that were associated with a trough at the 500 hPa surface. More recently, based on the analysis of the improved spatial and temporal resolution of the Canadian Large Fire Database, in conjunction with monthly 500 hPa height data over a northern North American region, Skinner *et al.* (2002) uncovered a statistically significant positive correlation between atmospheric circulation anomalies in the mid-troposphere and monthly burnt area in Canada. Using the amalgamated dataset of wildfire and burned area from the U.S. Department of the Interior's Bureau of Land Management (BLM), U.S. Department of Agriculture's Forest Service (USFS), National Park Service (NPS) and Bureau of Indian Affairs (BIA) for the western United States, Westerling *et al.* (2003) established links between antecedent moisture anomalies and anomalous summer wildfire activity which varied both regionally and temporally. Westerling *et al.* (2004) studied the outstanding 2003 fire season in California and highlighted the crucial role played by large-scale atmospheric circulation patterns, further exacerbated by configurations of local winds. Pereira *et al.* (2005) used the fire data set, between 1980 and 2000, from the Portuguese Forest Service, to describe the spatial and temporal variability of wildfire characteristics over continental Portugal. The authors have shown that the most severe wildfire episodes were related to a typical atmospheric circulation pattern dominated by a strong ridge located over the Iberian Peninsula. The devastating 2003 fire season in Portugal was investigated by Trigo *et al.* (2006) who pointed out that the days with highest amounts of burned area were characterized by large anomalies in the daily surface maximum and minimum temperatures, relative humidity, and wind speed and direction. The authors further remarked that the 2003 fire season was preceded by a wet winter followed by a very dry month of May. Rasilla *et al.* (2010) analyzed the atmospheric conditions associated with the occurrence of very large wildfires in Spain. Their results emphasize the need to combine short- and long-term climate variability to explain the occurrence of episodes of very large wildfires. Using the daily burnt area in Portugal as the parameter to be correlated with atmospheric fields provided by the European Centre for Medium-Range Weather Forecasts Reanalysis (ECMWF) data, Hoinka *et al.* (2009), concluded that the cross-covariance regression between the Iberian thermal low and burnt area showed that the peak amount of burnt area occurred up to three days after the appearance of a thermal low. Good *et al.* (2008) have investigated the meteorological conditions associated to fire risk in Italy and Greece, paying special attention to the long- and short-time scale components involved, as derived from a weather-based index of fire risk.

Detection of fire activity has long been identified as a task with great potential to be derived either from polar-orbiters (Giglio *et al.*, 1999; 2003) and geostationary satellites (Prins and Menzel, 1992; Calle *et al.*, 2006) and, since the last decade of the 20th century, more and more sophisticated fire detection algorithms have been successively developed. Because of their capacity to provide data at sub-hourly resolution, even data from earlier geostationary satellites have proven to be adequate to study fire activity at the continental (Prins and Menzel, 1994) and the global scales (Prins and Schmetz, 2000). The launch in 2002, by the European Space Agency (ESA) in cooperation with the European Organization for the Exploitation of Meteorological Satellites (EUMETSAT), of Meteosat-8, the first geostationary satellite of the Meteosat Second Generation (MSG) opened up new perspectives in active fire monitoring (Cihlar *et al.*, 1999; Pereira and Govaerts, 2001) thanks to the improved characteristics in the temporal (one image every 15 minutes), the spatial (a sampling distance of 3 km at the sub-satellite point) and the spectral (12 channels) domains provided by the Spinning Enhanced Visible and Infrared Imager (SEVIRI), the main payload of the MSG series (Schmetz *et al.*, 2002). The potential of Metosat-8 was in fact promptly explored, namely with the goal of studying the spatial distribution and the temporal organization of fire activity in the African continent, (Amraoui *et al.*, 2010) as well as of quantifying the respective fire intensity and biomass consumption (Roberts *et al.*, 2005; Roberts and Wooster, 2008).

In the above described context, information about fire activity, as provided by the SEVIRI instrument on-board Meteosat-8, appears as an especially adequate tool to monitor fire activity over Europe. The aim of the present study is to assess the potential of Meteosat-8 imagery to investigate the role of meteorological factors on fire activity in Mediterranean Europe. Based on information provided by Meteosat-8 covering the period of July and August 2007-2009, the spatial distribution of fire events is analysed and the number and persistence of fire events is related to the types of land cover affected. Special attention is then devoted to two extreme events of fire activity, respectively on July 24-25 and August 22-27, 2007 that stroke Italy and the Balkan Peninsula. The role of meteorological factors in the two periods is investigated by analysing composites of meteorological fields as well as vertical profiles of meteorological variables. Finally, the impact of long- and short-term meteorological components is assessed by analysing the associated meteorological fire risk based on weather-based indices of fire risk.

II. Data and methods

II.1. Fire activity

Information about fire events was derived from the so-called Fire Detection and Monitoring (FD&M) product that is currently running, in near real time, in the framework of EUMETSAT's Satellite Application Facility on Land Surface Analysis (LSA SAF) whose main scope is to take full advantage of remotely sensed data to support land, land-atmosphere interactions and biosphere applications with a strong emphasis on developing and implementing algorithms that will allow an operational use of data from EUMETSAT satellites (Trigo *et al.*, 2010). Identification of active fires relies on a contextual fire detection algorithm (FiDAlgo) that was specifically designed to process data provided by Meteosat-8/SEVIRI. The algorithm takes advantage of the 15-minute temporal resolution of SEVIRI and makes use of information from several SEVIRI channels (namely 0.6, 0.8, 3.9, 10.8 and 12.0 μm) together with information on illumination and viewing angles. The method is based on heritage from contextual algorithms designed for polar, sun-synchronous instruments, namely NOAA/AVHRR and MODIS/TERRA-AQUA. A potential fire pixel is compared with the neighbouring ones and the decision is made based on relative thresholds as derived from the pixels in the neighbourhood. A full description of the algorithm is given by Amraoui *et al.* (2010).

The FiDAlgo algorithm allows detecting both fire pixels and active fires which are defined as follows:

- fire pixels are those where at least one active fire was detected by the FiDAlgo algorithm;
- active fires are given by the number of fire occurrences continuously detected in a given fire pixel. Active fires may be viewed as an indicator of persistence (and therefore of severity) of a given fire event.

The algorithm (for Europe) is applied over a fixed window defined within the Meteosat disk, which is represented in Figure 3.1 together with information about land cover. Four types of land cover were assigned to each Meteosat-8 pixel by degrading to the Meteosat disk resolution the so-called Global Land Cover (GLC) 2000, a widely used dataset (Bartholomé & Belward, 2005);

- forest, which correspond to GLC2000 classes 1, 2, 3, 4 and 6, and represents 30% of land pixels,
- shrubland, which correspond to GLC2000 classes 11, 12, 13, 14 and 15, and represents 23% of land pixels;
- cropland, which correspond to GLC2000 classes 16, 17 and 18, and represents 40% of land pixels;
- other types (bare areas, snow and ice, and artificial surfaces),which represent the remaining 7% of land pixels, were masked because of the inexistence of fire activity.

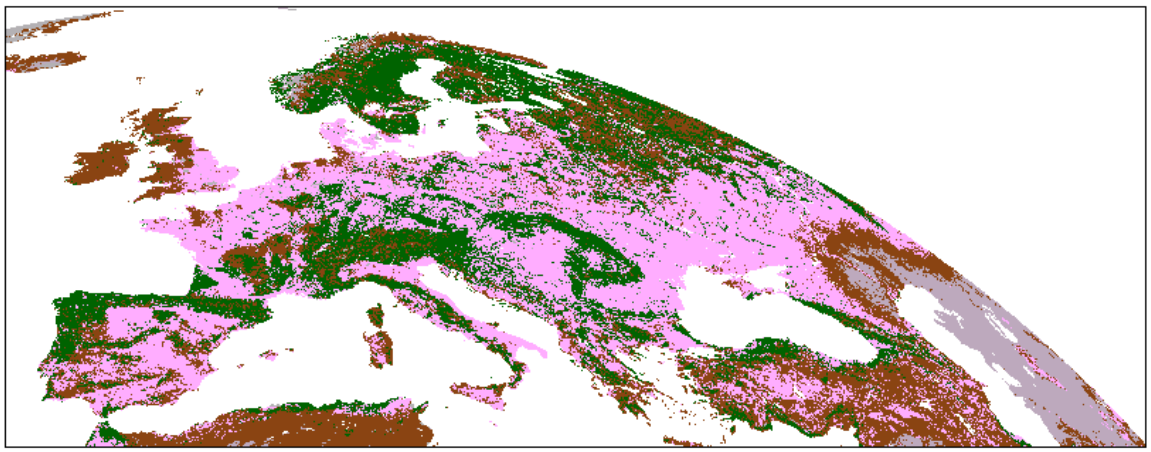

Figure 3.1. GLC2000-based land cover types over the European window; forest (green), shrubland (brown), cropland (pinkish) and other (grey).

II.2. Meteorological parameters

Meteorological data consist of horizontal fields, as well as of vertical profiles. The latter consist of soundings of temperature, dew point temperature and wind, and were obtained from the Department of Atmospheric Science of the University of Wyoming (http://www.uwyo.edu). Data extracted respect to July 25, 2007 (12 UTC) at the station of Belgrade (Serbia) and to August 25, 2007 (00 UTC) at Athens (Greece).

Horizontal fields consist of Interim Reanalyses (ERA-Interim) as obtained from the ECMWF. ERA-Interim is the latest ECMWF global atmospheric reanalysis available since 1989 up to the present (Dee and Uppala, 2009; Berrisford *et al.*, 2009). The following meteorological variables were extracted, at 12 UTC, over the European sector (12°W-55°E, 24°N-57°N) for July and August 1989-2009, and then projected onto a 0.75×0.75 latitude/longitude grid;

- mean Sea Level pressure (hereafter SLP);
- air temperature at 2 metres height (hereafter T2);
- dew point temperature at 2 meters height (hereafter Td2);
- 24 hours accumulated precipitation (hereafter P24);
- zonal and meridional wind components at 10 metres and respective wind speed (hereafter U10);
- 250, 500 and 850 hPa geopotential height (hereafter Z250, Z500 and Z850);
- temperature and relative humidity at 850hPa (hereafter T850 and RH850);
- wind speed at 250 hPa (hereafter U250).

Composites of the above-mentioned meteorological variables will be computed for short selected periods, and consist of arithmetic means (over the periods) of the considered 12 UTC fields, as well as of the respective anomalies. It may be noted that daily anomalies are defined as departures of the considered field (for a given day of July-August 2007) from the reference field (for that day), which is given by the average of the field for the same day over the reference period of 1989-2009. The seasonal cycle of the considered meteorological variables was therefore removed when computing the respective anomaly fields.

II.3. Fire risk

Atmospheric conditions favouring the onset and spreading of large wildfires may in fact be assessed by means of weather-based indices that rely on meteorological variables, alone or combined with vegetation and topographical information. Several fire risk indices have been developed which are used around the world. An early example is the Nesterov Index, initially developed for use in the former Soviet Union and based on fuel inflammability, mean and dew point temperatures, and daily precipitation (Nesterov, 1949; Shetinsky, 1994). Other indices include the McArthur Forest Fire Danger Index (FFDI) (McArthur, 1967) used in the eastern parts of Australia, the Forest Fire Behaviour Tables (FFBT) (Sneeuwjagt and Peet, 1998), developed for use in Western Australia, and the National Fire Danger Rating System (Deeming *et al.*, 1977) used in the USA.

Although, originally developed for use in the boreal forests of Canada, the Canadian Forest Fire Weather Index System (CFFWIS) (van Wagner, 1987) has been widely adapted for operational use (Viegas *et al.*, 1999; 2001; 2004; Raínha and Fernandes, 2002; Cruz and Plucinski, 2007; Good *et al.*, 2008) and is the basis for a global fire weather index (de Groot *et al.* 2006). CFFWIS is also a reference index for producing fire risk maps at the European Union level by the Joint Research Centre (JRC). CFFWIS consists of six components that account for the effects of fuel moisture and wind on fire behaviour. The first three components, *i.e.* the Fine Fuel Moisture Code (FFMC), the Duff Moisture Code (DMC) and the Drought Code (DC) respectively rate the average moisture content of surface litter, decomposing litter, and organic (humus) layers of the soil. Wind effects are then added to FFMC leading to the Initial Spread Index (ISI) that rates fire spread. The remaining two fuel moisture codes (DMC and DC) are in turn combined to produce the Build-Up Index (BUI) that is a rating of the total amount of fuel available for combustion. BUI is finally combined with ISI to produce the Fire Weather Index (FWI) and the Daily Severity Rating (DSR) that respectively rate fire intensity and the difficulty of controlling fires. Further details may be found in van Wagner (1987) and at http://cfs.nrcan.gc.ca/.

ERA-Interim reanalysis data, namely T2, Td2, U10 and P24 were used to compute BUI, ISI and FWI at 12 UTC for the period 1989-2009. As pointed out by Good *et al.* (2008), FWI may be viewed as a function of two quantities, namely ISI which has a timescale of the order of a day and of the so-called duff moisture function that is a non-linear function of BUI and has a timescale of the order of two weeks up to 50 days. Choice of BUI, ISI and FWI was in fact motivated by the aim of qualitatively assessing, for different situations, the contribution of short- and long-term meteorological components to meteorological fire risk.

III. Results

III.1. Fire activity over Europe

Figure 3.2 presents, for each July-August period of 2007, 2008 and 2009, the spatial distribution of fire pixels together with the respective persistence (in hours). Table 3.1 presents the number of active fires, the number of fire pixels and the ratio of former to the latter as detected over southern Europe for each July-August period; the respective grand totals for the three periods of 2007-2009 are also given in the rightmost column.

It may be observed that during the three considered periods, a grand total of 59 848 active fires were detected, distributed over 10 404 fire pixels. Almost half of the total number of active fires was detected in July-August 2007, distributed over 40% of all fire pixels. In fact, this year was characterized by extreme fire activity in northern Africa (Algeria) and southern Europe, especially in Italy, the Balkans, around the Black Sea; Moldavia, Ukraine and South Russia. The year of 2008 was characterized by low fire activity over Mediterranean Europe (with the exception of Italy) with 18% of the total number of active fires detected in this period, distributed over 31% of the fire pixels. In the above-mentioned period, extreme fire activity has occurred in Eastern Europe, especially in Romania, Bulgaria and Ukraine. It may be noted that 30% of active fires were detected in July-August 2009, distributed over 29% of fire pixels, mostly located in the north-western Iberia (Northern Portugal and Galicia) as well as in countries around the Black Sea. The extremely severe fire episodes that occurred close to Athens in August 22-24, 2009 are also conspicuous in Figure 3.2.

There are contrasts in fire activity among the individual years that are worth being noted. For instance, although the number of fire pixels in 2008 and 2009 is very similar (around three thousand) the total amount of active fire is much larger in 2009, indicating the existence of severe episodes in the latter period, which were observed at the end of August 2009 in the northwest of the Iberian Peninsula (Northern Portugal and Galicia) and east of Athens. The ratio of active fires to fire pixels is in fact about 6 in 2009, *i.e.*

the double of the ratio observed in 2008. The year 2007 is the one having the largest number of active fires and fire pixels as well as the largest ratio of active fires to fire pixels that is about 7.6.

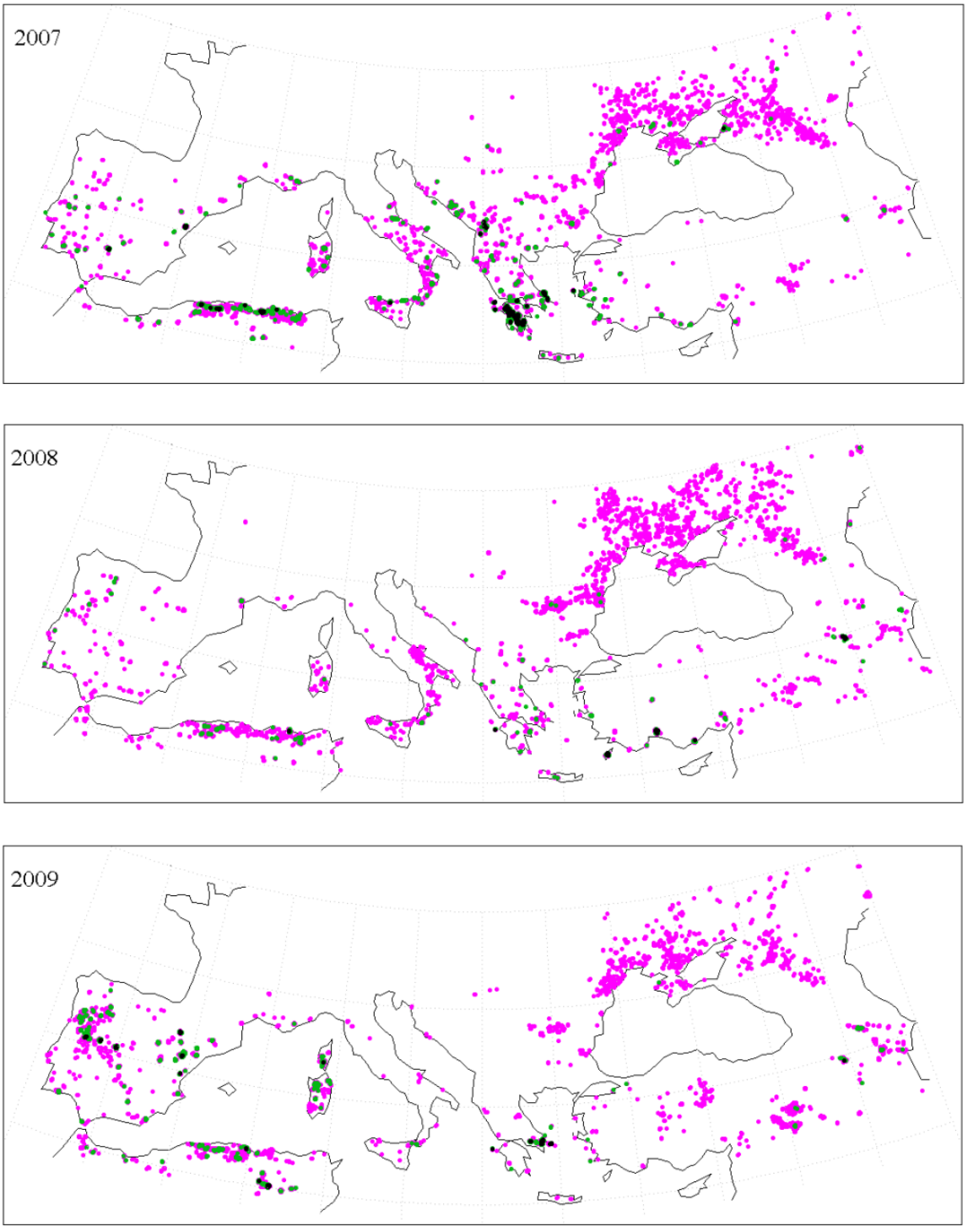

Figure 3.2. Fire pixels over Southern Europe during July-August of 2007 (upper panel), 2008 (middle panel) and 2009 (lower panel). Persistence of fires is indicated by the colour of the pixel; less than 2 hours (magenta), 2-10 hours (green), above 10 h (black).

Tables 3.2 and 3.3 present the distribution of total number of fire pixels and persistence in time of active fires among the three relevant GLC2000 land cover classes. The contrast between the distribution per class of number of fire pixels and the persistence of active fires is worth being noted. Around half of fire pixels were detected in croplands, the remaining half being evenly distributed between forests and shrublands (Table 3.2). If the distribution of the less persistent active fires (Table 3.3, left column) is relatively similar to the one of fire pixels (Table 3.2, right column), there is however a strong contrast in the case of the more persistent fires (Table 3.3, right column) since 90% of them occurred in forests and shrublands, roughly evenly distributed among these two classes. These results imply that fire events are most common but less persistent in croplands, whereas in forest and shrub the events are less frequent but more severe.

Table 3.1. Active fires, fire pixels and ratio of active fires to fire pixels as detected over Europe during July-August 2007, 2008 and 2009.

	2007	2008	2009	2007-2009
Active fires	31772	10497	17579	59848
Fire pixels	4195	3233	2976	10404
Ratio	7.6	3.2	5.9	5.8

Table 3.2. Distribution of fire pixels among the different GLC2000 land cover groups for Europe, during July-August 2007 to 2009.

	2007		2008		2009		2007-2009	
	Fire pixels	%	Fire pixels	%	Fire pixels	%	Fire pixels	%
Forest	1331	32	577	18	767	26	2675	26
Shrublands	1072	25	593	18	855	29	2520	24
Croplands	1792	43	2063	64	1354	45	5209	50
Total	4195	100	3233	100	2976	100	10404	100

Table 3.3. As in Table 3.2 but respecting to persistence (in hours) of active fires.

	Persistence of active fires					
	< 2 h		2-10 h		> 10 h	
Class	Fire pixels	%	Fire pixels	%	Fire pixels	%
Forest	1889	20	662	46	119	44
Shrublands	2818	29	551	39	126	47
Croplands	4963	51	219	15	26	9
Total	9670	100	1432	100	271	100

III.2. Analysis of two extreme fire events

The year of 2007 was characterised by warmer-than-average conditions covering most of Europe, including Southern Europe and the Middle East. Surface air temperature anomalies were one to two degrees above the 1961-90 average over most of the continent and according to Luterbacher *et al.* (2007) the winter of 2006-07 was extremely likely the warmest for more than 500 years, temperature anomalies in January having reached more than 11ºC in far eastern Europe. The annual average land surface temperature, as derived from the Climate Research Unit dataset (Brohan *et al.*, 2006) was 1.23±0.08ºC for the European region between 35º-75ºN and 10ºW-30ºE and it is virtually certain that 2007 is one of the five warmest years in the 1850-2007 series (Obregón *et al.*, 2008). During this period, a number of heat waves hit the south-eastern Europe, leading to extremely high temperatures and very low air humidity. For instance, the summer of 2007 ranks as the warmest summer according to the National Observatory of Athens' instrumental history; the maximum temperature has exceeded the 1961-90 mean by 3.3°C (an excess of up to 3.7 standard deviations). These unprecedented extreme conditions have triggered numerous excess deaths in several countries (Hungary, Romania, Bulgaria etc) and originated serious problems in electricity supply in many regions (Founda and Giannakopoulos, 2009). It may be finally noted that the total precipitation for the year 2007 was below average in most of Mediterranean Europe, especially in south-eastern Europe and the Middle East, where precipitation totals were less than 80% of the average (Rudolf *et al.*, 2005).

As pointed out in the previous section July-August 2007 is also the one with the largest number of fire pixels and of active fires. This is especially apparent over Greece where 1 035 fire pixels out of a grand total of 1 311 in 2007-2009 (*i.e.* 79%) occurred in 2007 and where 13 010 active fires out of 15 893 (*i.e.* 82%) occurred in the same year. In the case of Italy, the period of July-August 2007 also dominates the three-year period of 2007-2009, with 436 fire pixels out of 763 (*i.e.* 57%) and 1 551 active fires out of 2 186 (*i.e.* 71%) also occurred during July-August 2007.

Figures 3.3 and 3.4 respectively present time series of daily amounts and the spatial distribution of fire pixels during July-August 2007 over Greece and Italy. Fire activity concentrates into two periods, namely July 24-25 and August 22-27, the first one mainly respecting to Italy and the second one to both Italy and Greece. It may be noted that, in Italy, 30% of fire pixels (129 out of 436) and 36% of active fires (552 out of 1 551) occur in the extremely short first period of July 24-25. Similar amounts occur in the second period of August 22-27, namely 32% of fire pixels (138 out of 436) and 36% of active fires (566 out of 1 551) whereas, in Greece, the impressive amounts of 76% of fire pixels (783 out of 1 035) and 87% active fires (11 263 out of 13 010) were observed in the latter 6-day period.

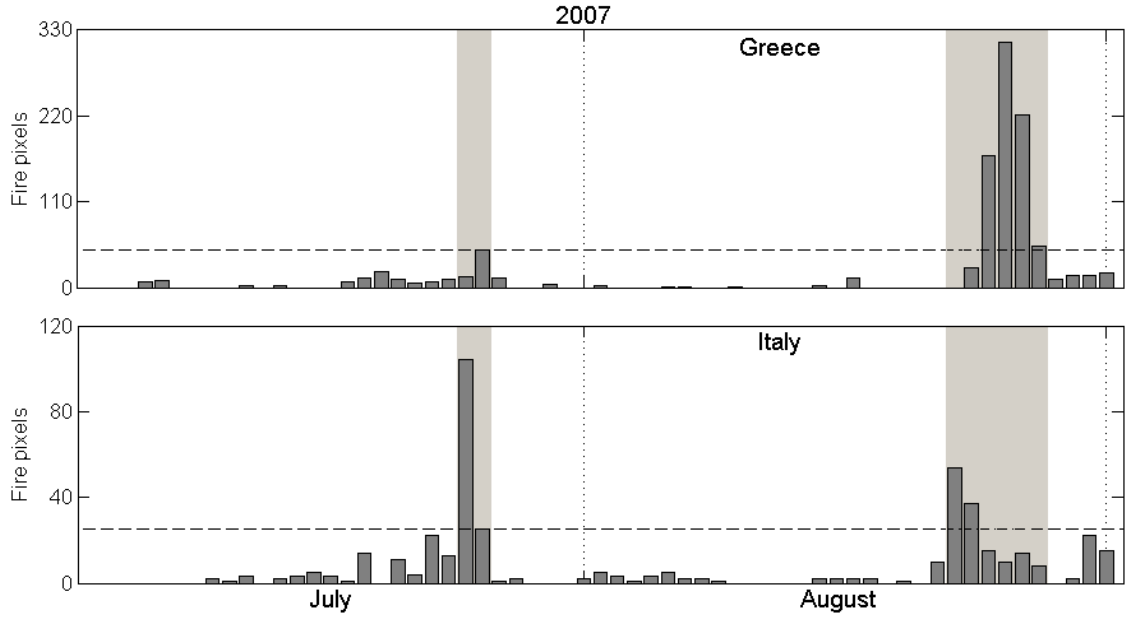

Figure 3.3. Time series of daily amounts of fire pixels during July-August 2007 for Greece (top panel) and Italy (bottom panel). Dashed lines in each region identify the 95th percentiles of fire pixels for July-August of 2007-2009. The two periods of extreme fire activity are shaded.

III.2.1. The episode of July, 24-25

Composites and corresponding anomalies of multiple low, mid and upper atmospheric fields associated with the episode of July 24-25, 2007 are shown in Figure 3.5. During the considered period the synoptic conditions that prevailed are characterized by the Azores high extending from the Atlantic to Central and Eastern Europe and by the location of a thermal low centred on southern Turkey and eastern Mediterranean. The surface conditions associated may be inferred from composites (12 UTC averages) and composite anomalies of sea-level pressure and surface air temperature (Figure 3.5a). The dynamical field associated to the ridge and the thermal low is responsible for the strong northerly advection of continental dry and hot air resulting in high surface air temperatures (over 30˚C) over the Mediterranean basin and by the extreme temperature anomalies (exceeding 8˚C both on T2 and on T850) that may be observed over some regions of Greece, Romania, Bulgaria and Turkey.

The overall configuration of the height field at 850 hPa is similar to the one of sea-level pressure but the gradients of Z850 (Figure 3.5b) tend to be stronger than those of SLP. Relative humidity composites at the same level (Figure 3.5b) clearly indicate the presence of very dry air (RH850 lower than 30%) over the entire Mediterranean basin and the Middle East, with anomalies greater than 25% on a large region extending from southern Italy and Greece up to the Black Sea basin. It is worth stressing that this region

of high temperature and low relative humidity closely matches the identified regions of extreme fire activity (Figure 3.4).

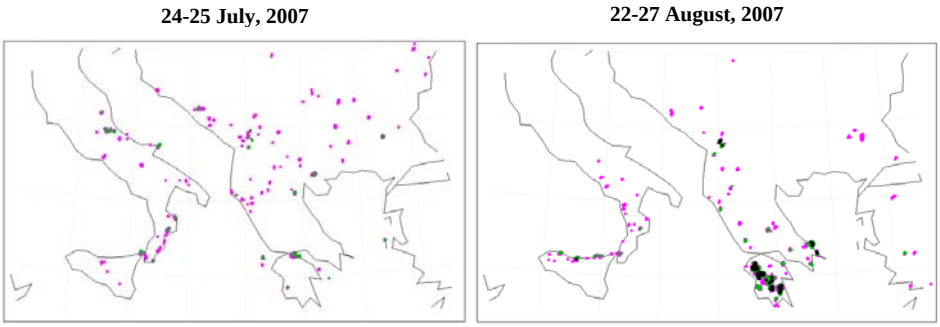

Figure 3.4. As in Figure 3.2 but respecting to Italy and the Balkan Peninsula during the two selected extreme events in 2007, *i.e.* July 24-25 (left panel) and August 22-27 (right panel).

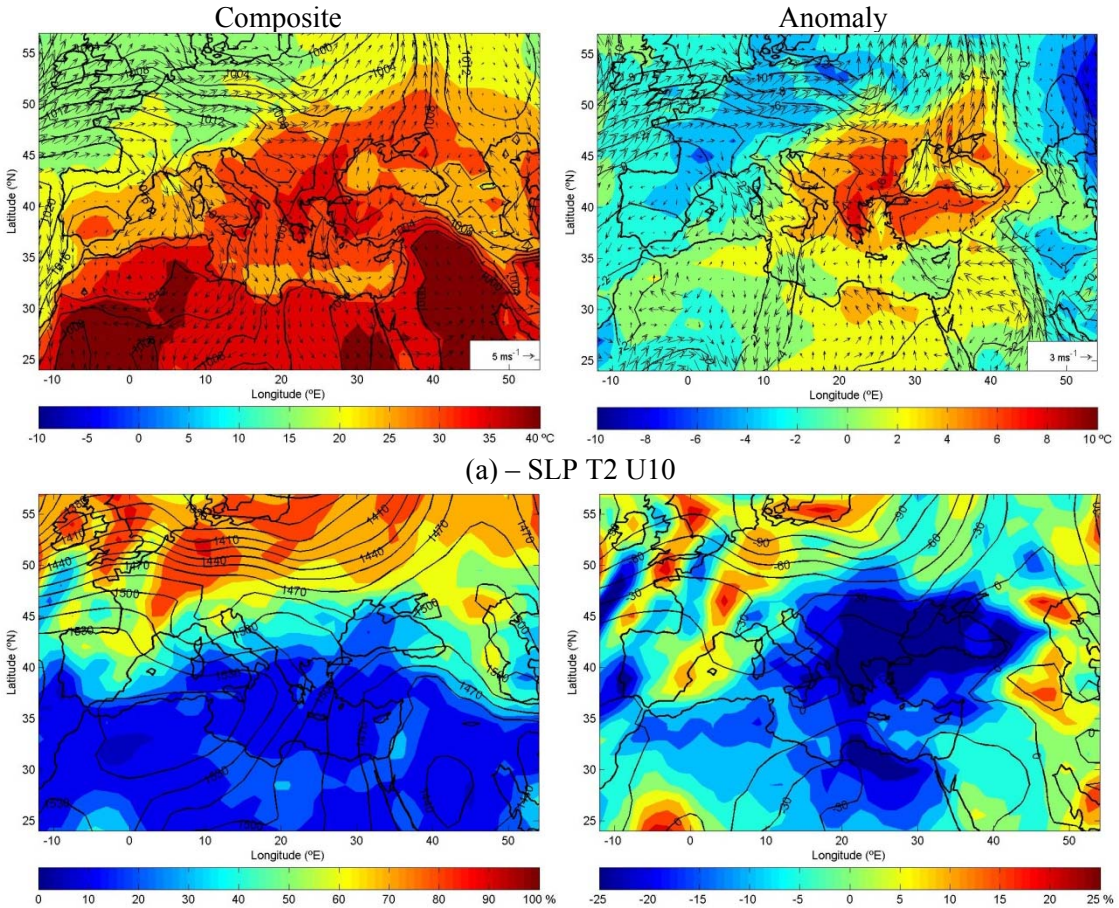

Figure 3.5. Colour patterns represent composites (left panels) and corresponding anomalies (right panels), of fields of (a) air temperature (°C) at 2 m (T2) with wind vectors at 10 m, (b) relative humidity (%) at 850 hPa (RH850), (c) air temperature (°C) at 850hPa (T850) and (d) wind speed (ms^{-1}) at 250hPa, for the period July 24 to 25, 2007. Contour lines show the corresponding (a) Sea Level Pressure (SLP) and geopotential height (gpm) at (b) 850 hPa, (c) 500 hPa and (d) 250 hPa.

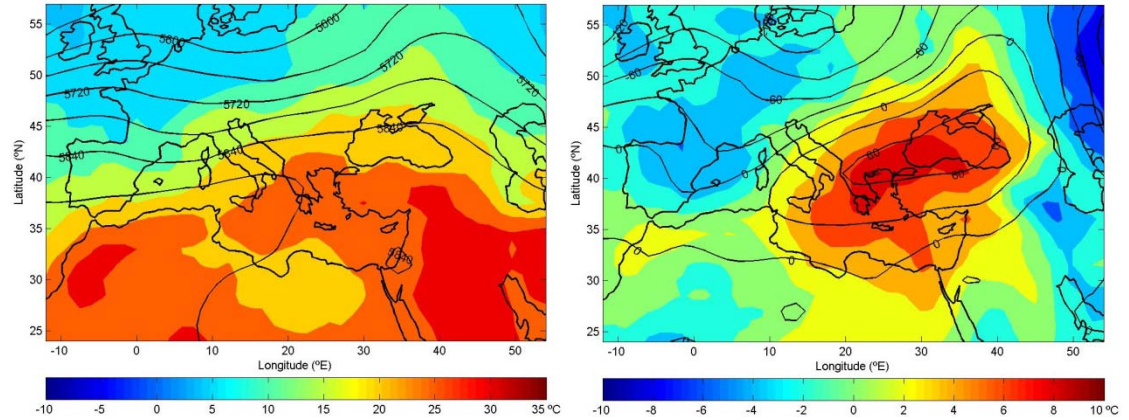

(c) – Z500 T850

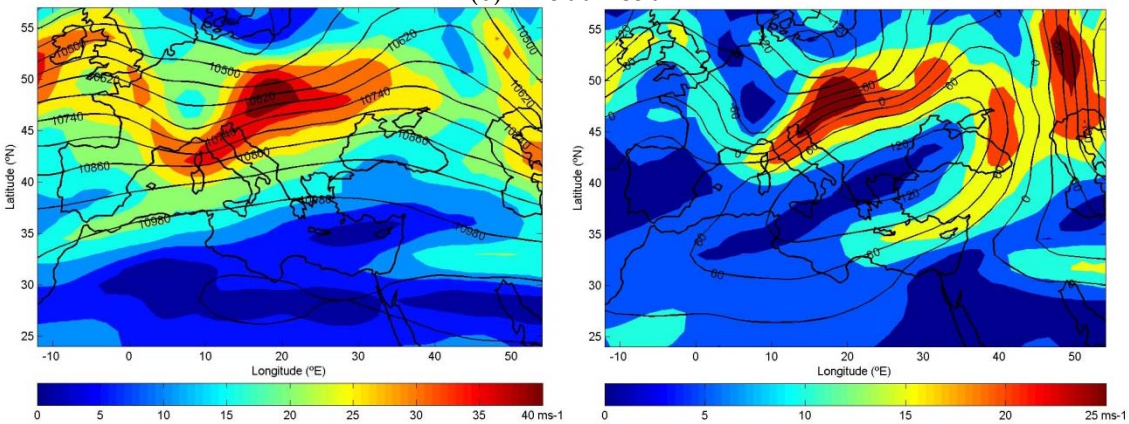

(d) – Z250 U250

Figure 3.5. Continued

The atmospheric flow at the 500 and 250 hPa levels is dominated by a synoptic baroclinic wave, with a pronounced ridge whose axis is directed from SW to NE (Figures 3.5c and 3.5d, left panels). The meandering of the jet stream is clearly reflected in the wind field at the 250 hPa level and it is worth noting that during the considered two-day period the jet stream axis is located over Central Europe, at abnormally high latitudes as suggested by the anomaly composites in Figure 3.5d (right panel). It is also worth noting that the patterns of composite anomalies at the 500 and 250 hPa levels (Figure 3.5c and 3.5d, right panels) exhibit positive departures of over 60 gpm and 120 gpm, respectively, revealing a region where there is an enhancement of the subsidence of air into the troposphere, and thus an increase of air temperature through adiabatic heating at lower levels. This effect, which is associated to the presence of the jet streak is also clear in the skew-T log-P diagram at Belgrade (Figure 3.6) where a layer of stable dry air region is conspicuous around 600-650 hPa, associated to westerly strong winds of the jet stream, over a turbulent layer of northerly winds.

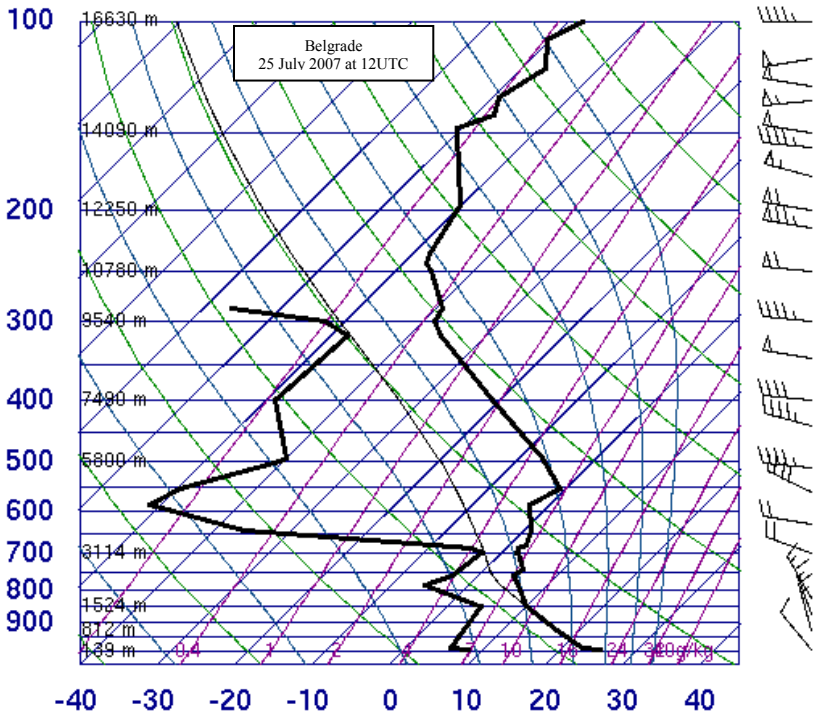

Figure 3.6. Skew-T log-P diagram as derived from the sounding of wind, temperature and dew point temperature on July 25, 2007 (12 UTC) at the station of Belgrade (Serbia). Source: http://www.uwyo.edu.

The impact of the above-described synoptic conditions on meteorological fire risk is shown in Figure 3.7. Composites and anomaly composites of FWI show a large region of high values of FWI (and of extremely high anomalies) over the Balkan Peninsula and Italy, which closely matches i) the already described region of hot and dry air that resulted from the intense hot and dry northerlies, ii) the subsidence associated to the extended ridge in the troposphere and iii) the subsidence at the upper tropospheric levels associated to the jet streak. The fingerprint of the described atmospheric conditions is well apparent in both composites and anomaly composites of ISI, but it may be noted that the impact of this short-term component is further increased by the long-term accumulation of vegetation stress, as indicated by the positive anomalies of BUI. Finally, it is worth stressing that the regions where severe fire events took place (*i.e.* fire pixels with a large number of active fires) are located along the Adriatic coasts of Italy (Marche, Abruzzo and Molise) and of the Balkan Peninsula (Croatia, Bosnia and Herzegovina, Montenegro and North of Albania).

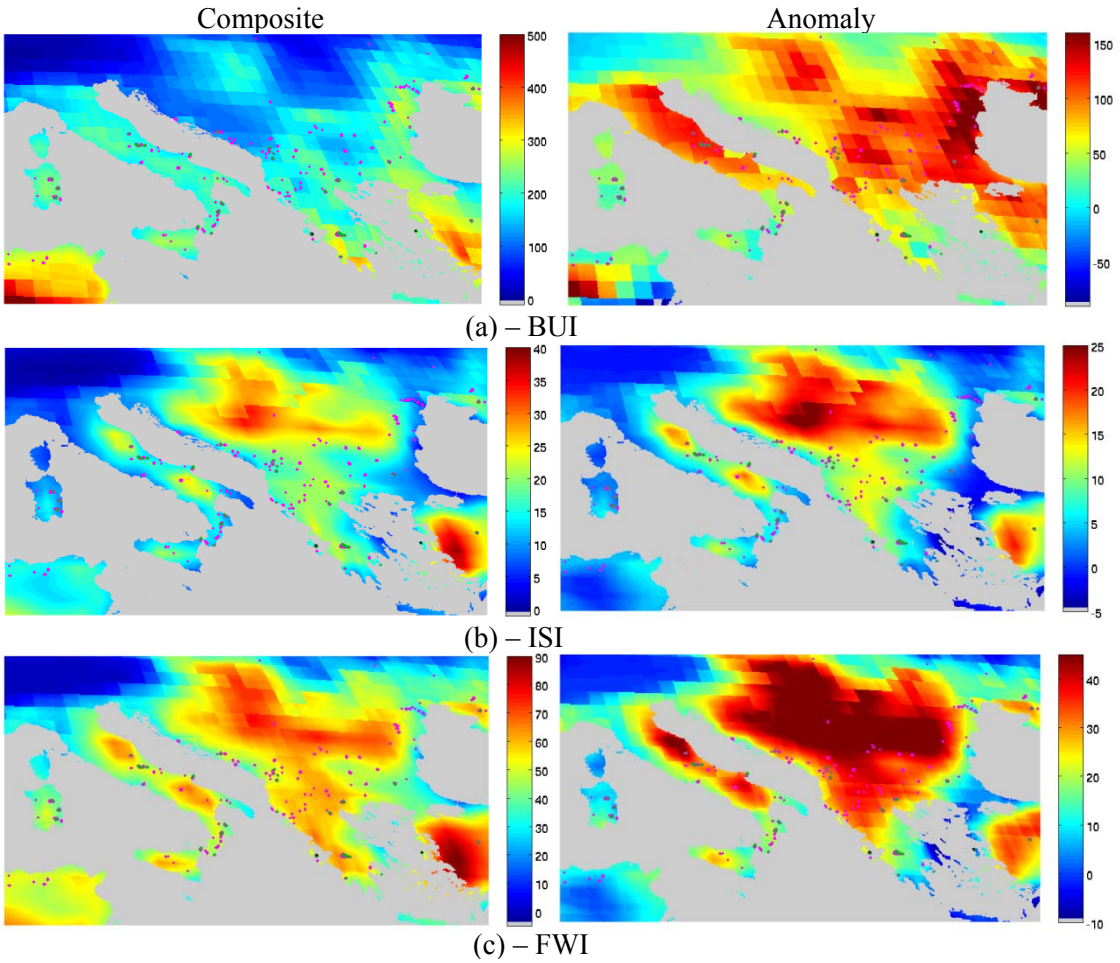

Figure 3.7. Composites (left panels) and anomalies (right panels) of (a) BUI, (b) ISI and (c) FWI for the period July 24-25, 2007. Fires represented in Figure 3.4 (left panel) are also represented, the colour codes indicating the respective persistence.

III.2.2. The episode of August, 22-27

Composites and associated anomalies of considered meteorological fields for the episode of August 22-27, 2007 are shown in Figure 3.8. The synoptic conditions that prevailed during the considered period are characterized by a Rex-type blocking over the Eastern Atlantic, which evolved into an omega pattern. The circulation at the surface is dominated by an extremely intense northerly advection of continental hot and dry air (Figure 3.8a, left panel), as steered by the anticyclonic circulation over central Europe associated to the cyclonic flow due to the presence of a deep thermal depression centred over southwest Asia. The intense northerlies are the well known etesian winds, which dominate the Adriatic, Ionian, and Aegean Seas and the adjacent countries from about mid-May to mid-September. The associated high values of surface air temperature (over 30˚C) and low values of relative humidity (below 40%) are well apparent over the

eastern Mediterranean basin, mainly in some regions of Italy and southern Greece, Romania, Bulgaria and Turkey (Figures 3.8a and 3.8b).

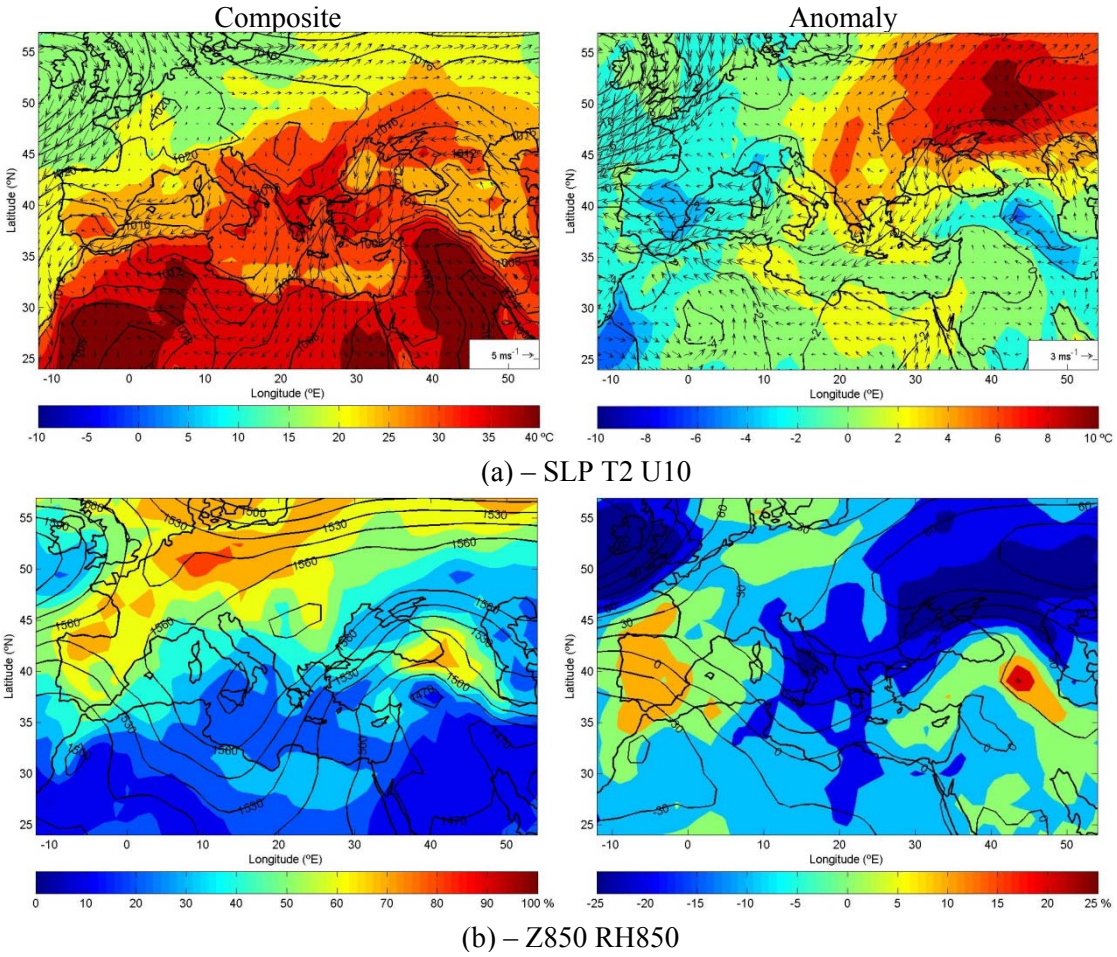

Figure 3.8. As in Figure 3.5, but respecting to the period of August, 22 to 27, 2007.

At the 500 and 250 hPa levels (Figures 3.8c and 3.8d) a synoptic baroclinic wave is well apparent, with a pronounced trough over Eastern Mediterranean and a pronounced ridge extending from northern Europe through Russia, with the axis directed from SW to NE (Figure 3.8d, left panel). As suggested by the wind field at the 250 hPa level, the meandering of the jet stream is even more pronounced than in the previous period, and the jet is also abnormally located at high latitudes. The abnormal location of the jet streak is associated to positive departures of Z500 and Z250 (Figures 3.8c and 3.8d) as large as 80 gpm and 120 gpm, respectively) which delimit a region over Italy and Greece characterised by a strong enhancement of the subsidence of air into the troposphere, leading to an increase of air temperature through adiabatic heating at lower levels. This effect is also clear on the skew-T log-P diagram at Athens (Figure 3.9) where a stable dry air layer may be identified around 650-750 hPa, associated to north-easterly strong winds associated with the ridge, over a turbulent layer of winds of 50 kt about the 800 hPa level.

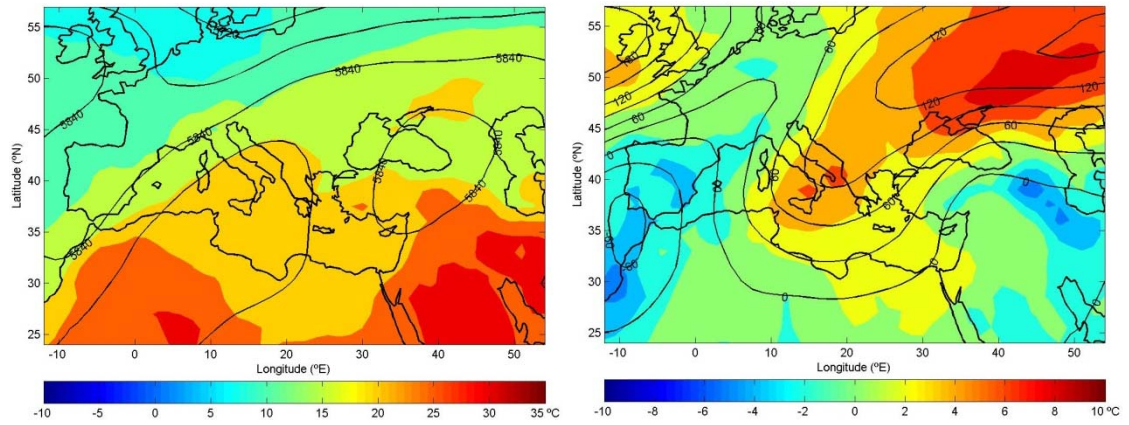

(c) – Z500 T850

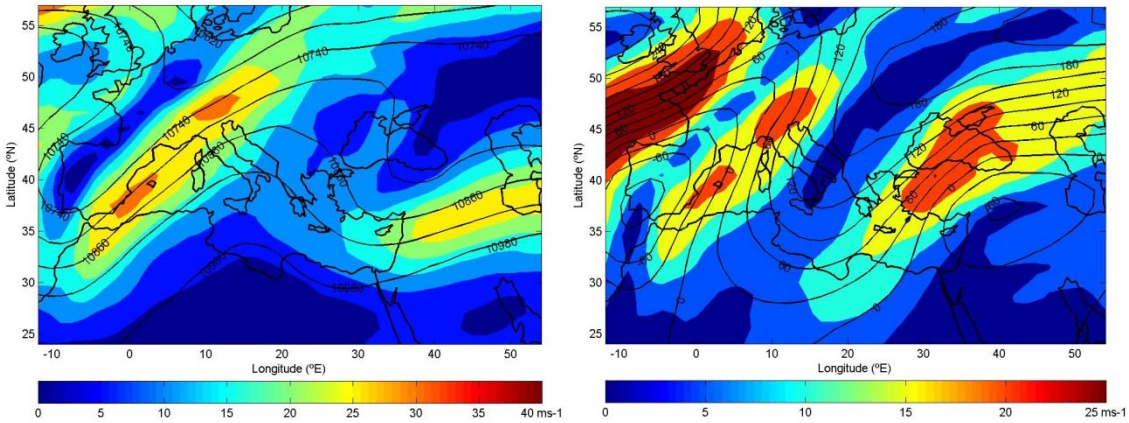

(d) – Z250 U250

Figure 3.8. Continued

Maps of composites and of anomaly composites of BUI, ISI and FWI respecting to this episode are presented in Figure 3.10. The region of high values and of high positive anomalies of FWI is more concentrated than in the previous episode, mainly locating over the Peloponnese and Attica peninsulas. The same region is also associated to high values and high positive anomalies of ISI, the short-term component of FWI displaying an arch-like structure along the coasts of the Adriatic and Black Seas which reflects the influence of the etesian winds. The extremely severe fires that occurred in the Peloponnese are located in the area of higher values and more positive anomalies of FWI, as a result of the contribution of ISI but also of BUI, *i.e.* of the long-term component. The impact of the long-term component is also well apparent in southern Italy and Sicilia, where other fires may be observed despite the lower values of FWI.

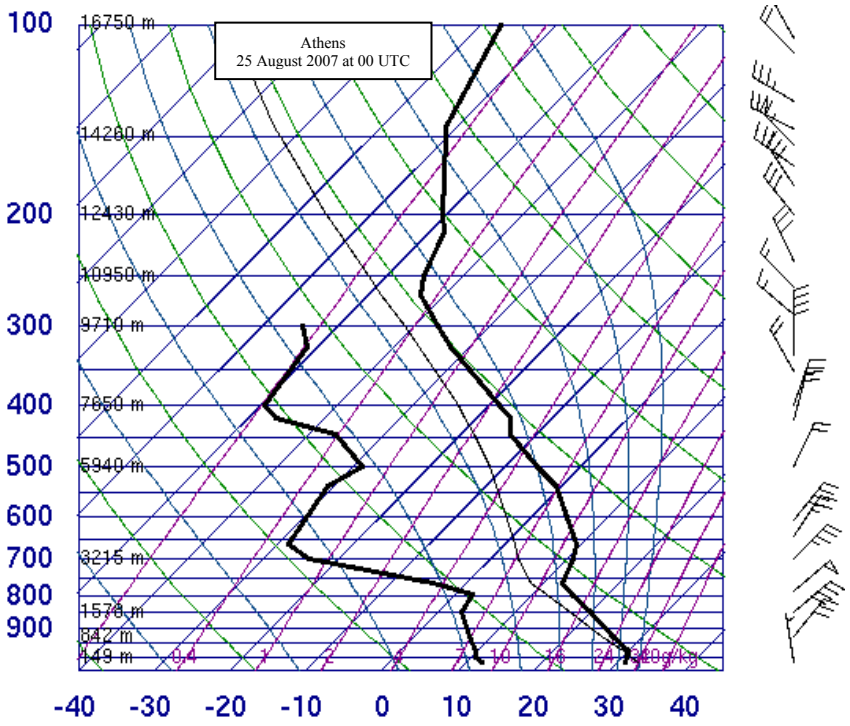

Figure 3.9. As in Figure 3.6, at Athens, respecting to 00 UTC Aug. 25, 2007 (Athens Airport). Source: http://www.uwyo.edu.

IV. Results

Mediterranean regions are some of the most affected by wildfires and although the majority of fire events are human caused (both arson and negligence), natural conditions like the morphology of the landscape, land cover and vegetation, and weather and climate strongly affect wildfire activity. In particular, meteorological factors play a crucial role in the case of the larger fire events and, as discussed in the Introduction, fire regimes depend on the type of land-use and land-cover, as well as on the temperature and precipitation regimes preceding the fire season and on the establishment of atmospheric circulation patterns which induce extremely hot and dry spells over a given area (even if of short duration).

In such context satellite information appears as a very appealing tool to monitor fire activity, especially if provided by instruments on-board geostationary platforms that are able to observe the target with a high temporal resolution (*e.g.* 15 minutes in the case of Meteosat-8). Remote sensing is also becoming a more and more reliable source of information for land cover monitoring.

The spatial distribution of fire events over Europe during the period of July and August 2007-2009 was investigated based on information on active fires as detected by a contextual algorithm (FiDAlgo) that was designed to process data provided by

Meteosat-8/SEVIRI. Contrasts were found in fire activity among the three years in what respects to both fire pixels (*i.e.* those pixels where at least one active fire was detected) and active fires (*i.e.* all fire occurrences continuously detected in a given pixel). For instance, the number of fire pixels in 2008 and 2009 is very similar but the ratio of active fires to fire pixels is about three in 2008 and about 6 in 2009, an indication that fire events in 2009 tended to be more severe. The severity of 2007 is particularly striking taking into account that the almost half of the total number of fire pixels and about 40% of active fires were detected in that year and given the fact that it presents a ratio of active fires to fire pixels of about 7.6.

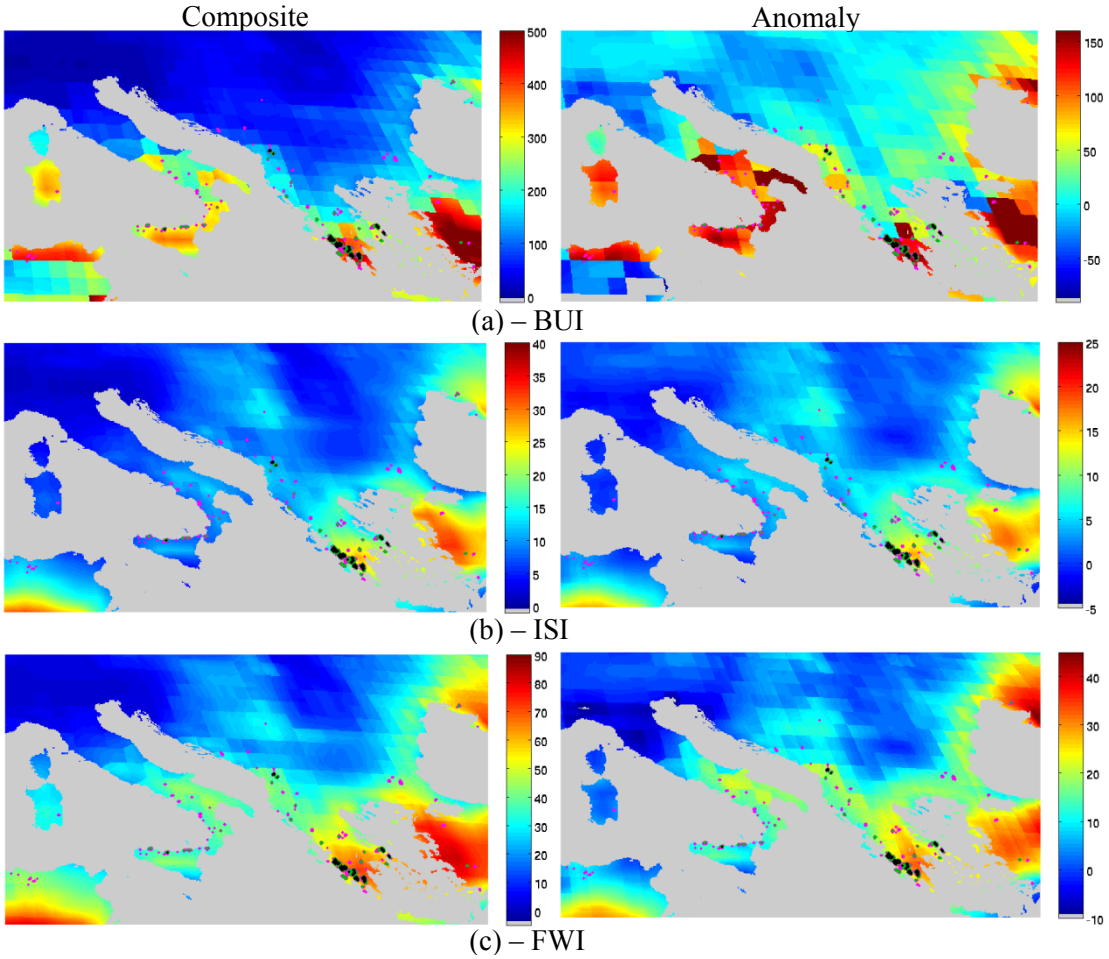

Figure 3.10. As in Figure 3.7, but respecting to the period of August 22-27, 2007. Fires represented in Figure 3.4 (right panel) are also represented, the colour codes indicating the respective persistence.

Contrasts were also found between the distribution, among vegetation cover types, of number of fire pixels and persistence of active fires. Around half of fire pixels were detected in croplands, the remaining half being evenly distributed between forests and shrublands as opposed to the distribution of persistent fire events (more than 10 h)

where 90% of them occurred in forests and shrublands, evenly distributed among these two classes. This may be attributed to human intervention which tends to be more effective in cultivated areas as opposed to forest and shrublands where prevention and fighting is more difficult and where meteorological conditions are a key factor.

The role of meteorological conditions on large fire events was assessed by studying two extreme events of fire activity, respectively on July 24-25 and August 22-27, 2007 that stroke Italy and the Balkan Peninsula. The assessment was based on the analysis of vertical profiles of temperature, dew point temperature and wind as well as of composites of meteorological fields, namely sea-level pressure and geopotential height at 850, 500 and 250 hPa, temperature at 2m and 850 hPa, wind at 10m, relative humidity at 850 hPa and wind speed at 250 hPa. Despite the differences (to be expected) between the two periods in both the atmospheric circulation and the thermo-hydrodynamic processes, structural similarities were found that allow inferring a conceptual model for meteorological conditions strongly favouring the occurrence of severe wildfire episodes in Italy and the Balkan Peninsula. According to the proposed model which is in close agreement with the results of Xoplaki *et al.* (2003) and with the findings of Founda and Giannakopoulos (2009) for the summer 2007, there is, on the one hand, strong northerly advection at the surface of very hot and very dry air over the region. As suggested by the composites of sea-level pressure, 2m-temperature and 10m-wind, the northerly flow is steered by the presence of a ridge over central Europe together with a thermal depression over southwest Asia. Such northerly flow is usually referred to as etesian winds which blow over the Adriatic, the Ionian and the Aegean Seas and affect the adjacent countries from May to September.

On the other hand, the advected air is further heated by adiabatic compression associated to strong subsidence from around 700 up to 250 hPa. As suggested by the composites of height fields at 850, 500 and 250 hPa as well as by the composites of temperature and relative humidity at 850 hPa and by the vertical profiles of temperature and dew point temperature, subsidence in the layer 800-500 hPa is related to the presence of a ridge over the Eastern Mediterranean, associated to a synoptic baroclinic wave. The anomalous displacement of the jet streak towards the northwest, as indicated by the composites of geopotential height and wind speed at 250 hPa, is associated to subsidence of air over the Eastern Mediterranean, which further contributes to the adiabatic heating.

The impact of synoptic conditions on meteorological fire risk was also assessed by analysing composite maps of weather-based indices, namely the Build-Up Index (BUI), the Initial Spread Index (ISI) and the Fire Weather Index (FWI) that are part of the Canadian Forest Fire Weather Index System (CFFWIS). Regions of high values of FWI (and of extremely high anomalies) were found over the Balkan Peninsula and Italy, closely matching the areas of hot and dry air that resulted from the intense etesian or etesian-like winds and from enhanced subsidence. The fingerprint of short-term atmospheric conditions is well apparent in the composites of ISI, but the long-term contribution is also present as indicated by the positive anomalies of BUI. Fire events

(although not as much persistent) may also be observed in regions of high values of BUI stressing the importance of long-term atmospheric conditions that lead to vegetation stress. Such long-term conditions were in fact observed, temperatures in spring ranking among the highest ever recorded in several European countries and temperature anomalies being unusually high in March (>7ºC), with the largest departures over eastern Europe (Obregón *et al.*, 2008). On the other hand, according to the Global Precipitation Climatology Centre (GPCC) (Rudolf *et al.*, 2005), spring 2007 was drier than average, and many countries in Europe had their driest April on record, followed by an extremely wet May for all but eastern Europe.

Results obtained provide a strong indication about the usefulness of monitoring fire activity over Europe using information from geostationary satellites. Besides allowing an almost continuous monitoring of fire events in quasi-real time and the generation of accurate maps of wildfire events, the developed procedure may also lead to an assessment of the respective severity by analysing fire pixels together with fire activity. Last, but not least, the relationships of fire activity and fire persistence with landcover types, on the one hand, and with atmospheric circulation and meteorological risk, on the other hand, suggest using Meteosat-8 information on fire activity to calibrate weather-based indices of fire risk, statistically compute the risk associated to a given class of vegetation when subject to a given type of atmospheric circulation and then disseminate improved maps of fire risk.

In the above-described context satellite information on fire activity, namely the one provided by the MSG series, that appears as a very appealing tool in assisting local authorities to better fulfil reporting obligations and more effectively managing natural resources. This is especially relevant if one takes into account that fire risk is likely to increase over the Mediterranean in the near future according to most scenarios of future climate (Moriondo *et al.*, 2006). In this regard, the current state-of-the-art regional climate models constitute an important tool to provide information not only about the average conditions but also on extreme events over smaller regions under climate change projections. Recent studies have shown that the occurrence of major droughts in southern Europe during the preceding winter and spring seasons may enlarge the amplitude of heatwaves in the following summer (Fisher *et al.*, 2007). This is of particular interest within the scope of the present study because the vast majority of modelling studies agrees in that the Mediterranean will become hotter and drier in the future (IPCC, 2007) favouring the increase in frequency and amplitude of heatwaves over the Mediterranean basin (Fisher and Schär, 2010). The use of regional climate models, together with weather-based indices of fire risk, like BUI, ISI and FWI, that allow assessing the contribution of the short- and the long-term meteorological component, accompanied by adequate conceptual models of the atmospheric circulation favouring the occurrence of extreme fire events and by reliable maps of fire risk will most likely contribute to establish improved scenarios of fire activity in Mediterranean Europe.

Acknowledgements

The work was partly supported by the Portuguese Science Foundation (FCT) through project FLAIR (PTDC/AAC-AMB/104702/2008). FCT has also supported the research performed by the first author (Grant No. SFRH/BD/36964/2007) and by the second author (SFRH/BPD/45080/2008). Part of the work was also supported by the EU 7th Framework Program (FUME) contract number 243888.

References

Amraoui, M., DaCamara, C.C., Pereira, J.M.C., 2010. Detection and monitoring of African vegetation fires using MSG-SEVIRI imagery. Remote Sensing of Environment, 114, 1038-1052.

Barbosa, P., Amatulli, G., Boca, R., Camia, A., Kucera, J., Libertà, G., San-Miguel Ayanz, J., Schmuck, G., Schulte, E., Dierks, H.-H., 2007. Forest Fires in Europe 2006. EUR 22931 EN – Joint Research Centre – Institute for Environment and Sustainability, Luxembourg: Office for Official Publications of the European Communities, EUR, Scientific and Technical Research series, ISSN 1018-5593.

Bartholomé, E., Belward, A.S., 2005. GLC2000: A new approach to global land cover mapping from Earth observation data. International Journal of Remote Sensing, 26, 1959-1977.

Benson, R.P., Roads, J.O., Wiese, D.R., 2009. Climatic and weather factors affecting fire occurrence and behaviour, in: Bytnerowicz, A., Arbaugh, M., Riebau, A., Andersen, C. (Eds.), Developments in Environment Science, 8, pp. 37-59. ISSN: 1474-8177, DOI: 10.1016/S1474-8177(08)00002-8.

Berrisford, P., Dick, D., Fielding, K., Fuentes, M., Kallberg, P., Kobayashi, S., Uppala, S., 2009. The ERA-Interim archive, ERA report series, European Centre for Medium Range Weather Forecasts, ERA Report Series No.1.

Brohan, P., Kennedy, J.J., Haris, I., Tett, S.F.B., Jones, P.D., 2006. Uncertainty estimates in regional and global observed temperature changes: A new dataset from 1850. Journal of Geophysical Research, 111, D12106, doi:10.1029/2005JD006548.

Brotak, E.A., Reifsnyder, W.E., 1977. An investigation of the synoptic situation associated with major wildland fires. Journal of Applied Meteorology, 16, 867-870.

Calle, A., Casanova, J.L., Romo, A., 2006. Fire detection and monitoring using MSG Spinning Enhanced visible and Infrared Imager (SEVIRI) data. Journal of Geophysical Research, 111, G04S06, doi: 10.1029/2005JG000116G04S06.

Chuvieco, E., Salas, J., Vega, C., 1997. Remote sensing and GIS for long-term fire risk mapping, in: Chuvieco, E. (Eds.), A review of remote sensing methods for the study of large wildland fire, Megafires Project ENV-CT96-0256 , Alcalà de Henares (Spain), pp. 91-108.

Cihlar, J., Belward, A., Govaerts, Y., 1999. Meteosat Second Generation opportunities for land surface research and applications. EUMETSAT Scientific Publications EUM SP 01.

Cruz, M.G., Plucinski, M.P., 2007. Billo Road fire: Report on fire behavior phenomena and suppression activities, Ensis Client Rep. No. 1798.

Dee, D., Uppala, S., 2009. Variational bias correction in ERA-Interim, ECMWF Newsletter, No. 119, ECMWF, Reading, United Kingdom, 21-29.

Deeming, J.E., Burgan, R.E., Cohen, J.D., 1977. The National Fire-Danger Rating System – 1978. USDA Forest Service Gen. Technical Report INT-39.

de Groot, W.J., Goldammer, J.G., Keenan, T., Brady, M.A., Lynham, T.J., Justice, C.O., Csiszar, I.A., O'Loughlin, K., 2006. Developing a global early warning system for wildland fire. Forest Ecology and Management, 234S, S10.

Dimitrakopulos, A.P., Mitsopoulos, I.D., 2006. Global forest resources assessment 2005 – Thematic report on forest fires in the Mediterranean region, FAO Fire Management Working Paper 8.

Directorate-General Joint Research Center (DG JRC), 2006. Forest fires in Europe 2005. European Community, EUR 22312 EN.

Fischer, E.M., Seneviratne, S.I., Vidale, P.L., Lüthi, D., Schär, C, 2007. Soil moisture-atmosphere interactions during the 2003 European summer heatwave. Journal of Climate, 20, 5081-5099.

Fischer, E.M., Schär, C., 2010. Consistent geographical patterns of changes in high-impact European heatwaves. Nature Geoscience, DOI: 10.1038/NGEO866.

Founda, D., Giannakopoulos, C., 2009. The exceptionally hot summer of 2007 in Athens, Greece – A typical summer in the future climate. Global and Planetary Change, 67, 227-236.

Giglio, L., Kendall, J.D., Justice, C.O., 1999. Evaluation of global fire detection algorithms using simulated AVHRR infrared data. International Journal of Remote Sensing, 20, 1947-1985.

Giglio, L., Descloitres, J., Justice, C.O., Kaufman, Y.J., 2003. An enhanced contextual fire detection algorithm for MODIS. Remote Sensing of Environment, 87, 273-282.

Good, P., Moriondo, M., Giannakopoulos, C., Bindi, M., 2008. The meteorological conditions associated with extreme fire risk in Italy and Greece: relevance to climate model studies. International Journal of Wildland Fire, 17, 155-165.

Hoinka, K.P., Carvalho, A., Miranda, A.I., 2009. Regional-scale weather patterns and wildland fires in central Portugal. International Journal of Wildland Fire, 18, 36-49.

Ichoku, C., Kaufman, Y.J., Giglio, L., Li, Z., Fraser, R.H., Jin, J.–Z., Park, W.M., 2003. Comparative analysis of daytime fire detection algorithms using AVHRR data for the 1995 fire season in Canada: Perspective for MODIS. International Journal of Remote Sensing, 24, 1669-1690.

Ichoku, C., Giglio, L., Wooster, M.J., Remer, A., 2008. Global characterization of biomass-burning patterns using satellite measurements of fire radiative energy. Remote Sensing of Environment, 112, 2950-2962.

Intergovernmental Panel on Climate Change (IPCC), 2007. Climate Change 2007. The Physical Science Basis, in: Solomon, S., Qin, D., Manning, M., Chen, Z., Marquis, M., Averyt, K.B., Tignor, M., Miller, H.L. (Eds.), Cambridge University Press, Cambridge, United Kingdom and New York, NY, USA.

Lavorel, S., Flannigan, M.D., Lambin, E.F., Scholes, M.C., 2007. Vulnerability of land systems to fire: Interactions among humans, climate, the atmosphere, and ecosystems. Mitigation and Adaptation Strategies for Global Change, 12, 33-53, doi: 10.1007/s11027-006-9046-5.

Le Page, Y., Pereira, J.M.C., Trigo, R.M., DaCamara, C.C., Oom, D., Mota, B., 2008. Global fire activity patterns (1996–2006) and climatic influence: An analysis using the World Fire Atlas. Atmospheric Chemistry and Physics, 8, 1911-1924.

Luterbacher, J., Liniger, M.A., Menzel, A., Estrella, N., Della-Marta, P.M., Pfister, C., Rutishauser, T., Xoplaki, E., 2007. Exceptional European warmth of autumn 2006 and winter 2007: Historical context, the underlying dynamics, and its phenological impacts. Geophysical Research Letters, 34, L12704, doi:10.1029/2007GL029951.

McArthur, A.G., 1967. Fire Behaviour in Eucalypt Forests. Commonwealth Australia Forest and Timber Bureau Leaflet Number 107.

Moriondo, M., Good, P., Durao, R., Bindi, M., Giannakopoulos, C., Corte-Real, J., 2006. Potential impact of climate change on fire risk in the Mediterranean area. Climate Research, 31, 85–95.

Nesterov, V., 1949. Combustibility of the Forest and Methods for its Determination, USSR State Industry Press.

Nikolov, N., 2006. Global forest resources assessment 2005 – Thematic report on forest fires in the Balkan region. FAO Fire Management Working Paper 11.

Obregón, A., Bissolli, P., Kennedy, J.J., Parker, D.E., 2008. Europe, in: Levinson, D.H., Lawrimore, J.H. (Eds.), State of the climate in 2007, Special supplement to the Bulletin of the American Meteorological Society, 89(7), pp. 140-144.

Pereira, J.M.C, 1999. A Comparative evaluation of NOAA/AVHRR vegetation indexes for burned surface detection and mapping. IEEE Transactions on Geoscience and Remote Sensing, 37, 217-226.

Pereira, J.M.C., Govaerts, Y., 2001. Potential fire applications from MSG/SEVIRI observations. EUMETSAT Programme Development Department, Technical Memorandum No. 7.

Pereira, J.M.C., Carreiras, J.M.B., Silva, J.M.N., Vasconcelos, M.J., 2006. Alguns conceitos básicos sobre os fogos rurais em Portugal, in: Pereira, J.S., Pereira, J.M.C., Rego, F.C., Silva, J.M.N., Silva, T.P. (Eds.), Incêndios Florestais em Portugal – Caracterização, Impactes e Prevenção, ISA Press, pp. 133-161.

Pereira, M.G., Trigo, R.M., DaCamara, C.C., Pereira, J.M.C., Leite, S.M., 2005. Synoptic patterns associated with large summer forest fires in Portugal. Agricultural and Forest Meteorology. 129, 11-25.

Prins, E.M., Menzel, W.P., 1992. Geostationary satellite detection of biomass burning in Southern America. International Journal of Remote Sensing, 13, 2783-2799.

Prins, E.M., Menzel, W.P., 1994. Trends in South American biomass burning detected with the GOES VAS from 1983-1991. Journal of Geophysical Research, 99, 16719-16735.

Prins, E.M., Schmetz, J., 2000. Diurnal active fire detection using a suite of international geostationary satellites, in: Ahern, F., Grégoire, J.-M., Justice, C. (Eds.), Forest Fire Monitoring and Mapping: A Component of Global Observation of Forest Cover (pp.139-148). European Commission Joint Research Centre, EUR19588EN.

Pyne, S.J., 2006. Fogo no jardim: compreensão do contexto dos incêndios em Portugal, in: Pereira, J.S., Pereira, J.M.C., Rego, F.C., Silva, J.M.N., Silva, T.P. (Eds.), Incêndios Florestais em Portugal – Caracterização, Impactes e Prevenção, ISA Press, pp. 115-131.

Raínha, M., Fernandes, P.M., 2002. Using the Canadian Fire Weather Index (FWI) in the Natural Park of Montesinho, NE Portugal: calibration and application to fire management, in: Forest Fire Research & Wildland Fire Safety, Viegas (Eds.), Millpress, Rotterdam, ISBN 90-77017-72-0.

Rasilla, D.F., García-Cordon, J.C., Carracedo, V., Concepción, D., 2010. Circulation patterns, wildfire risk and wildfire occurrence at continental Spain. Physics and Chemistry of the Earth, 35, 553-560.

Roberts, G., Wooster, M.J., Perry, G.L.W., Drake, N., Rebelo, L.-M., Dipotso, F., 2005. Retrieval of biomass combustion rates and totals from fire radiative power observations: application to southern Africa using geostationary SEVIRI Imagery. Journal of Geophysical Research, 110, D21111: doi: 10.1029/2005JD006018.

Roberts, G.J., Wooster, M.J., 2008. Fire detection and fire characterization over Africa using Meteosat SEVIRI. IEEE Transactions on Geoscience and Remote Sensing, 46, 1200-1218.

Rudolf, B., Beck, C., Grieser, J., Schneider, U., 2005. Global precipitation analysis products. Global Precipitation Climatology Centre (GPCC), DWD Publication, 1-8.

Shetinsky, E.A., 1994. Protection of forests and forest pyrology, Ecology, Moscow.

Skinner, W.R., Flannigan, M.D., Stocks, B.J., Martell, D.L., Wotton, B.M., Todd, J.B., Mason, J.A., Logan, K.A., Bosch, E.M., 2002. A 500 hPa synoptic wildland fire climatology for large Canadian forest fires. Theoretical and Applied Climatology, 71, 157-169.

Schmetz, J., Pili, P., Tjemkes, S., Just, D., Kerkmann, J., Rota, S., Ratier, A., 2002. An introduction to Meteosat Second Generation (MSG). Bulletin of the American Meteorological Society 83, 977–992. doi:10.1175/1520-0477(2002)083.

Sneeuwjagt, R.J., Peet, G.B., 1998. Forest Fire Behaviour Tables for Western Australia, Dept. of Conservation and Land Management, Perth, Western Australia.

Trigo, I.F., DaCamara, C.C., Viterbo, P., Roujean, J.-L., Olesen, F., Barroso, C., Camacho-de-Coca, F., Carrer, D., Freitas, S.C., García-Haro, J., Geiger, B., Gellens-Meulenberghs, F., Ghilain, N., Meliá, J., Pessanha, L., Siljamo, N., Arboleda, A., 2010. The Satellite Application Facility on Land Surface Analysis. International Journal of Remote Sensing, In Press.

Trigo, R.M., Pereira, J.M., Pereira, M.G., Mota, B., Calado, M.T., DaCamara, C.C., Santo, F.E., 2006. The exceptional fire season of summer 2003 in Portugal. International Journal of Climatology, 26, 1741-1757.

van Wagner, C.E., 1987. Development and structure of the Canadian Forest Fire Index System, Canadian Forestry Service, Ottawa, Ontario, Forestry Technical Report 35.

Ventura, J., Vasconcelos, M.J., 2006. O fogo como processo físico-químico e ecológico, in: Pereira, J.S., Pereira, J.M.C., Rego, F.C., Silva, J.M.N., Silva, T.P. (Eds.), Incêndios Florestais em Portugal – Caracterização, Impactes e Prevenção, ISA Press , pp. 93-113.

Viegas, D.X., Bovio, G., Ferreira, A., Nosenzo, A., Sol, B., 1999. Comparative study of various methods of fire danger evaluation in southern Europe. International Journal of Wildland Fire, 9, 235-246.

Viegas, D.X., Pinõl, J., Viegas, M.T., Ogaya, R., 2001. Estimating live fine fuels moisture content using meteorologically-based indices. International Journal of Wildland Fire, 10, 223-240.

Viegas, D.X., Reis, R.M., Cruz, M.G., Viegas, M.T., 2004. Calibration of Canadian Fire Danger Rating System for application to Portugal. Silva Lusitana, 12, 77-93.

Westerling, A.L., Gershunov, A., Brown, B.L., Cayan, D.R., Dettinger, M.D., 2003. Climate and wildfire in the western United States. Bulletin of the American Meteorological Society, 84, 595-604.

Westerling, A.L., Cayan, D.R., Brown, T.J., Hall, B.L., Riddle, L.G., 2004. Climate, Santa Ana winds, and autumn wildfires in southern California. EOS, 85, 289-296.

Xoplaki, E., González-Rouco, J.F., Gyalistras, D., Luterbacher, J., Rickli, R., Wanner, H., 2003. Interannual summer air temperature variability over Greece and its connection to the large-scale atmospheric circulation and Mediterranean SSTs 1950-1999. Climate Dynamics, 20, 537-554.

CHAPTER 4: Using active fires derived from MSG-SEVIRI imagery to calibrate the Fire Weather Index and generate maps of risk of fire over Mediterranean Europe

Teresa J. Calado[a,b], Carlos C. DaCamara[a] , Malik Amraoui[a,c]

[a] University of Lisbon, Instituto Dom Luiz (IDL), Lisbon, Portugal

[b] Instituto de Meteorologia, Lisbon, Portugal

[c] School of Sciences and Technology, University of Trás-os-Montes e Alto Douro (UTAD), Vila Real, Portugal

This Chapter has been submitted to Agricultural and Forest Meteorology in October 2010.

Abstract

A procedure is presented that allows operationally generating daily maps of fire risk over three regions of Mediterranean Europe (the Iberian Peninsula, Italy and Greece) which are very prone to the occurrence of large fire events. The rationale of the developed methodology is to provide the user community with information on meteorological risk that will allow adopting the adequate measures to mitigate fire damage. The generated maps of fire risk are based on an integrated use of meteorological information from ECMWF forecasts, on vegetation land cover from GLC2000 and on occurrences of active fires as detected by MSG-SEVIRI. The obtained levels of fire danger are associated to probabilities of occurrence of fires exceeding specified magnitudes. It is shown that statistical models based on two-parameter Generalized Pareto (GP) distributions adequately fit the observed samples of duration of active fires and that these models are significantly improved when the Fire Weather Index (FWI) is used as a covariate to model both the shape and scale parameters of the GP distributions. A set of five coherent classes of fire risk is then derived by defining a "reference value" of active fire duration associated to the geographical location and the vegetation type and by analysing the risk departure from the "background" due to meteorological factors. Validation of results is performed in the period of July-August 2007-2009 and it is shown that all three regions present an overall similar behaviour, with a virtual absence of fire occurrences of large duration in the classes of very low and low risk of fire. On the other hand, fires of small duration concentrate in the classes of moderate, high and very high risk and there is a displacement of the modal class towards classes of higher risk with increasing duration. The procedure will be operationally run in the very nearby future within the framework of the Land Surface Analysis Satellite Application Facility (LSA SAF), a specialized development and processing centre, which is part of EUMETSAT distributed Applications Ground Segment.

I. Introduction

Meteorological factors play a crucial role in the setting and spreading of wildfires and are determinant in the resulting fire severity (*e.g.* Bovio and Camia, 1997). Meteorological factors are therefore frequently used, alone or combined with vegetation and topographical information, to develop indices of fire risk. However, because the majority of fires that occur in Europe are anthropogenic, it is difficult to calibrate fire risk indices in order to generate realistic maps of fire danger.

Fire danger is usually defined by means of the factors affecting the ignition, propagation, difficulty of control and fire effects on the ecosystem (Helms, 1988). An appropriate knowledge of the spatial and temporal variation associated to these factors is requires in order to establish pro-active fire management (Palheiro *et al.*, 2006).

There are a number of fire danger rating systems (van Wagner, 1987; Deeming *et al.*, 1972, 1977), but the Canadian Forest Fire Danger Rating System (CFFDRS) is one of the most used throughout the world (Stocks *et al.*, 1989). For instance, in a study conducted by the European Commission, the performance of six methods of rating fire index was assessed for Italy, France, Portugal and the Fire Weather Index (FWI) was the method that presented better results, both in the discrimination of fire occurrences and in the amount of daily burnt areas. According to these results, the European Commission, in 1995, recommended the community countries to adopt CFFDRS to predict fire danger. The use of a single method has, among others, the advantage of allowing a common language, with indices of easy recognition and interpretation by all users. The same decision was taken by the European Forest Fire Information System (EFFIS) network, who adopted in 2007 the FWI, to assess fire danger over Europe.

The FWI System (van Wagner, 1987) is the first major subsystem of CFFDRS and consists of six numerical sub-indices that are relative indicators of potential fire behaviour in common boreal fuel type (Stock *et al.*, 1989; Alexander and Lanoville, 1989; Forestry Canada Fire Danger Group, 1992). It is nevertheless worth noting that FWI was developed for boreal forest types in Canada, which means that calibration is required when applied to different regions in order to take into account specific characteristics of climate and fuel type, fire regime and structure of prevention and fire fighting of the region. Some authors (Haines *et al.*, 1988; van Wagner, 1987; Lynham and Stocks, 1989; Viegas *et al.*, 2004) have calibrated the system through analyses of fire weather history and temporal data series of the FWI System components.

It may be noted that FWI is usually computed based on point measurements of meteorological variables, which in some locations may be difficult either because the sparsity of meteorological stations may lead to less precise estimates for areas between stations, or because the measurements at the meteorological stations do not adequately represent the properties of the surrounding vegetation. Hernandez-Leal *et al.* (2004) proposed the use of remote sensing as way to circumvent this problem, mainly because

the time and spatial resolution of remote-sensed parameters is of great value in the generation of risk indices that express the water stress of vegetation and the surface temperature, both of them key variables in fire risk assessment. For instance, the SEVIRI instrument on-board the MSG satellite series has been identified as having an especially good potential in the domain of fire risk management (Pereira and Govaerts, 2001), namely in what respects to the identification of pre-fire indicators (*e.g.* signals of water vegetation stress).

The severity of wildfire-related problems, together with the demands from environment monitoring and risk management and a growing number of users in agricultural and forestry applications, has led EUMETSAT's (European organization for the Exploitation of Meteorological Satellites) LSA SAF (Satellite Application Facility on Land Surface Analysis) to commit to the development of two new lines of research aiming to explore the capability of Meteosat-8/SEVIRI to detect and monitor: (1) active fires over Africa and Europe, leading to the operational dissemination of the Fire Detection and Monitoring (FD&M) product; (2) signals of vegetation stress and of meteorological risk of fire, leading to the operational dissemination of the Fire Risk Map (FRM) product. The LSA SAF (Trigo *et al.*, 2010) is part of the SAF Network, a set of specialised development and processing centres, serving as EUMETSAT distributed Applications Ground Segment. The SAF network complements the product-oriented activities at the EUMETSAT Central Facility in Darmstadt. The main purpose of the LSA SAF is to take full advantage of remotely sensed data, particularly those available from EUMETSAT sensors, to measure land surface variables, which will find primarily applications in meteorology (http://landsaf.meteo.pt/). In fact, since the last quarter of the 20th century, several studies have stressed the role of land surface processes on weather forecasting and climate modelling (*e.g.* Dickinson *et al.*, 1983; Mitchell *et al.*, 2004; Ferranti and Viterbo, 2006). The LSA SAF has been especially designed to serve the needs of the meteorological community, particularly Numerical Weather Prediction (NWP). However, there is no doubt that the LSA SAF addresses a much broader community, which includes users from: weather forecasting and climate modelling; environmental management and land use; agricultural and forestry applications; renewable energy resources assessment, particularly biomass, depending on biophysical parameters, and solar energy; natural hazards management; climatological applications and climate change detection.

The present work discusses the first results related to the generation of maps of fire risk over Mediterranean Europe, whose climate is characterised by rainy and mild winters followed by warm and dry summers which make the region very prone to the occurrence of a large number of fire events (Ventura and Vasconcelos, 2006; Pyne, 2006), in particular Portugal, Spain, France, Italy, Greece and Croatia (Pereira *et al.*, 2006; Barbosa *et al.*, 2007). The generated maps of fire risk are based on an integrated use of meteorological information from the European Centre for Medium-Range Weather Forecasts Reanalysis (ECMWF) forecasts, on vegetation land cover from Global Land Cover 2000 (GLC2000) and on occurrences of active fires as detected by

MSG-SEVIRI. The obtained levels of fire danger are associated to probabilities of occurrence of fires exceeding specified magnitudes.

The rationale of the developed methodology is to provide the user community with information on meteorological risk that will allow adopting the adequate measures to mitigate fire damage. The main difference of the adopted method when compared to other proposed ones is that it takes full advantage of the temporal resolution of SEVIRI that, by detecting fire events every 15 minutes, allows estimating the duration of active fires that is essential to determine classes of fire danger. Usually fire risk maps are computed using the amount of burnt area or number of fire occurrences as detected by firemen, which are not as reliable, since its computation not only depends on the countries policy but is also evaluated by visual inspection, which makes their accuracy doubtful. Moreover, the use of satellite data prevents us from being dependent on the availability of ground fire records from each country. It is also worth noting that, despite the worst spatial resolution of SEVIRI when compared to *e.g.* MODIS, the sensor 3.9 μm is very sensitive to fires, even to sub-pixel ones, making it an adequate sensor to monitor active fires.

II. Data and methods

All data are retrieved for the European window within Meteosat disk (covering all EUMETSAT member states). The study area was however, restricted to three regions in Southern Europe, since they are amongst the countries more prone to burn; Iberian Peninsula, comprehended between 10ºW and 3ºE in longitude and between 36ºN and 44ºN, Italy, comprehended between 8ºE and 17ºE in longitude and between 36ºN and 45ºN, and Greece, comprehended between 17ºE and 29ºE in longitude and between 34ºN and 42ºN (Figure 4.1).

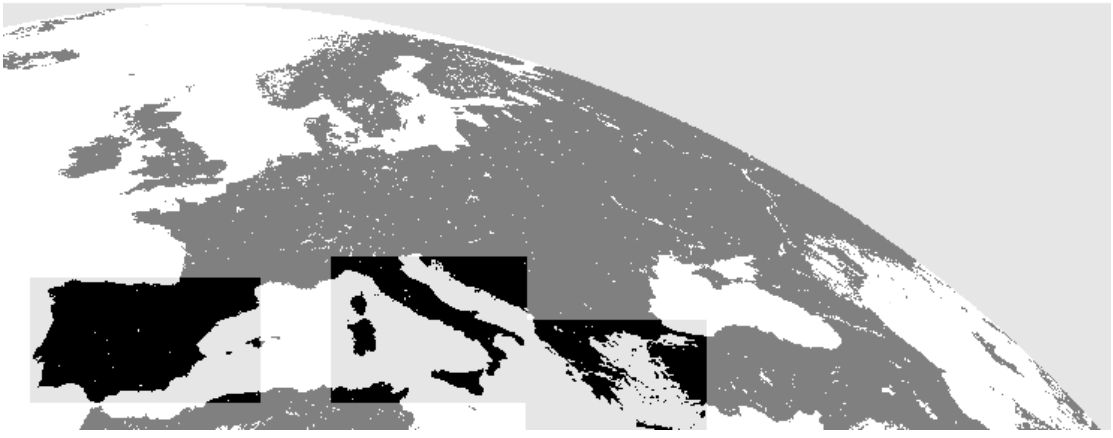

Figure 4.1. Pixels in black correspond to the sub region of Europe selected for the study.

The Canadian Forest Fire Weather Index System, CFFWIS (van Wagner, 1987) consists of six components that account for the effects of fuel moisture and wind on fire behaviour. The System comprehends three levels of information: (i) fire weather observations (*e.g.* 12 h, in local time, daily observations of air temperature, relative humidity, 10 m wind speed and 24 h cumulative precipitation); (ii) fuel moisture codes: Fine fuel Moisture Code (FFMC), Duff Moisture Code (DMC) and Drought Code (DC) and (iii) fire behaviour indexes: Initial Spread Index (ISI), Build-Up Index (BUI) and Fire Weather Index (FWI). FFMC, DMC and DC rate the average moisture content of all layers of the soil, *i.e.*, surface litter, decomposing litter and organic (humus) layer, respectively. ISI combines wind effects with FFMC to rate fire spread that may be different according to the type of fuel. BUI is a combination of DMC and DC and is a rating of the total amount of fuel available for combustion. Finally, BUI is combined with ISI to produce the Fire Weather Index (FWI) and the Daily Severity Rating (DSR) that respectively rate fire intensity and the difficulty of controlling fires.

FWI was obtained from meteorological data as derived from ECMWF analysis, within the period July and August, 2007 to 2009. Originally defined on a 0.25°×0.25° latitude/longitude grid and retrieved at 12 UTC, meteorological data were mapped onto the MSG grid and spatially interpolated for 2-meter air temperature, 2-meter dew point temperature, 10-meter wind speed and 24-hour cumulated precipitation. Air relative humidity was computed combining dew point temperature and temperature according to Magnus' expression. An example of a map of FWI produced by FRM product is shown in Figure 4.2.

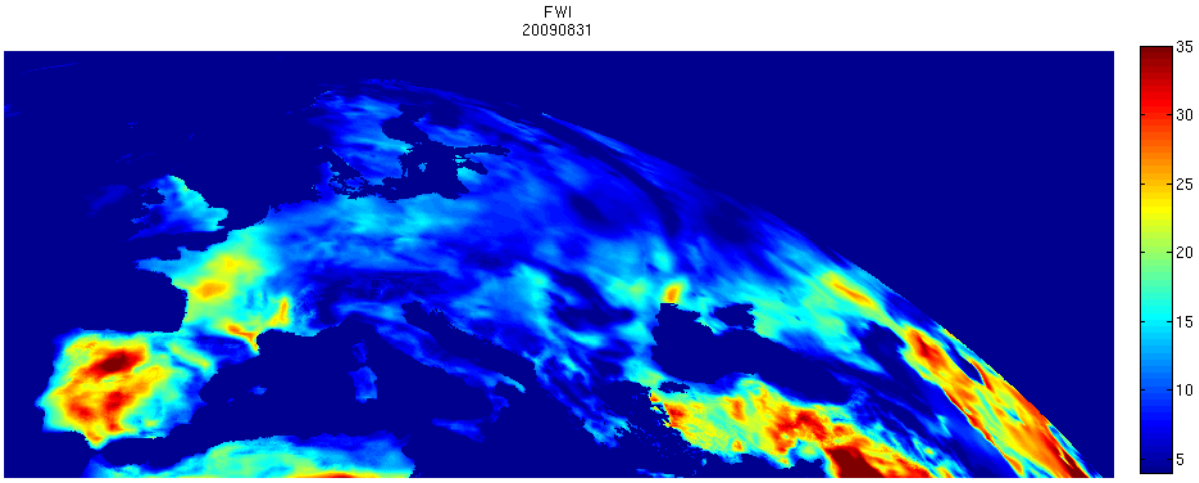

Figure 4.2. Fire Weather Index (FWI) at 12h of 31/08/2009 over the LSA SAF European window.

Vegetation types associated to each pixel were obtained from GLC2000 over the European window. GLC2000 was reprojected from its original regular

latitude/longitude grid onto the MSG projection, *i.e.* onto the Normalized Geostationary Projection (NGP), using the most frequent value in the resampling of the data.

In order to determine which types of vegetation are more sensitive to fires we analysed the spatial distribution of fire pixels and active fires over forests, shrub and cultivated areas (Figure 4.3), according to classification given by GLC2000, for the three Mediterranean regions mentioned above (Figure 4.1). The chosen GLC2000 classes were 1, 2, 3, 4, 6 for forests; 11, 12, 13, 14 for shrub and 16 for cultivated areas.

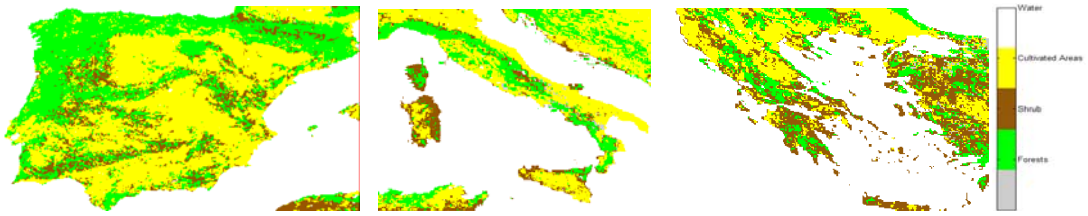

Figure 4.3. The three main types of vegetation cover as identified by GLC2000, over Iberian Peninsula (left panel), Italy (middle panel) and Greece (right panel). Pixels in white, yellow, brown, green and gray correspond to water bodies, cultivated areas, shrub, forests and other types, respectively.

Finally, active fire data were obtained from the FD&M product, covering the same period as the fire-risk data. The FD&M product relies on FiDAlgo (*Fi*re *D*etection *Algo*rithm), an operational procedure that allows active fire detection in near real time, based on information from Meteosat-8/SEVIRI. FiDAlgo is based on contextual algorithms that have been successfully developed for different sensors, namely NOAA-AVHRR and MODIS (see Doc: SAF/LAND/IM/ATBD_FD&M).

The Fire Detection and Monitoring (FD&M) is a product that was developed in the framework of LSA SAF Project (DaCamara *et al.*, 2007; Amraoui *et al.*, 2008), to detect and monitor active fires, particularly over Africa and Europe (Figure 4.4). FiDAlgo uses information provided by SEVIRI at the maximum temporal resolution, namely the TOP Of the Atmosphere (TOA) radiances for visible channels centred at 0.635 µm (VIS0.6) and 0.81 µm (VIS0.8) and infrared channels centred at 3.92 µm (IR3.9), 10.8 µm (IR10.8) and 12.0 µm (IR12.0). For each pixel and time-step, FiDAlgo also makes use of the respective solar zenith angle. The procedure allowed identifying both active fires (*i.e.* occurrences in a given pixel of a given image) and fire pixels (*i.e.* pixels where at least one active fire was detected). A full description of the algorithm is given by Amraoui *et al.* (2010).

III. Results

As shown in Table 4.1, during the validation period of July-August 2007-2009, cultivated areas are the predominant vegetation type in all three considered regions, namely 51% in Iberian Peninsula, 65% in Italy and 38% in Greece, but the percentage of recorded fire pixels reduces to 27%, 35% and 20%. On the other hand both forests and shrubland types, although occupying a much smaller amount of the territory, are associated to a larger percentage of fire events. As an example, it may be noted that the relevance of shrub in what respects to fire incidence is quite conspicuous in Italy where the few percentage of shrub pixels (2%) is associated to 28% of fire events.

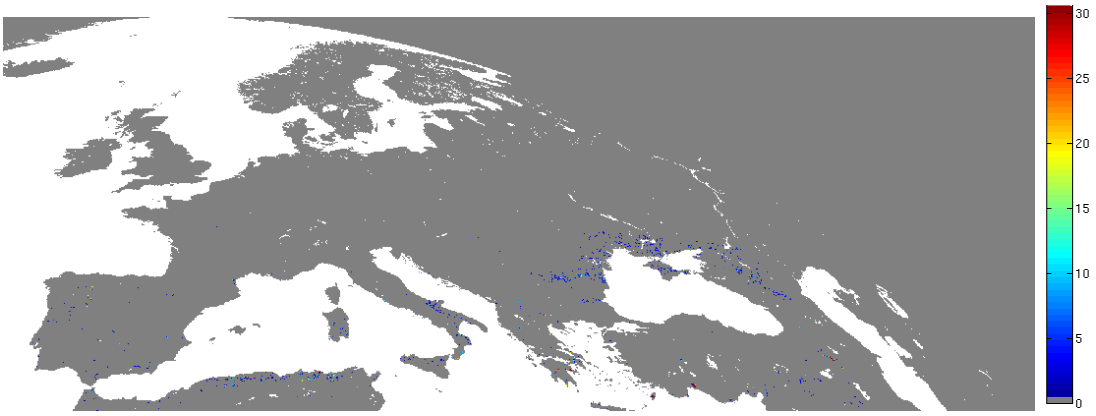

Figure 4.4. Number of active fires in July and August 2008-2009 as identified by FiDAlgo. Red pixels represent number of fires greater or equal to 30.

Table 4.1. Total number of pixels and number of fire pixels (during July-August 2007-2009) and respective percentages (in brackets) for the three considered types of vegetation, for (a) Iberian Peninsula, (b) Italy and (c) Greece.

	(a) Iberian Peninsula			(b) Italy			(c) Greece		
	Forest	Shrub	Cultivated	Forest	Shrub	Cultivated	Forest	Shrub	Cultivated
N. Pixels	15685	6102	22776	7050	382	13814	3957	6726	6485
[%]	[35]	[14]	[51]	[33]	[2]	[65]	[23]	[39]	[38]
N. Fire events	1151	451	606	644	503	624	434	991	355
[%]	[52]	[21]	[27]	[36]	[28]	[35]	[24]	[56]	[20]

Table 4.2 presents, for each region and vegetation type, the persistence in time (in hours) of active fires. It is well apparent that intense fire events (with persistence in time greater than 10 hours) are virtually inexistent in Italy during the study period, but are quite important in Iberian Peninsula and Greece. It is also worth noting that fire events are much less persistent in cultivated areas than in forests and shrubland types, with a

total of 8% for fires with persistence greater than 10 hours for Iberian Peninsula (6% for Greece) against 57% (31%) for forests and 35% (63%) for shrubland.

Table 4.2. Persistence in time (in hours) of active fires (during July-August 2007-2009) and respective percentages (in brackets) for the three considered types of vegetation, for (a) Iberian Peninsula, (b) Italy and (c) Greece.

	(a) Iberian Peninsula			(b) Italy			(c) Greece		
	<5h	[5,10]h	>10h	<5h	[5,10]h	>10h	<5h	[5,10]h	>10h
Forest	4735	1403	42	2333	216	0	1987	2345	1016
[%]	[57]	[45]	[57]	[40]	[28]	[0]	[26]	[30]	[31]
Shrub	1450	674	388	1945	497	0	4356	4775	2022
[%]	[17]	[22]	[35]	[34]	[64]	[0]	[56]	[61]	[63]
Cultivated	2184	1015	94	1507	64	0	1362	733	183
[%]	[26]	[33]	[8]	[26]	[8]	[0]	[18]	[9]	[6]

Results presented in Tables 4.1 and 4.2 suggest investigating whether the temporal organization of active fires tends to follow a long-tailed distribution. For instance, Amraoui *et al.* (2010) have successfully fitted a Generalized Pareto (GP) distribution to the samples of duration of active fires over Northern and Southern Africa.

The GP distribution is able to model the tails of a wide variety of distributions, based on theoretical arguments. The GP is a right-skewed distribution parameterized with a shape or "tail index" (α), a scale ($\sigma > 0$) and a location (θ). When $\theta = 0$, one has the so-called two-parameter GP, whose cumulative distribution is given by:

$$F(\alpha, \sigma)(x) = 1 - \left(\alpha \frac{x}{\sigma}\right)^{-\frac{1}{\alpha}} \qquad (4.1)$$

and corresponding probability density function is given by:

$$f(x|\alpha, \sigma) = \left(\frac{1}{\sigma}\right)\left(1 + \alpha \frac{x}{\sigma}\right)^{-1-\frac{1}{\alpha}} \qquad (4.2)$$

It may be noted that, according to the definition of GP, if $\alpha < 0$ then the distribution has zero probability above the upper limit $x_{max} = -\sigma/\alpha$. When $\alpha > 0$, the GP distribution is not upper bounded.

Using maximum likelihood estimation, Generalized Pareto distributions were fitted to the samples of daily records of decimal logarithm of active fire duration during the

period of July-August 2007-2009, for each Mediterranean region and type of land cover. Active fire duration is measured in MSG slots (1 slot = 15 minutes) and since daily values range from 1 slot (*i.e.* 15 minutes) to 96 slots (*i.e.* 24 hours), the corresponding decimal logarithms range from 0 to log10 (96).

Table 4.3 presents the obtained estimated values for the shape (α), and scale (σ) parameters of the fitted GP distributions for the three types of vegetation over the three considered geographical areas. Table 4.3 also presents the respective 95% confidence intervals as obtained by generating 5,000 samples using the bootstrapping technique (*e.g.* Wilks, 1995). Graphical representations of the fitted density distribution functions are provided in Figure 4.5 and the different roles of vegetation types on fire duration is well apparent, especially when comparing cultivated areas with shrub and forests. The difference is especially conspicuous in Italy and Greece.

Figure 6 allows visually assessing the quality of fit of the GP distributions to the respective samples for three cases, namely forest in the Iberian Peninsula, shrub in Italy and cultivated areas in Greece. It may be noted that the three presented cases are representative of the total of 9 cases (*i.e.* 3 geographical areas × 3 vegetation types).

Table 4.3. Estimated values of the shape and scale parameters and respective confidence interval of 95% for the adjusted Generalized Pareto.

	(a) Iberian Peninsula					
	Forests		Shrub		Cultivated Areas	
Parameter	Estimated	Conf. Int. (95%)	Estimated	Conf. Int. (95%)	Estimated	Conf. Int. (95%)
α	-0.46	[-0.52,-0.45]	-0.34	[-0.41,-0.28]	-0.53	[-0.63,-0.50]
σ	0.90	[0.87, 0.95]	0.71	[0.65,0.79]	0.92	[0.87,1.01]

	(b) Italy					
	Forests		Shrub		Cultivated Areas	
Parameter	Estimated	Conf. Int. (95%)	Estimated	Conf. Int. (95%)	Estimated	Conf. Int. (95%)
α	-0.41	[-0.49,-0.36]	-0.42	[-0.50,-0.32]	-0.35	[-0.40,-0.32]
σ	0.65	[0.60, 0.72]	0.71	[0.62,0.80]	0.52	[0.49,0.56]

	(c) Greece					
	Forests		Shrub		Cultivated Areas	
Parameter	Estimated	Conf. Int. (95%)	Estimated	Conf. Int. (95%)	Estimated	Conf. Int. (95%)
α	-0.84	[-0.93,-0.80]	-0.73	[-0.79,-0.70]	-0.39	[-0.51,-0.25]
σ	1.56	[1.48, 1.70]	1.34	[1.28,1.42]	0.77	[0.64,0.91]

Goodness of GP model fits were further assessed by means of appropriate non-parametric tests (Kotz *et al*., 1982), namely the Anderson-Darling (A^2) test which is especially appropriate since it gives more weight to the tails than do other tests, *e.g.* the Kolmogorov-Smirnov (K-S) test. Significance levels for A^2 were obtained by randomly generating 5,000 data samples from the GP distribution characterised by each parameter from the original data set, as obtained by maximum likelihood estimation. Figure 4.6

(a), (b), (c), shows examples of the obtained curves for A^2, as well as the results that were obtained from the sample data for the Iberian Peninsula, Italy and Greece in shrubland, forests and cultivated areas, respectively.

Significance levels obtained for A^2 were higher than 5% for all 9 fitted distributions, an indication that the GP model is appropriate to describe the statistical behaviour of the decimal logarithm of active fire duration for the three considered vegetation types in the three geographical regions. Figure 4.7 provides three examples of results obtained, respectively for shrub over the Iberian Peninsula, forests in Italy and cultivated areas in Greece.

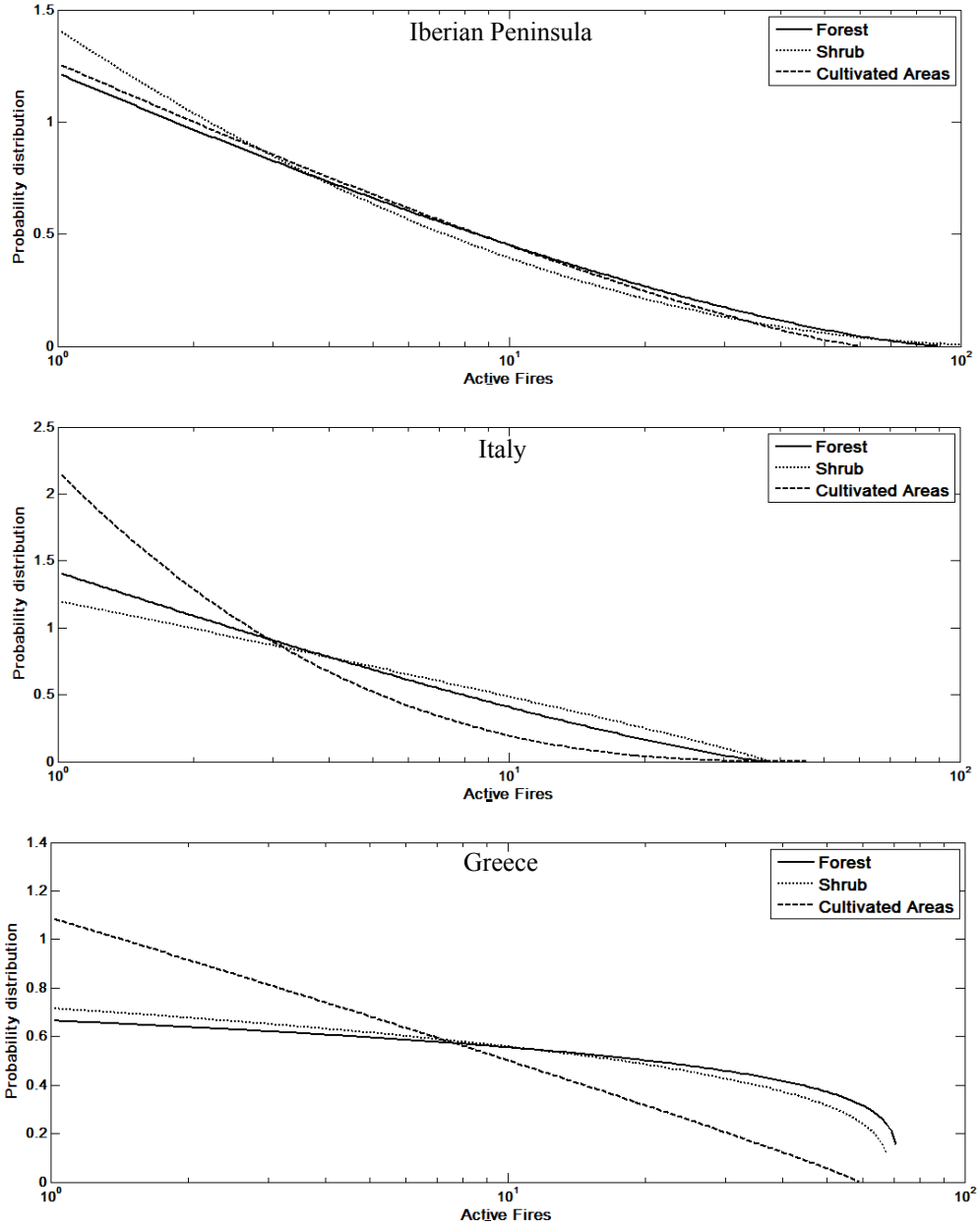

Figure 4.5. Probability density functions for the fitted GP models, for each region and type of vegetation.

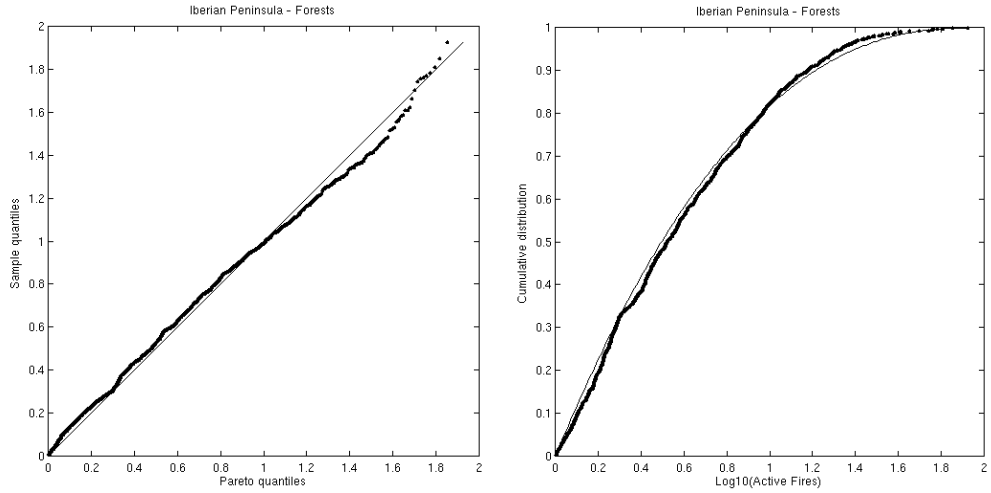

(a) Iberian Peninsula - Forests

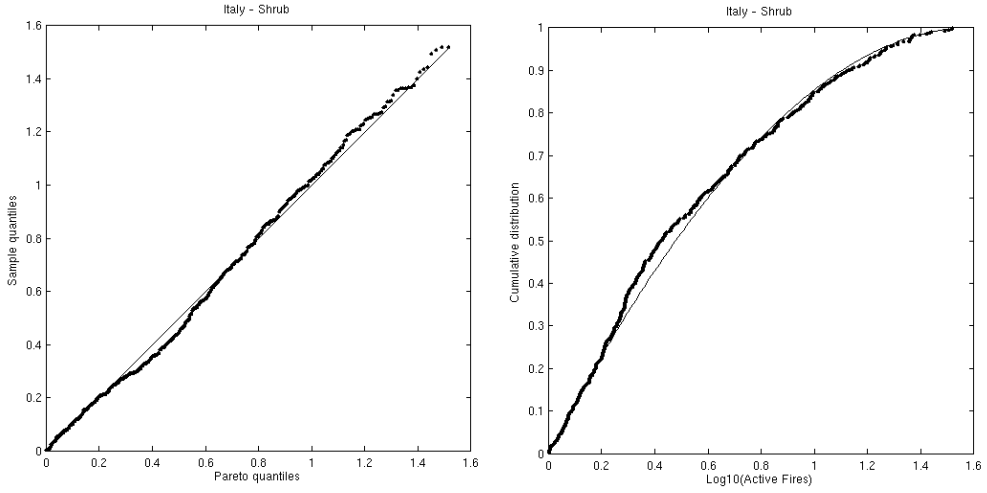

(b) Italy - Shrub

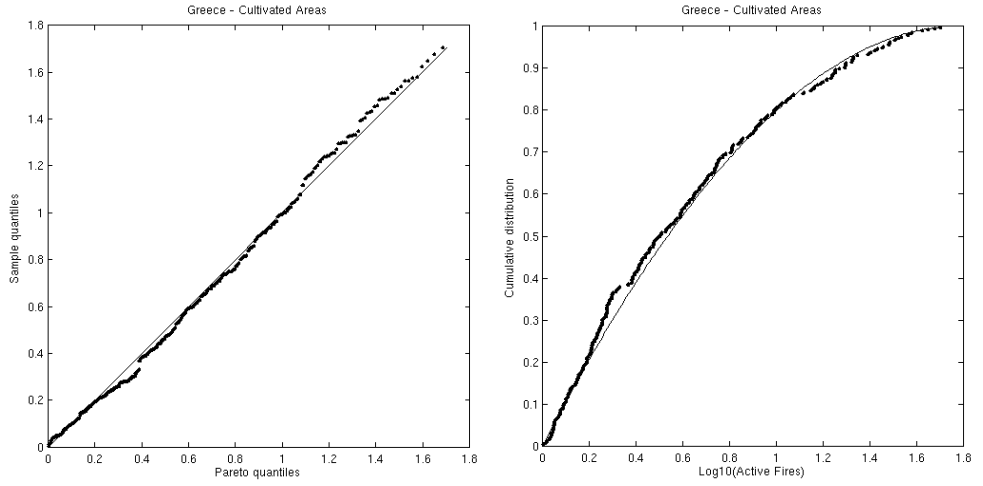

(c) Greece – Cultivated area

Figure 4.6. Probability plots (left panels) and cumulative distributions (right panels) for the fitted model (solid curve) and sample data (dots), for the Generalized Pareto distribution, for (a) forests in Iberian Peninsula, (b) shrub in Italy and (c) cultivated areas in Greece.

It is worth stressing that when fitting GP distributions to the samples of fire duration only geographical location and vegetation type was considered and no account was given to the role played by meteorological factors. However, as already discussed, FWI is a meteorological index closely linked to fire activity, and large fires are expected to be associated to high values of FWI.

In order to assess the impact of FWI on fire activity we divided the active fire dataset in groups of active fires associated to different ranges of associated FWI. Accordingly, 51 groups of active fires respectively associated to values of FWI between percentile 0 and percentile 50, percentile 1 and percentile 51, up to percentile 51 and percentile 100. GP distributions were then adjusted to each subset of active fires and plots were made of estimated values of shape (α) and scale (σ) parameters versus the mean value of FWI in the considered range. An example of such a plot is shown in Figure 4.8, respecting to shrubland in the Iberian Peninsula. The presented plot is representative of all plots obtained and it is well apparent that α linearly decreases with increasing of FWI while σ linearly increases with increasing FWI. Moreover, values of α are always negative and therefore an upper limit of duration, given by $-\sigma/\alpha$, has to be imposed. A plot of the upper limit versus FWI is presented in Figure 4.9 and it may be noted that there seems to be no clear dependence of the upper limit on FWI.

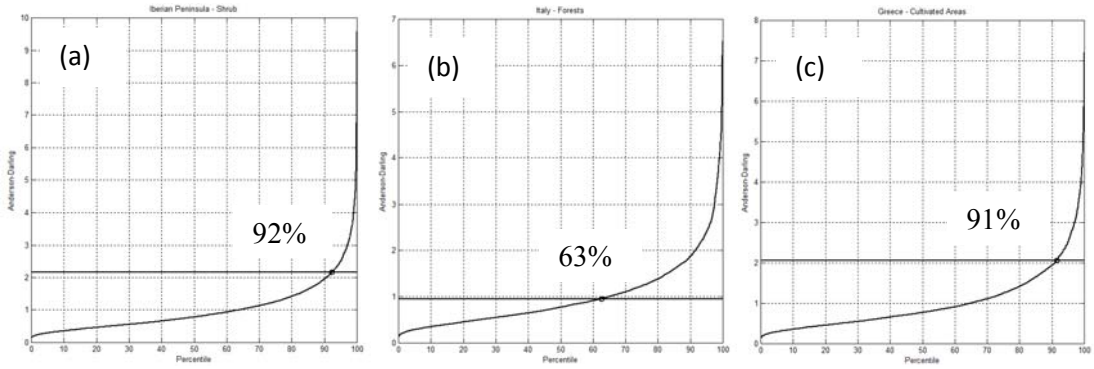

Figure 4.7. Significance levels of Anderson-Darling as derived from 5,000 uniform random samples, for (a) Iberian Peninsula and shrubland, (b) Italy and forests, (c) Greece and cultivated areas. Dots indicate obtained results from sample data and the respective confidence levels are shown in the boxes.

Assuming a linear dependence of shape α and scale σ on FWI and assuming that the ratio $-\sigma/\alpha$ is constant leads to the following improved model where FWI is a covariate of the two-parameter GP distributions:

$$\begin{cases} \alpha = A * FWI + B \\ \sigma = AF_{max} * (A * FWI + B) \end{cases} \quad (4.3)$$

where A and B are parameters to be estimated.

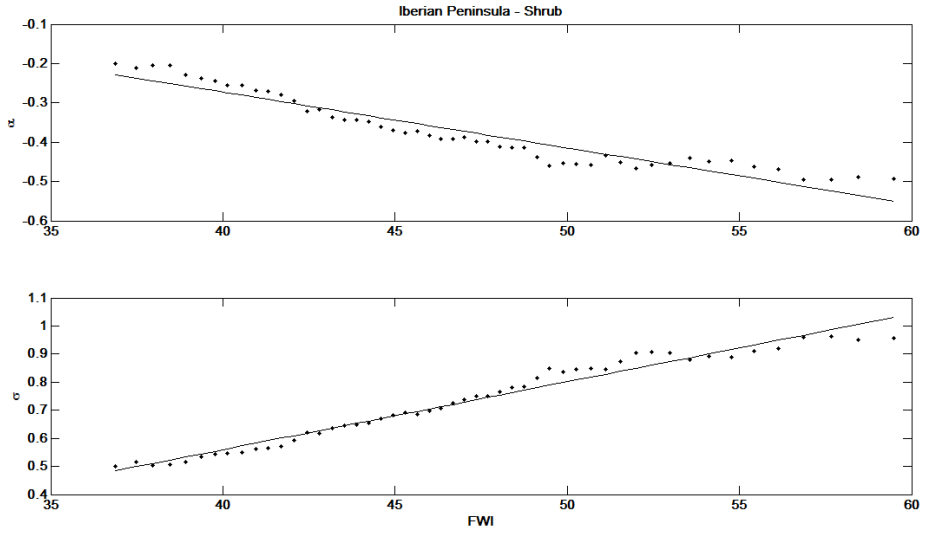

Figure 4.8. Dependence of α (upper panel) and σ (lower panel) on FWI, respecting to shrubland in the Iberian Peninsula.

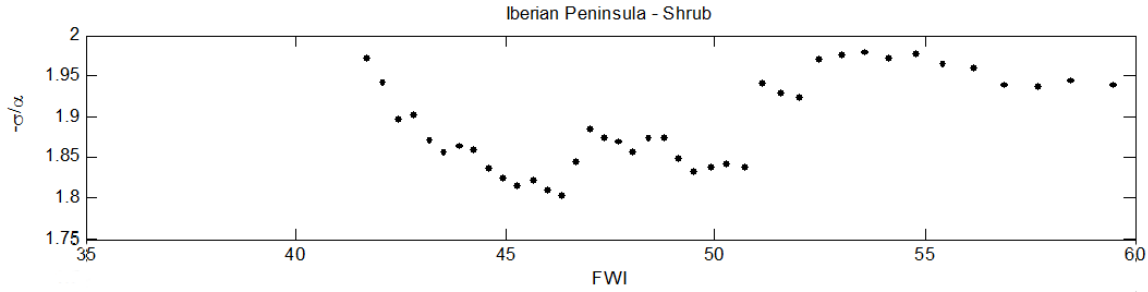

Figure 4.9. As in Figure 4.8 but respecting to the dependence of the ratio $-\sigma/\alpha$ on FWI.

The fit of the new models (using FWI as a covariate) may be compared against the respective models (that have no co-variate) by using the so-called standard likelihood ratio test, based on likelihood ratio statistic Λ defined by:

$$\Lambda = 2 * (L' - L) \qquad (4.4)$$

where L is the maximum likelihood function of the model with no-covariate and L' is the maximum likelihood function of the new model. The likelihood ratio test is used to compare the fit of two models, one of which is nested within the other and the likelihood ratio statistic Λ is asymptotically distributed as a χ^2_p with p degrees of

freedom. Obtained parameters for each region and land cover type are shown in Table 4.4, together with the values of Λ and respective p-values.

Table 4.4. Estimated values of the parameters when using GP with the co-variant FWI.

	(a) Iberian Peninsula		
Parameter	Forests	Shrub	Cultivated Areas
AF_{max}	88	108	56
A	0.0061	0.0044	0.0064
B	0.1506	0.1476	0.1400
Λ	8.53×10^{-10}	0.0012	1.93×10^{-7}
[p-value]	$[7.58\times10^{-14}]$	$[7.41\times10^{-7}]$	$[3.86\times10^{-11}]$

	(b) Italy		
Parameter	Forests	Shrub	Cultivated Areas
AF_{max}	37	38	31
A	0.0028	0.0061	0.0044
B	0.3409	0.2156	0.1163
Λ	0.4153	5.05×10^{-5}	7.13×10^{-11}
[p-value]	$[1.92\times10^{-5}]$	$[3.33\times10^{-16}]$	[0.0787]

	(c) Greece		
Parameter	Forests	Shrub	Cultivated Areas
AF_{max}	72	69	51
A	0.0098	0.0098	0.0110
B	0.1795	0.1344	-0.1294
Λ	6.58×10^{-8}	1.11×10^{-16}	9.55×10^{-15}
[p-value]	$[1.11\times10^{-16}]$	$[3.21\times10^{-5}]$	[0.07]

Figures 4.10 to 4.12 show examples of the impact of FWI on the density function (upper panels) and the cumulative density functions (lower panels) for the three types of vegetation in the Iberian Peninsula for the period July and August 2007-2009. Plots of the density and cumulative density functions are depicted corresponding to four different values of FWI, namely percentiles 5 and 95 and the values of first and third quartiles of the samples. The impact of FWI in increasing the probability of occurrence of active fires with high duration is well apparent. In fact, in all three regions and vegetation types, the probability of having fires greater than a pre-defined threshold increases with increasing FWI (Figures 4.13-4.15, left panels) and for pre-defined risks of fire occurrences, the duration of fires is larger for higher values of FWI (Figure 4.13-4.15, right panels).

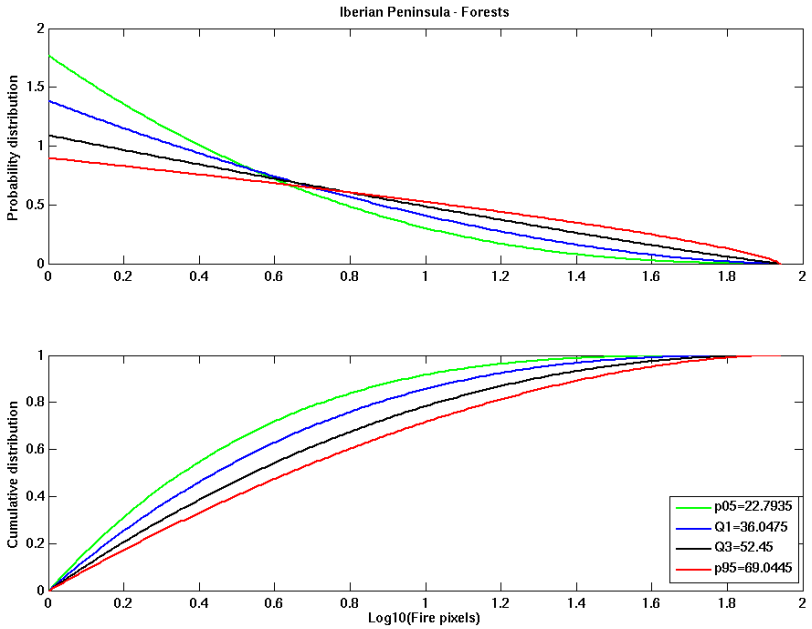

Figure 4.10. Probability density functions (upper panel) and cumulative density functions (lower panel) for the adjusted Pareto distribution using FWI as a covariate respecting to forests in the Iberian Peninsula for the period July and August 2007-2009. The four curves respect to different values of percentiles of FWI, namely percentile 5 (curve in green), first quartile (curve in blue), third quartile (curve in black) and percentile 95 (curve in red).

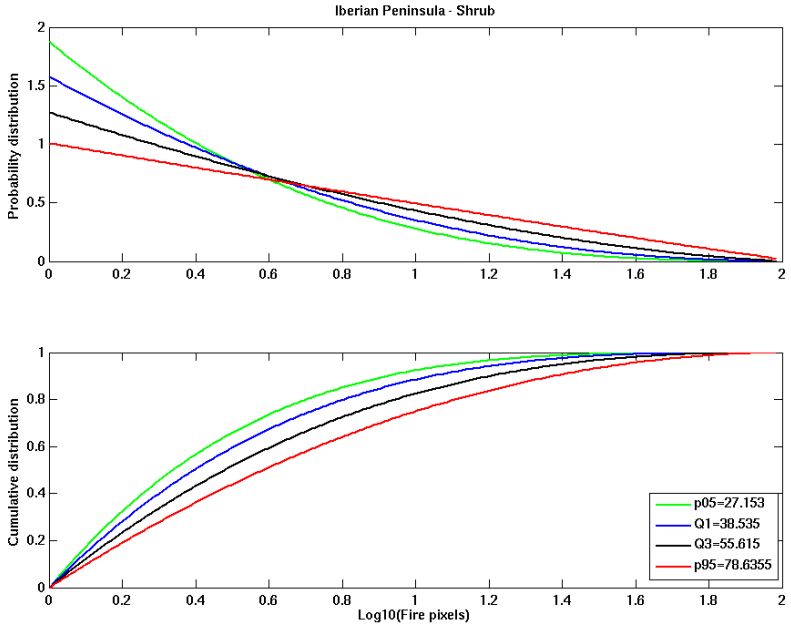

Figure 4.11. As in Figure 4.10 but respecting to shrub in the Iberian Peninsula.

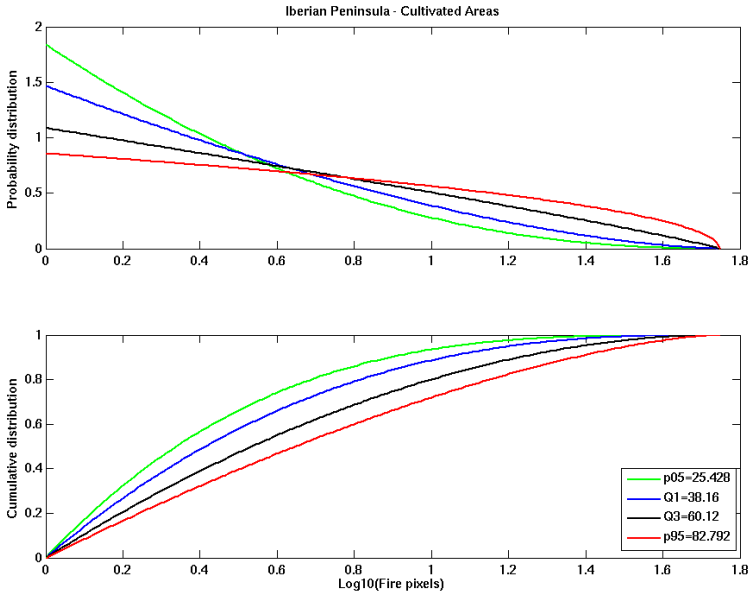

Figure 4.12. As in Figure 4.10 but respecting to cultivated areas in the Iberian Peninsula.

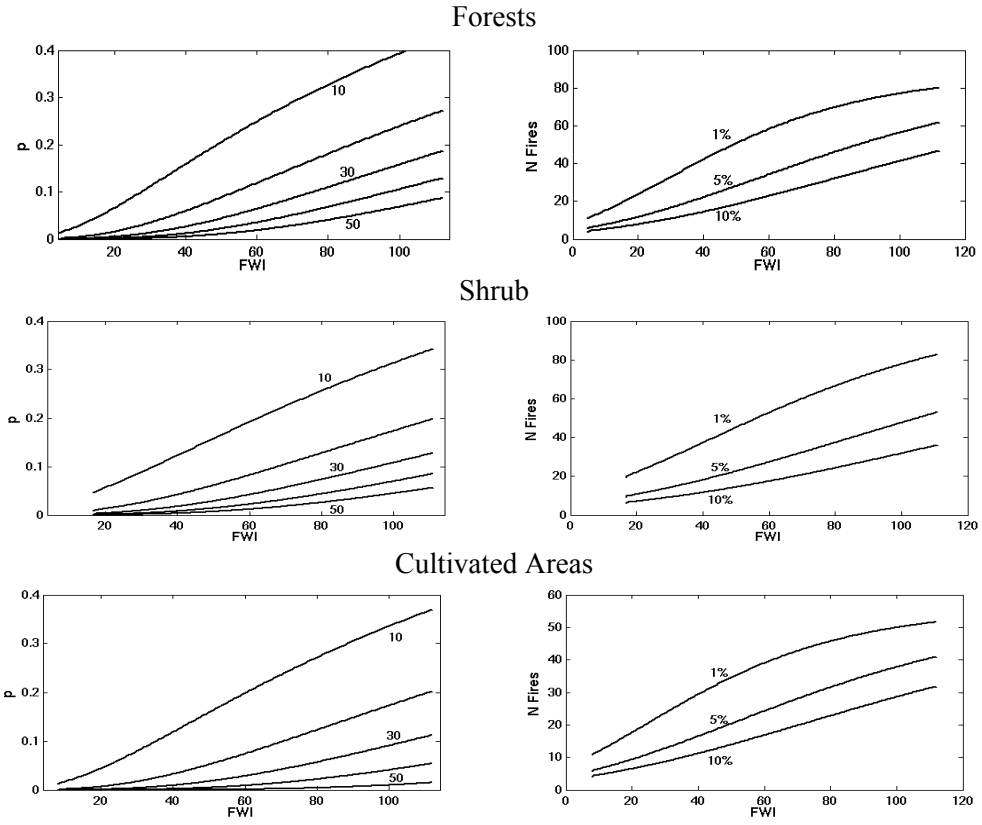

Figure 4.13. Dependence on FWI of probability of occurrence of active fires (left panels) larger than five selected thresholds (10, 20, 30, 40, 50) and number of active fires for three selected thresholds (1%, 5%, 10%) of risk (right panels) in the Iberian Peninsula.

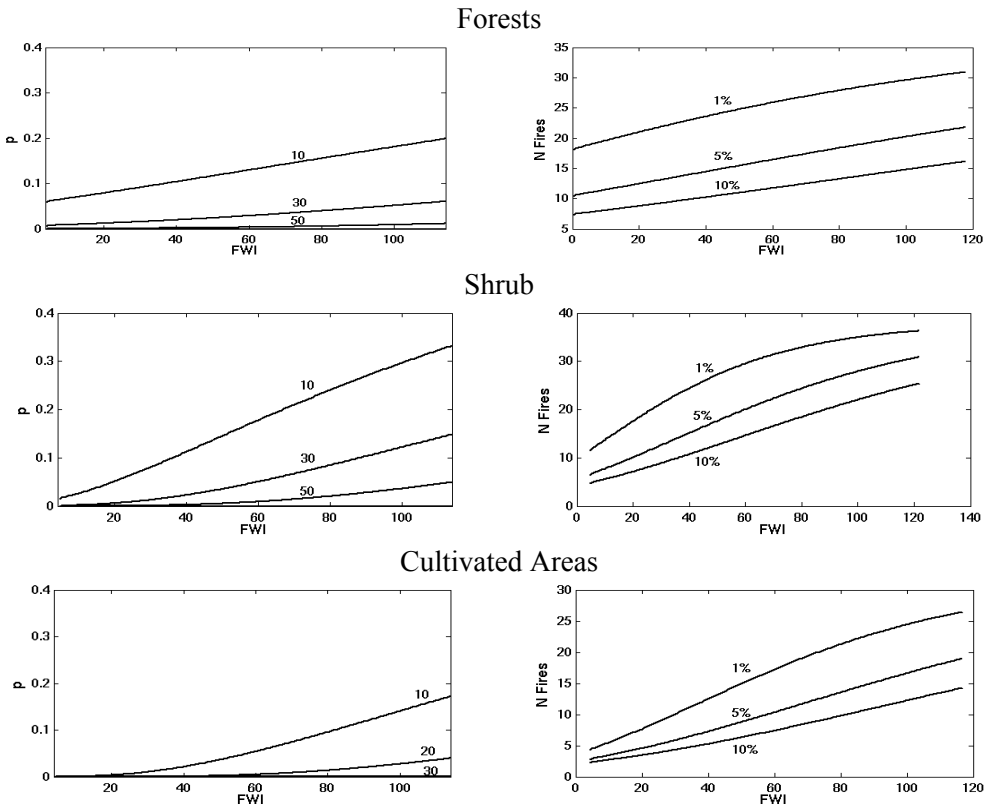

Figure 4.14. As in Figure 4.13 but respecting to Italy.

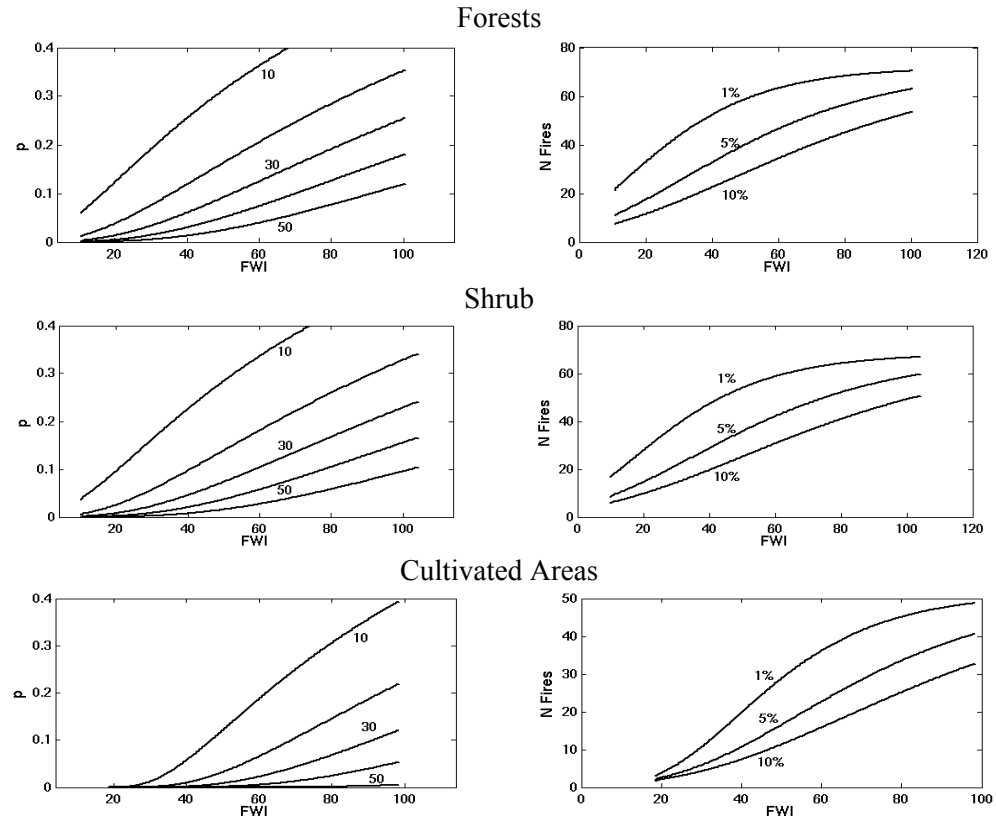

Figure 4.15. As in Figure 4.13 but respecting to Greece.

Results presented in Figures 4.13 to 4.15 allow producing daily charts of fire risk, *i.e.* of probability of occurrence of active fires with duration exceeding a prescribed threshold or charts with active fire duration associated to a prescribed risk level. Figures 4.16-4.18 (Figures 4.19-4.21) present examples of the former type (latter type) of charts, respectively for the Iberian Peninsula, Italy and Greece. It is worth noting that the impact of FWI may be qualitatively assessed by comparing the charts with the corresponding ones of vegetation cover (Figure 4.3) since the models that do not use FWI as a covariate would lead to constant values over each type of vegetation.

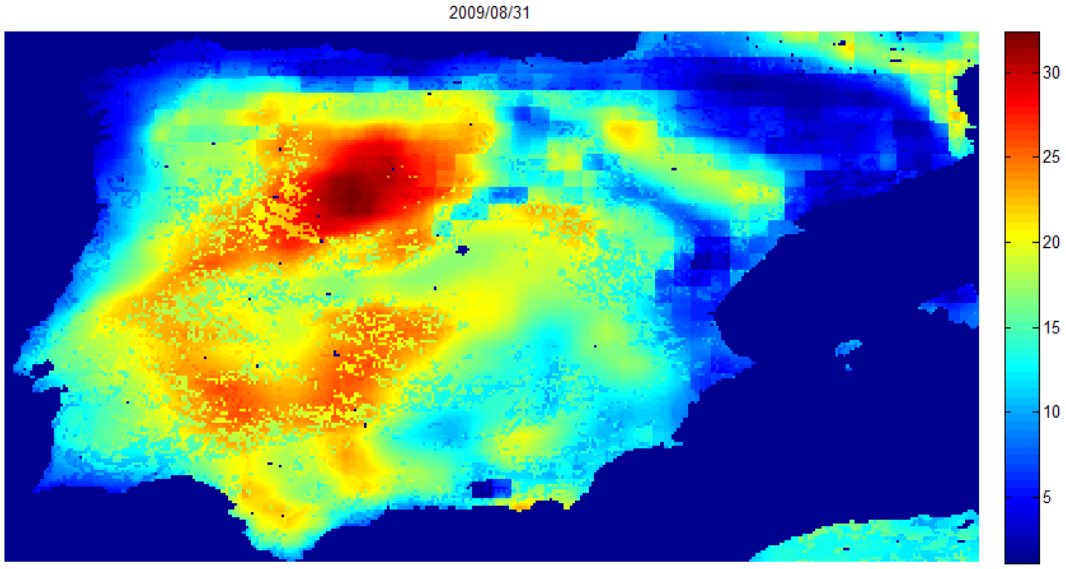

Figure 4.16. Risk of occurrence of active fires with a duration exceeding than 10 MSG slots (*i.e.* 2.5 hours), in the Iberian Peninsula on August, 31 2009.

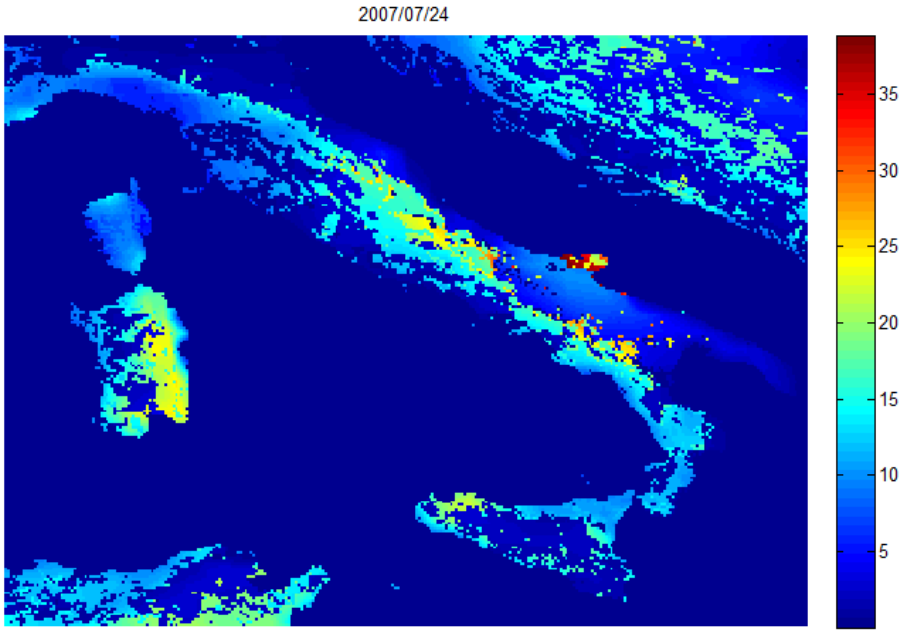

Figure 4.17. As in Figure 4.16 but for Italy on July, 24 2007.

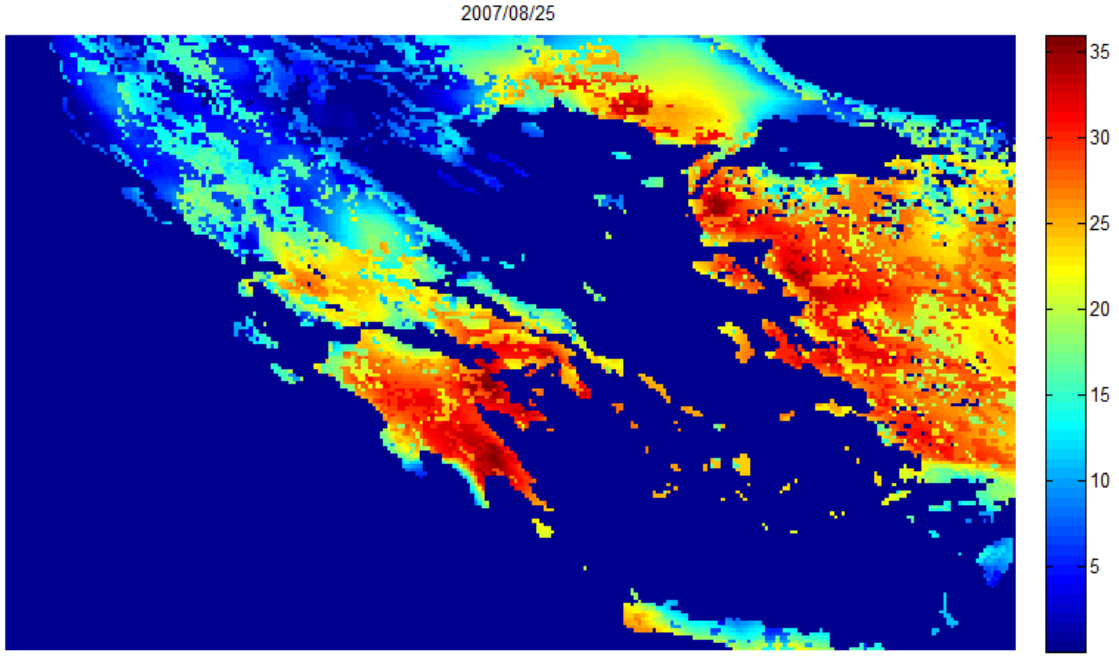

Figure 4.18. As in Figure 4.16 but for duration exceeding than 20 MSG slots (*i.e.* 5 hours), for Greece on August, 28 2007.

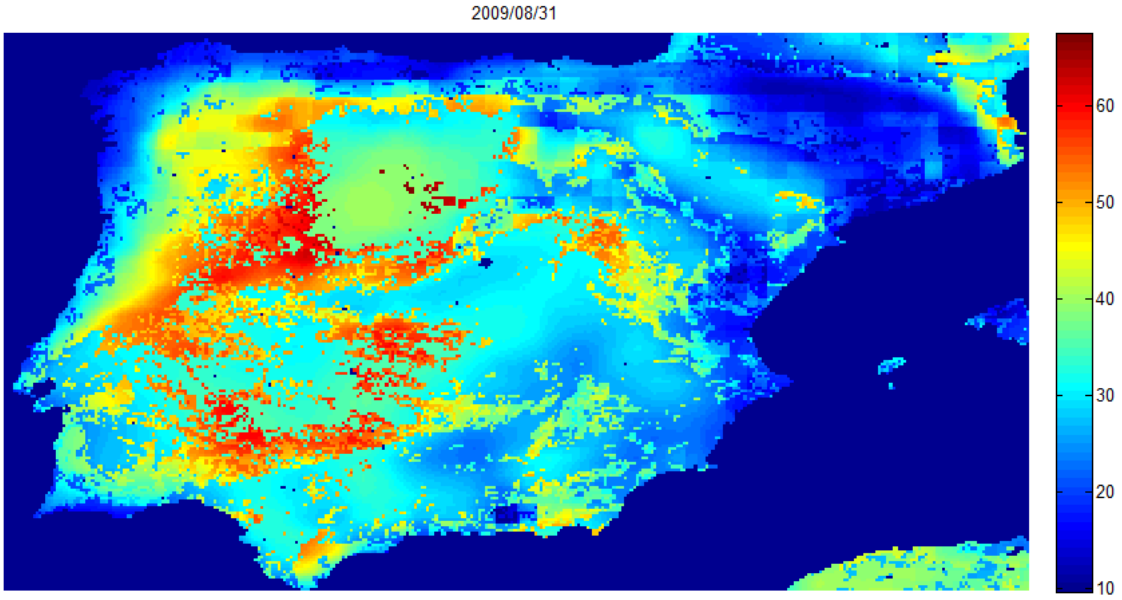

Figure 4.19. Active fire duration (in MSG slots) associated to a risk of occurrence of 1% in the Iberian Peninsula on August, 31 2009.

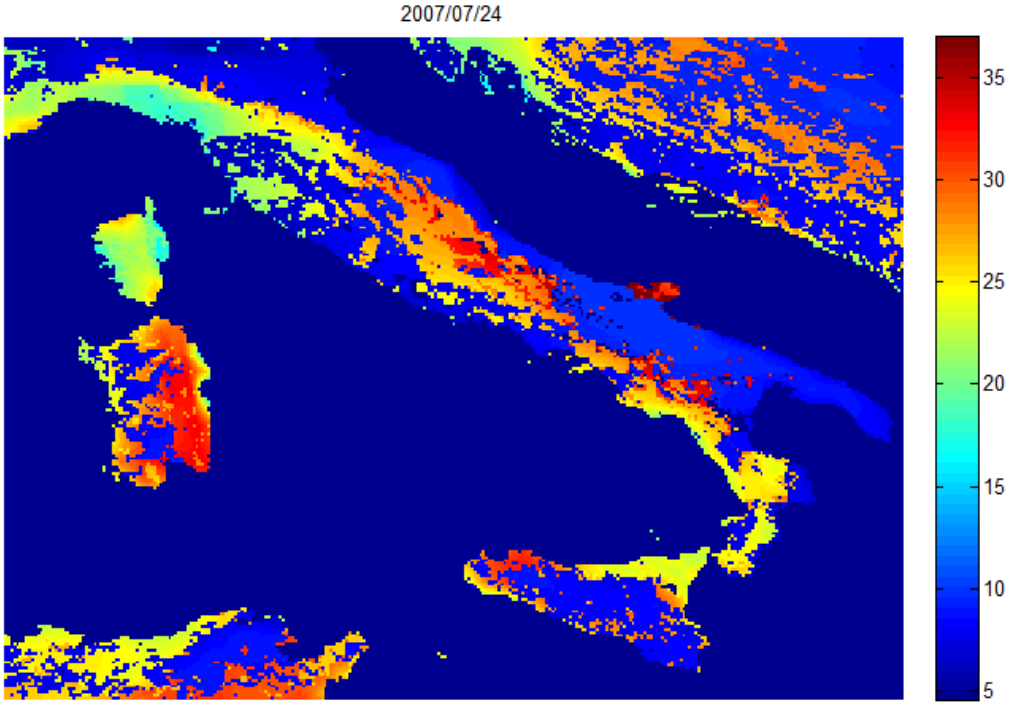

Figure 4.20. As in Figure 4.19 but for Italy on July, 24 2007.

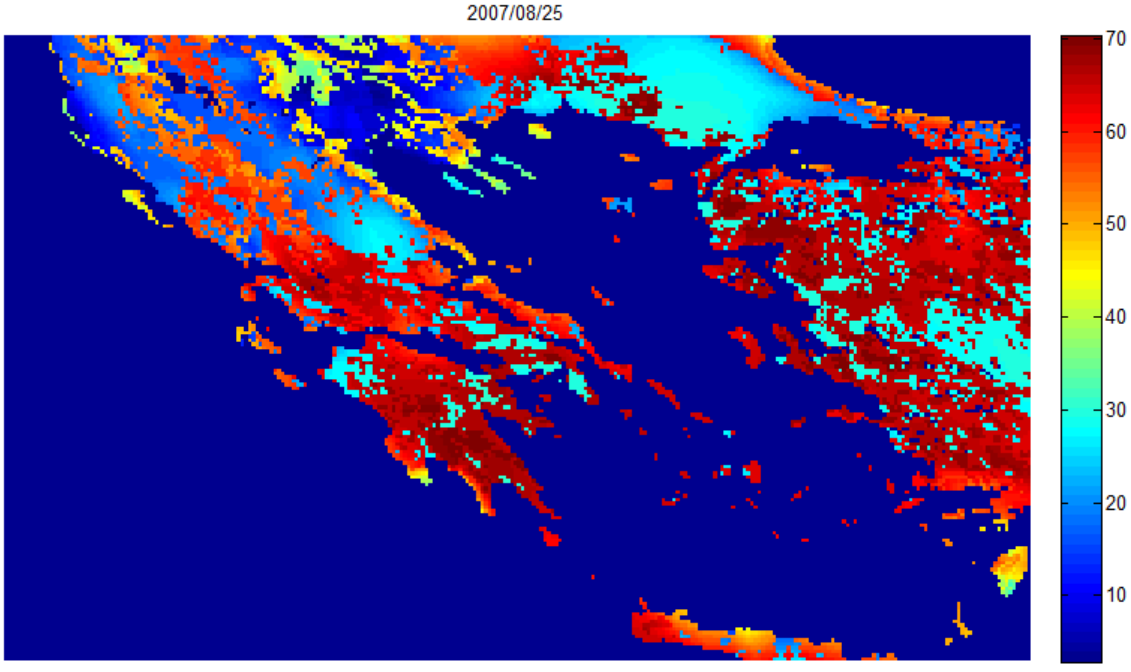

Figure 4.21. As in Figure 4.19 but for Greece on August, 28 2007.

IV. Discussion and concluding remarks

As already mentioned, the aim of the present work is to build on operational basis daily maps of fire risk for three regions of Mediterranean Europe, taking into account vegetation types and meteorological factors. Results obtained in the previous section clearly suggest that statistical models based on two-parameter Generalized Pareto (GP) distributions adequately fit the observed samples of duration of active fires and that these models are significantly improved when FWI is used as a covariate to model both the shape (α) and scale (σ) parameters of the GP distributions.

Coherent classes of fire risk in what respects to geographical location, vegetation type and meteorological conditions may be derived from obtained results by:

1) relying on the derived GP models (not using FWI as a co-variate) derived for each region and vegetation type to estimate a "reference value" of active fire duration associated to a common prescribed value of "background" risk;

2) using the GP models (integrating FWI as a co-variate) for each region, vegetation type and considered day to estimate the risk departure from the "background" due to meteorological factors.

Table 4.5 presents, for each region and vegetation type, the "reference values" obtained of duration of active fires when considering a "background risk" of 25%. Based on these "reference" values, a large set of maps of departures of risk was produced for different days associated to a wide range of meteorological conditions.

Table 4.5. Reference values of duration of active fires associated to a common "background" risk of 25%.

	Duration of active fires (in MSG slots)		
	Forest	Shrubland	Cultivated areas
Iberian Peninsula	7	6	7
Italy	5	7	3
Greece	18	16	8

Obtained results led to the definition of five classes of fire risk (Table 4.6), respectively referred to as of "very low", "low", "moderate", "high", and "very high" risk. For instance, in the case of Greece, if the risk of active fires lasting more than 18 MSG slots in forest, 16 slots in shrubland or 8 slots in cultivated areas is lower than 1% then the risk is very low, if the risk is in the range [1, 5[% then the risk is low, if the risk is in the range [5, 10[% then the risk is moderate, if the risk is in the range [10, 20[% then the risk is high and finally, if the risk is higher than 20 then the risk is very high. It may be noted that, as expected, the limits between classes of risk differ from region to region.

Table 4.6. Classes of fire risk and respective levels of risk, R (%) of exceeding the "reference values" of duration associated to the "background" risk of 25% (as shown in Table 4.5).

Class of Risk	Iberian Peninsula R (%)	Italy R (%)	Greece R (%)
Very Low	$R < 8$	$R < 8$	$R < 1$
Low	$8 \leq R < 13$	$8 \leq R < 15$	$1 \leq R < 5$
Moderate	$13 \leq R < 20$	$15 \leq R < 20$	$5 \leq R < 10$
High	$20 \leq R < 27$	$20 \leq R < 27$	$10 \leq R < 20$
Very High	$R > 27$	$R > 27$	$R > 20$

Examples of obtained maps of fire risk are shown in Figures 4.22 to 4.25 and the good agreement between duration of fire occurrences and classes of fire risk is worth being stresses. In fact, visual inspection of the distribution of observed fires and respective duration in the three study regions, namely over the zoomed areas, clearly reveals that the fires with higher duration (higher number of active fires) restrict to regions of high meteorological risk.

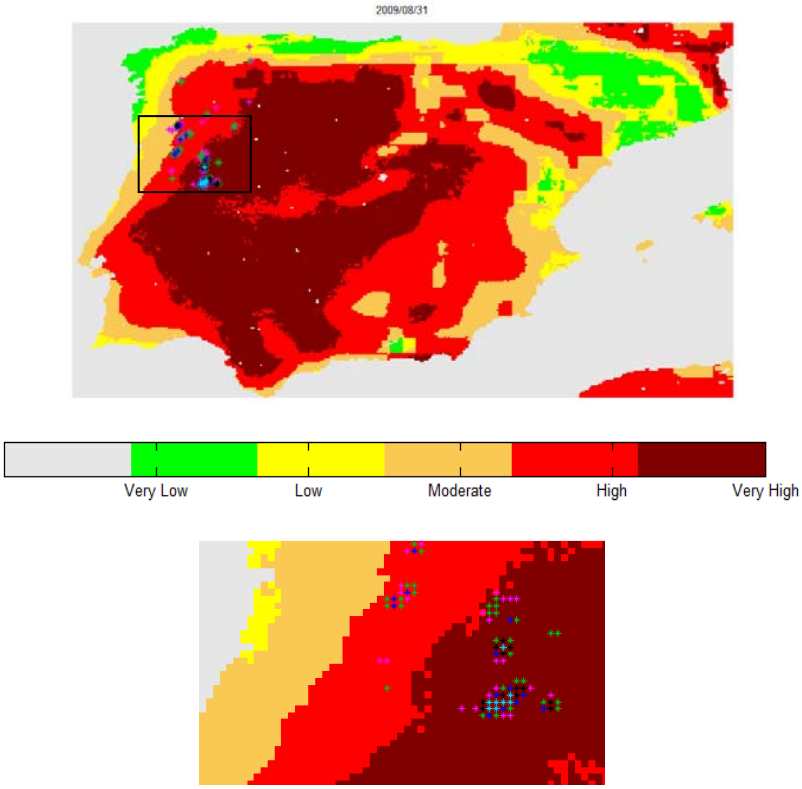

Figure 4.22. Map of classes of fire risk for the Iberian Peninsula on August 25 2007. Green, yellow, orange, red and brown respectively identify pixels belonging to classes of very low, low, moderate, high and very high risk of fire. Coloured asterisks respect to observed active fires, as obtained from the FD&M product, with duration less or equal than 2 MSG slots (pink asterisks), greater than 2 and less or equal than 10 slots (green asterisks), greater than 10 and less or equal than 20 slots (blue asterisks), greater than 20 and less or equal 30 slots (black asterisks) and greater than 30 slots (cyan asterisks). The lower panel is a zoomed view of the area identified by the black frame in the upper panel.

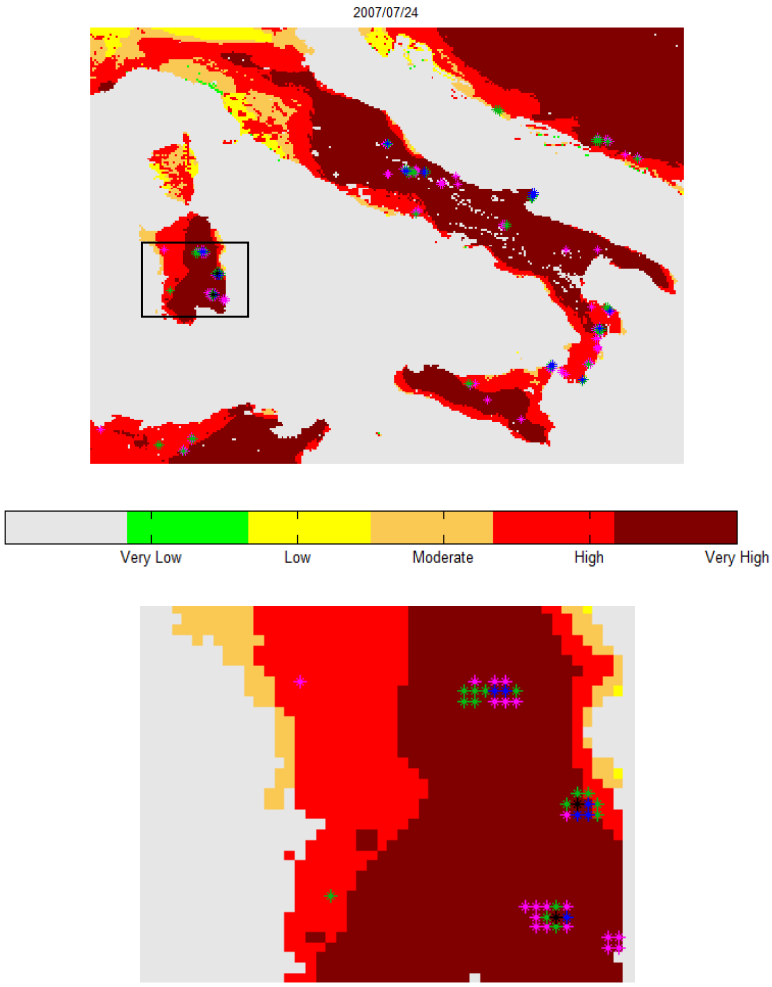

Figure 4.23. As in Figure 4.22, but for Italy on July 24 2007.

A quantitative validation of obtained results is provided in Tables 4.7 to 4.9 which show the distribution of duration of observed fires during the entire considered period of July-August 2007-2009, for the three considered geographical regions. All three regions present an overall similar behaviour, with a virtual absence of fire occurrences of large duration in the classes of very low and low risk of fire. On the other hand, fires of small duration concentrate in the classes of moderate, high and very high risk and there is a displacement of the modal class towards classes of higher risk with increasing duration.

It is therefore well apparent that the defined classes of fire risk constitute useful information for wildfire management, in particular for fire prevention. The proposed methodology has the advantage of relying on information on active fires as detected by remote sensing instruments, which makes the estimation of fire risk easily updated and tuned on a continuous basis. The procedure is currently running in the parallel chain of the LSA SAF System and will be operationally run in the very nearby future.

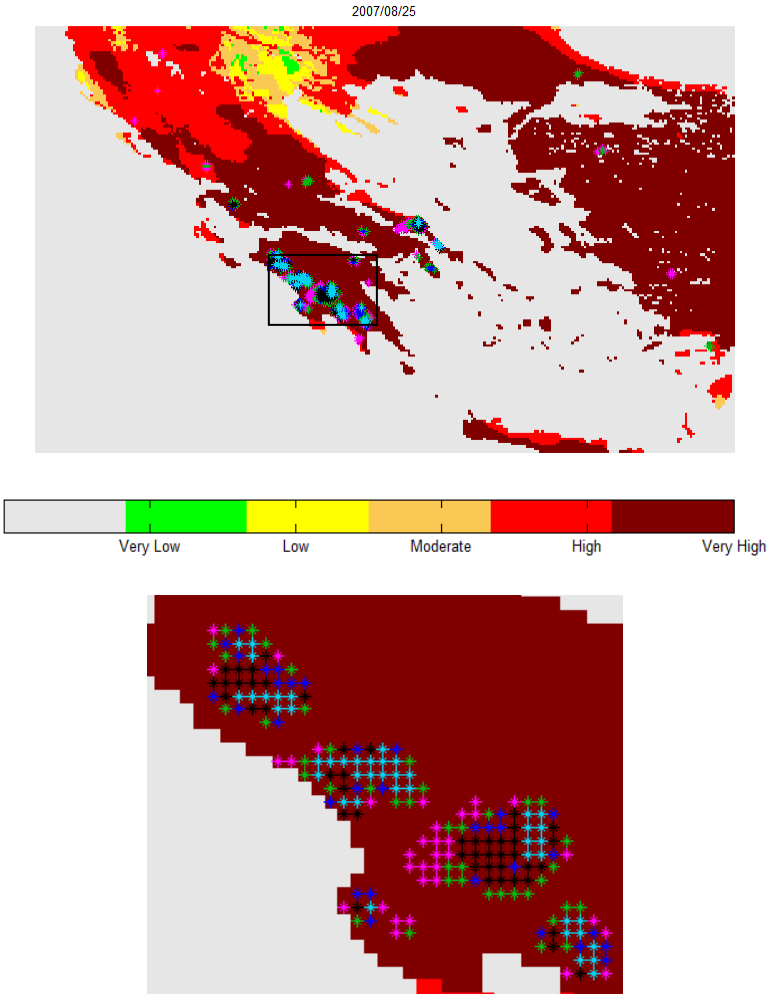

Figure 4.24. As in Figure 4.22, but for Greece on August 25 2007.

Table 4.7. Distribution of duration of observed active fires in the Iberian Peninsula among the five classes of fire risk, during the entire considered period of July-August 2007-2009. Each cell presents the number of observed fire events and the respective percentage (in brackets).

	Iberian Peninsula (2007-2009)				
	Classes of Risk				
Duration [MSG slots]	Very low	Low	Moderate	High	Very High
]0,2]	11	46	234	515	338
[%]	[1]	[4]	[20]	[45]	[29]
]2,10]	7	20	94	292	310
[%]	[1]	[3]	[13]	[40]	[43]
]10,20]	0	1	39	69	113
[%]	[0]	[0]	[17]	[31]	[51]
]20,30]	0	0	11	32	39
[%]	[0]	[0]	[13]	[39]	[47]
>30	0	0	2	12	29
[%]	[0]	[0]	[5]	[28]	[37]

Table 4.8. As in Table 4.7 but respecting to Italy.

	Italy (2007-2009)				
	Classes of Risk				
Duration [MSG slots]	Very low	Low	Moderate	High	Very High
]0,2]	5	75	270	520	236
[%]	[0]	[7]	[24]	[47]	[21]
]2,10]	1	16	72	288	158
[%]	[0]	[3]	[13]	[54]	[29]
]10,20]	0	3	12	49	57
[%]	[0]	[2]	[10]	[40]	[47]
]20,30]	0	0	2	8	11
[%]	[0]	[0]	[9]	[38]	[52]
>30	0	0	1	3	0
[%]	[0]	[0]	[25]	[75]	[0]

Table 4.9. As in Table 4.7 but respecting to Greece.

	Greece (2007-2009)				
	Classes of Risk				
Duration [MSG slots]	Very low	Low	Moderate	High	Very High
]0,2]	2	19	47	186	349
[%]	[0]	[2]	[8]	[31]	[58]
]2,10]	0	10	19	168	394
[%]	[0]	[2]	[3]	[28]	[67]
]10,20]	0	1	8	56	215
[%]	[0]	[0]	[3]	[20]	[77]
]20,30]	0	2	0	19	165
[%]	[0]	[1]	[0]	[10]	[89]
>30	0	0	0	3	134
[%]	[0]	[0]	[0]	[2]	[98]

Acknowledgements

The work was partly supported by the Portuguese Science Foundation (FCT) through project FLAIR (PTDC/AAC-AMB/104702/2008). FCT has also supported the research performed by the third author (Grant No. SFRH/BD/36964/2007). Part of the work was also supported by the framework of the Project Satellite Application Facility on Land Surface Analysis (LSA SAF).

References

Alexander, M.E., and Lanoville, R.A., 1989. Predicting Fires Behaviour in the Black Spruce-Lichen Woodland Fuel Type of Western and Northern Canada. For. Can., North. For. Cent., Edmonton, Albert and Gov. Northwest Territ., Dep. Renewable Resor., Territ. For. Fire Cent., Fort Smith, Northwest Territories.

Amraoui, M., DaCamara, C.C., and Pereira, J.M.C., 2008. Fire detection and monitoring over Africa. 2008 EUMETSAT Meteorological Satellite Conference, Darmstadt, Germany, 08 - 12 September. EUMETSAT P.52, ISBN 978-92-9110-082-8.

Amraoui, M., DaCamara, C.C., and Pereira, J.M.C., 2010. Detection and monitoring of African vegetation fires using MSG-SEVIRI imagery. Remote Sensing of Environment, 114, 1038-1052.

Barbosa, P., Amatulli, G., Boca, R., Camia, A., Kucera, J., Libertà, G., San-Miguel Ayanz, J., Schmuck, G., Schulte, E., and Dierks, H.-H., 2007. Forest Fires in Europe 2006. EUR 22931 EN – Joint Research Centre – Institute for Environment and Sustainability, Luxembourg: Office for Official Publications of the European Communities, EUR – Scientific and Technical Research series – ISSN 1018-5593.

Bovio, G., and Camia, A., 1997. Meteorological Indices for Large Fires Danger Rating. In: "A review of remote sensing methods for the study of large wildland fires", Ed. by E. Chuvieco, Megafires Project ENV-CT96-0256, Alcalà de Henares (Spain), 73-90.

DaCamara, C.C., Calado, T.J., Amraoui, M., and Pereira, J.M.C, 2007. The SAF for Land Surface Analysis: wildfire applications. 2007 EUMETSAT Meteorological Satellite Conference and the 15th Satellite Meteorology & Oceanography Conference of the American Meteorological Society, Amsterdam, Netherlands, 24 - 28 September. EUMETSAT P.50, ISBN 92-9110-079-X.

Deeming, J.E., Lancaster, J.W., Fosberg, M.A., Furman, R.W., and Shroeder, M.J., 1972. The National Fire Danger Rating System. USDA Forest Service, Rocky Mountain Forest and Range Experiment Station, Research paper RM-84, Ft. Collins, Colorado, 165 pp.

Deeming, J.E., Burgan, R.E., and Cohen, J.D., 1977. The National Fire Danger Rating System – 1978. Gen. Tech. Rep. INT-39 USDA Forest Service; Intermountain Forest and Range Experiment Station, Ogden, Utah, 63 p.

Dickinson, R.E., 1983. Land-surface processes and climate, surface albedos and energy balance. Advances in Geophysics 25: 305–353.

Ferranti, L., and Viterbo, P., 2006. The European summer of 2003: sensitivity to soil water initial conditions. J. Climate, 19, pp 3659-80.

Forestry Canada Fire Danger Group, 1992. Development and structure of the Canadian Forest Fire Behaviour Prediction system. Information Report ST-X-3. forestry Canada. Science and Sustainable Development Directories. Ottawa.

Haines, D.A., 1988. A lower atmosphere severity index for wildland fires. National Weather Digest, 13, 23-27.

Helms, J.A., 1988. The dictionary of forestry. The society of American Foresters, Bethesda, MD.

Hernandez-Leal, P.A., Arbelo, M., and Gonzalez-Calvo, A., 2004. Fire risk assessment using satellite data. Advances in space Research, 741-746. Elsevier.

Kotz, S., Johnson, N.L., and Read, C.B., (eds.), 1982. Encyclopedia of statistical Sciences, Vol. 1, John Wiley and Sons, New York.

Lynham, T.J., Stocks, B.J., 1989. Suitability of the Canadian Forest Fire Danger Ranting System for Use in the Daxingangling Forestry Management Bureau Heilongjiang Province, China. 10th Conference on Fire and Forest Meteorology, Ottawa, Canada.

Mitchell, K. E., Lohmann, D., Houser, P.R., Wood, E.F., Schaake, J.C., Robock, A., Cosgrove, B.A., Sheffield, J., Duan, Q., Luo, L., Higgins, R.W., Pinker, R.T., Tarpley, J.D., Lettenmaier, D.P., Marshall, C.H., Entin, J.K., Pan, M., Shi, W., Koren, V., Meng, J., Ramsay, B.H., and Bailey, A.A., 2004. The multi-institution North American Land Data Assimilation System (NLDAS): Utilizing multiple GCIP products and partners in a continental distributed hydrological modelling system. Journal Of Geophysical Research-Atmospheres, 109, D07S90, 32 pp. doi:10.1029/2003JD003823

Palheiro, P.M., Fernandes, P., and Cruz, M.G., 2006. A fire behaviour-based fire danger classification for maritime pine stands. In D.X. Viegas (Ed.), Comparison of two approaches. V International Conference on forest Fire Research, Elsevier.

Pereira, J.M.C., and Govaerts, Y., 2001. Potential fire applications from MSG/SEVIRI observations. EUMETSAT Programme Development Department, Technical Memorandum No. 7.

Pereira, J.M.C., Carreiras, J.M.B., Silva, J.M.N., and Vasconcelos, M.J., 2006. Alguns conceitos básicos sobre os fogos rurais em Portugal. In: Pereira, J.S., Pereira, J.M.C., Rego, F.C., Silva, J.M.N., Silva, T.P. (Eds.), Incêndios Florestais em Portugal – Caracterização, Impactes e Prevenção (pp 133-161). ISA Press.

Pyne, S.J., 2006. Fogo no jardim: compreensão do contexto dos incêndios em Portugal. In: Pereira, J.S., Pereira, J.M.C., Rego, F.C., Silva, J.M.N., Silva, T.P. (Eds.), Incêndios Florestais em Portugal – Caracterização, Impactes e Prevenção (pp 115-131). ISA Press.

Stocks, B.J., Lawson, B.D., Alexander, M.E., VanWagner, C.E., McAlpine, R.S., Lynham, T.J., and Dubé, D.E., 1989. The Canadian Forest Fire Danger Rating System: and overview. Forestry Chronicle, 65(6):258-265.

Trigo, I.F., DaCamara, C.C., Viterbo, P., Roujean, J.-L., Olesen, F., Barroso, C., Camacho-de-Coca, F., Carrer, D., Freitas, S.C., García-Haro, J., Geiger, B., Gellens-Meulenberghs, F., Ghilain, N., Meliá, J., Pessanha, L., Siljamo, N., Arboleda, A., 2010. The Satellite Application Facility on Land Surface Analysis. International Journal of Remote Sensing, In Press.

van Wagner, C.E., 1987. Development and structure of the Canadian Forest Fire Index System. Canadian Forestry Service, Ottawa, Ontario, Forestry Technical Report 35, 37 pp.

Ventura, J., and Vasconcelos, M.J., 2006. O fogo como processo físico-químico e ecológico. In: Pereira, J.S., Pereira, J.M.C., Rego, F.C., Silva, J.M.N., Silva, T.P. (Eds.), Incêndios Florestais em Portugal – Caracterização, Impactes e Prevenção (pp 93-113). ISA Press.

Viegas, D.X., Reis, R., Cruz, M.G., and Viegas, M.T., 2004. Calibração do Sistema Canadiano de Perigo de Incêndio para aplicação em Portugal. Silva Lusitana, 12(1):77-93.

Wilks, D.S., 1995. Statistical methods in the atmospheric sciences: an introduction. Academic Press, 464 pp.

CHAPTER 5: General Conclusions

Detection of fire activity has long been identified as a task with great potential to be derived either from polar-orbiters or from geostationary satellites. However, one of the major constraints in monitoring the vegetation fires over Europe and Africa was the lack of high frequency observations combined with high or coarse spatial resolution. In fact, geostationary meteorological satellite systems provide much higher frequency of observation of the land surface than sun-synchronous systems but, until recently, their spatial and spectral resolutions were sub-optimal for vegetation fire monitoring. New possibilities were opened up with the launch in 2002, by ESA in cooperation with the EUMETSAT, of Meteosat-8, the first satellite of the MSG series. Temporal, spatial and spectral characteristics of the MSG series were substantially improved, rendering its satellites very adequate for Earth surface observation, and namely for fire detecting and monitoring over Africa and Europe. The benefit results not only from the spectral and temporal capability of SEVIRI, but also from the MSG ground segment infrastructure that allows the dissemination in near real-time of products derived from combination of meteorological observations, forecast data and SEVIRI observations.

This research exploits the potential of Meteosat-8/SEVIRI for fire applications. First of all, a contextual algorithm (FiDAlgo) was developed for detecting active fires over Africa and Europe, using information provided by MSG at the maximum temporal resolution. The procedure is closely related with one of the activities developed within the framework of EUMETSAT's LSA SAF, the so-called Fire Detection and Monitoring (FD&M) product.

The spatial and temporal distributions of active fires over Africa and Europe as obtained from FD&M product, together with the obtained characteristics of fire incidence by land cover class showed a very good agreement with findings in previous works, namely Barbosa *et al.* (1999), Tansey, Grégoire, Stroppiana *et al.* (2004a) and Tansey, Grégoire, Binaghi *et al.* (2004b).

The duration of active fires in NAfr, SAfr windows and in Southern Europe was investigated. The high temporal resolution of SEVIRI allows investigating whether the temporal organization of active fires tends to follow a power-law distribution. In fact, the duration of active fires in all regions tends to follow two-parameter generalized Pareto distributions, with both the scale and the shape parameters presenting very similar values for NAfr and SAfr. The obtained results are consistent with the finding by Malamud *et al.* (1998) and Reed and McKelvey (2002).

An analysis of the daily cycle of the median of fire activity was also performed in two regions, respectively located in northern and southern hemisphere Africa, respectively during January and July 2007. The added value brought by the increased temporal resolution of the SEVIRI sensor is well apparent, especially when compared with the poorer sampling by polar-orbit sensors such as MODIS that may lead to severe biases when characterising the daily cycle of fire activity. In agreement with the findings by Roberts and Wooster (2007), the daily cycle of active fires presents a slightly asymmetric distribution in both regions, with a steeper increase before the maximum

and a slower decrease during the afternoon. Nevertheless there is virtually no fire activity between midnight and 08:00.

The very different sampling of the diurnal cycles of active fires provided by SEVIRI and MODIS severely impairs any attempt to make a direct comparison between information provided by the two sensors. A different approach was accordingly adopted which consisted in subdividing the study area and period in space-time blocks of N SEVIRI pixels×N SEVIRI pixels×T days, and then adjusting linear models that relate fire counts over each block as obtained from FiDAlgo with corresponding numbers from the MODIS active fire database. Results obtained with FiDAlgo matched well those from the MODIS fire product when adequate spatial and temporal scales are chosen.

The role of meteorological conditions on large fire events over Mediterranean Europe, as obtained by FD&M product, was assessed by studying two extreme events of fire activity, respectively on July 24-25 and August 22-27, 2007 that stroke Italy and the Balkan Peninsula. Structural similarities in the atmospheric circulation and the thermo-hydrodynamic processes between the two periods were found that allow inferring a conceptual model for meteorological conditions strongly favouring the occurrence of severe wildfire episodes in Italy and the Balkan Peninsula. According to the proposed model which is in close agreement with the results of Xoplaki *et al.* (2003) and with the findings of Founda and Giannakopoulos (2009) for the summer 2007, there is, on the one hand, strong northerly advection at the surface of very hot and very dry air over the region. As suggested by the composites of sea-level pressure, 2m-temperature and 10m-wind, the northerly flow is steered by the presence of a ridge over central Europe together with a thermal depression over southwest Asia. On the other hand, the advected air is further heated by adiabatic compression associated to strong subsidence from around 700 up to 250 hPa. As suggested by the composites of height fields at 850, 500 and 250 hPa as well as by the composites of temperature and relative humidity at 850 hPa and by the vertical profiles of temperature and dew point temperature, subsidence in the layer 800-500 hPa is related to the presence of a ridge over the Eastern Mediterranean, associated to a synoptic baroclinic wave. The anomalous displacement of the jet streak towards the northwest, as indicated by the composites of geopotential height and wind speed at 250 hPa, is associated to subsidence of air over the Eastern Mediterranean, which further contributes to the adiabatic heating.

The impact of synoptic conditions on meteorological fire risk was also assessed by analysing composite maps of weather-based indices, namely BUI, ISI and FWI that are part of CFFWIS. Regions of high values of FWI (and of extremely high anomalies) were found over the Balkan Peninsula and Italy, closely matching the areas of hot and dry air that resulted from the intense etesian or etesian-like winds and from enhanced subsidence. The fingerprint of short-term atmospheric conditions is well apparent in the composites of ISI, but the long-term contribution is also present as indicated by the positive anomalies of BUI. Fire events may also be observed in regions of high values

of BUI stressing the importance of long-term atmospheric conditions that lead to vegetation stress.

The problem of generating maps of fire risk over Mediterranean Europe was also investigated by developing and validated a procedure based on an integrated use of meteorological information from ECMWF forecasts, on vegetation land cover from GLC2000 and on occurrences of active fires as detected by MSG-SEVIRI. The obtained levels of fire danger are associated to probabilities of occurrence of fires exceeding specified magnitudes. The main difference of the adopted method when compared to other proposed ones is that it takes full advantage of the temporal resolution of SEVIRI that, by detecting fire events every 15 minutes, allows estimating the duration of active fires that is essential to determine classes of fire danger. Moreover, the use of satellite data prevents us from being dependent on the availability of ground fire records from each country.

During the period of July-August 2007-2009, it is shown that cultivated areas are the predominant vegetation type in all three considered regions but both forests and shrubland types, although occupying a much smaller amount of the territory, are associated to a larger percentage of fire events. Using maximum likelihood estimation, Generalized Pareto (GP) distributions were fitted to the samples of daily records of decimal logarithm of active fire duration during the period of July-August 2007-2009, for each Mediterranean region and type of land cover.

An improved model, using meteorological information, was then fitted to data, by assuming a linear dependence of the shape and scale parameters of the GP distributions on the Fire Weather Index (FWI). The impact of FWI in increasing the probability of occurrence of active fires with high duration is well apparent, the probability of having fires greater than a pre-defined threshold increasing with increasing FWI and for pre-defined risks of fire occurrences, the duration of fires being larger for higher values of FWI. Results obtained allowed producing daily charts of fire risk, *i.e.* of probability of occurrence of active fires with duration exceeding a prescribed threshold or charts with active fire duration associated to a prescribed risk level.

Coherent classes of fire risk in what respects to geographical location, vegetation type and meteorological conditions were accordingly derived by; 1) relying on the GP models (not using FWI as a co-variate) derived for each region and vegetation type to estimate a “reference value” of active fire duration associated to a common prescribed value of “background” risk and then 2) using the GP models (integrating FWI as a co-variate) for each region, vegetation type and considered day to estimate the risk departure from the “background” due to meteorological factors. A quantitative validation of obtained showed that the regions analysed present an overall similar behaviour, with a virtual absence of fire occurrences of large duration in the classes of very low and low risk of fire. On the other hand, fires of small duration concentrate in the classes of moderate, high and very high risk and there is a displacement of the modal class towards classes of higher risk with increasing duration. It is therefore well

apparent that the defined classes of fire risk constitute useful information for wildfire management, in particular for fire prevention.

Obtained results demonstrated that Meteosat-8 data allows detecting active fires and monitoring of fire dynamics from continental to regional scales and from diurnal cycles to inter-annual changes. The fire activity provided by the MSG series appears as a very appealing tool in assisting local authorities to better fulfil reporting obligations and more effectively managing natural resources. The major current challenge is the provision of a homogeneous, high quality, long-term data records of active fires, which will enable fire information to be used for many science applications including an improved characterization of fire regimes, land cover changes, ecosystem disturbance and emission studies (Csiszar *et al.*, 2005).

The development of the two above mentioned products (FD&M and FRM) represents a significant contribution to implement recommendations made by the Early Warning Programme, set up by the United Nations within the framework of the International Decade for Natural Disaster Reduction (Goldammer, 1997), and by the Disaster Management Support Group, of the Committee on the Earth Observation Satellites (CEOS/DMSG, 2000). Both of these organisations mention the capability of geostationary satellites to provide comprehensive global fire monitoring and assessment of biomass burning, and of its ecological, atmospheric, climatic and human health impacts (Pereira and Govaerts, 2001).

References (Introduction and Conclusions)

Agee, J.K., 1993. Fire Ecology of Pacific Northwest Forests. Washington, DC: Island Press.

Andreae M.O., 1991. Biomass burning: its history, use, and distribution and its impact on environmental quality and global climate. In: Global Biomass Burning. Atmospheric, Climatic, and Biospheric Implication. Ed. J.S. Levine. MIT Press, Cambridge, Massachusetts, 3-21.

Baker, W.L., 2009. Fire Ecology in Rocky Mountain Landscapes. Washington, DC: Island Press.

Barbosa, P.M., Stroppiana, D., Grégoire, J.-M., & Pereira, J.M.C. (1999). An assessment of vegetation fire in Africa (1981-1991): burned areas, burned biomass, and atmospheric emissions. *Global Biogeochemical Cycles, 13*, 933-950.

Benson, R.P., Roads, J.O., Wiese, D.R., 2009. Climatic and weather factors affecting fire occurrence and behaviour, in: Bytnerowicz, A., Arbaugh, M., Riebau, A., Andersen, C. (Eds.), Developments in Environment Science, 8, pp. 37-59. ISSN: 1474-8177, DOI: 10.1016/S1474-8177(08)00002-8

Bond, W.J., Keeley, J.E., 2005. Fire as a global "herbivore": the ecology and evolution of flammable ecosystems. Trends in Ecology & Evolution, 20, 287-394.

Brown, R.J.E., 1983. Effects of fire on the permafrost ground thermal regime. National Research Council Canada (pp. 17).

Bowman, D.M.J.S., Balch, J.K., Artaxo, P., Bond, W.J., Carlson, J.M., Cochrane, M.A., D'Antonio, C.M., DeFries, R.S., Doyle, J.C., Harrison, S.P., Johnston, F.H., Keeley, J.E., Krawchuk, M.A., Kull, C.A., Marston, J.B., Moritz, M.A., Prentice, I.C., Roos, C.I., Scott, A.C., Swetnam, T.W., van der Werf, G., Pyne, S.J., 2009. Fire in the Earth system. Science, 324 (5926), 481-484.

CEOS/DMSG, 2000. Fire Hazard Team Report. Disaster Management Support Group (DMSG), Committee on Earth Observation Satellites (CEOS). Available at: http://disaster.ceos.org/2000Ceos/progress/reports/pdf/fire.pdf

Chatfield, R.B., Vastano, J.A., Li, L., Sachse, G.W., Connors, V.S., 1998. The Great African plume from biomass burning: generalizations from a three-dimensional study of TRACE A carbon monoxide. Journal of Geophysical Research, 103 (D21), 28059-28077.

Csiszar, I., Denis, L., Giglio, L., Justice, C.O., Hewson, J., 2005. Global fire activity from two years of MODIS data. International Journal of Wildland Fire, 14, 117-130. doi: 10.1071/WF03078

DaCamara, C.C., Tavares, C.D., 2001. The SAF for Land Surface Analysis: its impacts on the NWP community. The 2001 EUMETSAT Meteorological Satellite Data User's Conference, Antalya, Turkey, 1-5 October 2001, EUMETSAT P.33, p. 420. ISBN 92-9110-044-7

DaCamara, C.C., 2006. The Land Surface Analysis SAF: one year of pre-operational activity. The 2006 EUMETSAT Meteorological Satellite Conference, Helsinki, Finland, 12-16 June 2006, EUMETSAT P.48, , 8pp. ISBN 92-9110-076-5. (available from http://www.eumetsat.int/Home/Main/Publications/index.htm).

Damoah, R., Spichtinger, N., Forster, C., James, P., Mattis, I., Wandinger, U., Beirle, S., Wagner, T., Stohl, A., 2004. Around the world in 17 days – hemispheric-scale transport of forest fire smoke from Russia in May 2003. Atmospheric Chemistry and Physics, 4, 1311-1321.

Dantonio, C.M., Vitousek, P.M., 1992. Biological invasions by exotic grasses, the grass fire cycle, and global change. Annual Review of Ecology and Systematics, 23, 63-87.

Flannigan, M.D., Krawchuck, M.A., de Groot, W.J., Wotton, B.M., Gowman, L.M., 2009. Implications of changing climate for global wildland fire. International Journal of Wildland Fire, 18, 483-507.

Founda, D., Giannakopoulos, C., 2009. The exceptionally hot summer of 2007 in Athens, Greece – A typical summer in the future climate. Global and Planetary Change, 67, 227-236.

Galanter, M., Levy II, H., Carmichael, G.R., 2000. Impacts of biomass burning on tropospheric CO, NOx and O3. Journal of Geophysical Research, 105, 6633-6653.

Goldammer, J.G., 1997. Report on Early Warning for Fire and Other Environmental Hazards. International Decade for Natural Disaster Reduction (IDNDR) Secretariat, United Nations, Geneva. Available at: http://wwwgfz-potsdam.de/ewc98/docs/reports/c-goldfire.pdf

Govaerts, Y.M., Pereira, J.M., Pinty, B., Mota, B., 2002. Impact of fire on surface albedo dynamics over the African continent. Journal of Geophysical Research, 107, D22, 4629. doi:10.1029/2002JD002388

Ito, A., Penner, J.E., 2004. Global estimates of biomass burning emissions based on satellite imagery for the year 2000. Journal of Geophysical Research, 109, D14S05. doi:10.1029/2003JD004423

Justice, C.O., Korontzi, S.A., 2001. A review of satellite fire monitoring and the requirements for global environmental change research. In: Global and regional vegetation fire monitoring from space: Planning a coordinated international effort. Ahern, F., Goldammer, J.G., Justice, C.O. (Eds.), pp. 1-18.

Justice, C.O., Giglio, L., Boschetti, L., Toy, D., Csiszar, I., Morisette, J., Kaufman, Y., 2006. MODIS fire products. Algorithm Technical Background Document, Version 2.3, October 2006, EOS ID#2741 (pp. 34).

Kafatos, M., Wang, X.S., Li, Z., Yang, R., Ziskin, D., 1998. Information technology implementation for a distributed data system serving earth scientists: seasonal to interannual ESIP. Proceedings of SSDBM.

Le Page, Y., Pereira, J.M.C., Trigo, R.M., DaCamara, C.C., Oom, D., Mota, B., 2008. Global fire activity patterns (1996-2006) and climatic influence: an analysis using the World Fire Atlas. Atmospheric Chemistry and Physics, 8, 1911-1924.

Levine, J.S., 1991. Global biomass burning: Atmospheric, climatic, and biospheric implications. Levine J.S. (Eds.), pp. 569. 0-262-12159-X

Levine, J.S., Bobbe, T., Ray, N., Witt, R.G., Singh, A., 1999. Wildland fires and the environment: A global synthesis. Eds. UNEP/DEIAEW/TR.99-1. 92-807-1742-1

Malamud, B.D., Morein, G., & Turcotte, D. L. (1998). Forest fires: An example of selforganized critical behavior. *Science, 281*, 1840-1842.

McCollum, J.R., Gruber, A., Ba, M., 2000. Discrepancy between gauges and satellite estimates of rainfall in equatorial Africa. Journal of Applied Meteorology, 39, 666-679.

Moritz, M.A., Morais, M.E., Summerell, L.A., Carlson, J.M., Doyle, J., 2005. Wildfires, complexity, and highly optimized tolerance. Proceedings of the National Academy of Sciences, 102, 17912-17917.

Muzy, A., Wainer, G., Innocenti, E., 2002. Comparing simulation methods for fire spreading across a fuel bed. Proceedings of AI, Simulation and Planning in High Autonomy Systems, vol. AIS'2002, pp. 219–224.

Parisien, M.A., Moritz, M.A., 2009. Environmental controls on the distribution of wildfire at multiple spatial scales. Ecological Monographs, 79, 127-54.

Pereira, J.M.C., Govaerts, Y., 2001. Potential fire applications from MSG/SEVIRI observations. EUMETSAT Programme Development Department, Technical Memorandum No. 7.

Pereira, M.G., Trigo, R.M., DaCamara, C.C., Pereira, J.M.C., Leite, S.M., 2005. Synoptic patterns associated with large summer forest fires in Portugal. Agricultural and Forest Meteorology. 129, 11-25.

Pyne, S., Andrews, P., Laven, R., 1996. Introduction to Wildland Fire. New York: Wiley.

Pyne, S.J., 2001. Fire: A brief history. Jeremy Mills Publishing (Eds.), pp. 204.

Pyne, S.J., 2006. Fogo no jardim: compreensão do contexto dos incêndios em Portugal. In: Pereira, J.S., Pereira, J.M.C., Rego, F.C., Silva, J.M.N., Silva, T.P. (Eds.), Incêndios Florestais em Portugal – Caracterização, Impactes e Prevenção, ISA Press, pp. 115-131.

Rasilla, D.F., García-Cordon, J.C., Carracedo, V., Concepción, D., 2010. Circulation patterns, wildfire risk and wildfire occurrence at continental Spain. Physics and Chemistry of the Earth, 35, 553-560.

Reed, W.J., & McKelvey, K. S. (2002). Power-law behavior and parametric models for the size-distribution of forest fires. *Ecological Modelling, 150*, 239-254.

Roberts, G., & Wooster, M.J. (2007). New perspectives on African biomass burning dynamics. *EOS, Transactions, American Geophysical Union, 88*, 369-370.

Roberts, G.J., Wooster, M.J., 2008. Fire detection and fire characterization over Africa using Meteosat SEVIRI. IEEE Transactions on Geoscience and Remote Sensing, 46, 1200-1218.

Rothermel, R.C., 1972. A mathematical model for predicting fire spread in wildland fuels. Ogden, UT, Research paper, INT-115. USDA Forest Service, Intermountain Research Station.

Scott, A.C., 2000. The pre-quaternary history of fire. Palaeogeography, Palaeoclimatology, Palaeoecology, 164, 281-329.

Schmetz, J., Pili, P., Tjemkes, S., Just, D., Kerkman, J., Rota, S., Ratier, A., 2002. An introduction to Meteosat Second Generation (MSG). Bulletin of the American Meteorological Society, 83, 977-992.

Tan, P.-N., Steinbach, M., Kumar, V., 2002. Finding spatio-temporal patterns in earth science data. NASA grant project, University of Minnesota.

Tansey, K.J., Grégoire, J.-M., Stroppiana, D., Sousa, A., Silva, J., Pereira, J.M.C., Boschetti, L., Maggi, M., Brivio, P., Fraser, R., Flasse, S., Ershov, D., Binaghi, E., Graetz, D., Peduzzi, P., 2004a. Vegetation burning in the year 2000: global burned area estimates from SPOT VEGETATION data. Journal of Geophysical Research, - Atmospheres, 109. doi:10.1029/2003JD003598

Tansey, K., Grégoire, J-M., Binaghi, E., Boschetti, L., Brivio, P.A., Ershov, D., Flasse, S., Fraser, R., Graetz, D., Maggi, M., Peduzzi, P., Pereira, J.M.C., Silva, J., Sousa, A., Stroppiana, D., 2004b. A global inventory of burned areas at 1 km resolution for the year 2000 derived from SPOT VEGETATION data. Climatic Change, 67, 345–377.

Tavares, C.D., DaCamara, C.C., 1999. The SAF for Land Surface Analysis: increasing the benefits from the new generation of EUMETSAT satellites. The 1999 EUMETSAT Meteorological Satellite Data User's Conference, Copenhagen, Denmark, 6-10 September 1999, EUMETSAT P.26, pp. 511-519. ISBN 92-9110-033-1

Tavares, C.D., DaCamara, C.C., 2002. The SAF for Land Surface Analysis: meeting the requirements of the Land Surface User Community. The 2002 EUMETSAT Meteorological Satellite Conference, Dublin, Ireland, 2-6 September 2002, EUMETSAT P.36, p. 300. ISBN 92-9110-049-8

Trigo, I.F., DaCamara, C.C., Viterbo, P., Roujean, J.-L., Olesen, F., Barroso, C., Camacho-de-Coca, F., Carrer, D., Freitas, S.C., García-Haro, J., Geiger, B., Gellens-Meulenberghs, F., Ghilain, N., Meliá, J., Pessanha, L., Siljamo, N., Arboleda, A., 2010. The Satellite Application Facility on Land Surface Analysis. International Journal of Remote Sensing, In Press.

Trigo, R.M., Pereira, J.M., Pereira, M.G., Mota, B., Calado, M.T., DaCamara, C.C., Santo, F.E., 2006. Atmospheric conditions associated with the exceptional fire season of 2003 in Portugal. International Journal of Climatology, 26, 1741-1757.

van der Werf, G.R., Randerson, J.T., Giglio, L., Collatz, G.J., Kasibhatla, P.S., Arellano, A.F., 2006. Interannual variability in global biomass burning emissions from 1997 to 2004. Atmospheric Chemistry and Physics, 6, 3423–3441.

Velben, T.T., Kitzberger, T., Donnegan, J., 2000. Climatic and human influences on fire regimes in ponderosa pine forests in the Colorado Front Range. Ecological Applications, 10, 1178-1195.

Ventura, J., Vasconcelos, M.J., 2006. O fogo como processo físico-químico e ecológico. In: Pereira, J.S., Pereira, J.M.C., Rego, F.C., Silva, J.M.N., Silva, T.P. (Eds.), Incêndios Florestais em Portugal – Caracterização, Impactes e Prevenção, ISA Press , pp. 93-113.

White, P.S., Pickett, S.T.A., 1985. The ecology of natural disturbance and patch dynamics. In: Pickett, S.T.A. & White, P.S. (Eds.), New York: Academic Press 3-13.

Whitlock, C., Higuera, P.E., McWethy, D.B., Briles, C.E., 2010. Paleoecological Perspectives on Fire Ecology: Revisiting the Fire-Regime Concept. The Open Ecology Journal, 3, 6-23.

Xoplaki, E., González-Rouco, J.F., Gyalistras, D., Luterbacher, J., Rickli, R., Wanner, H., 2003. Interannual summer air temperature variability over Greece and its connection to the large-scale atmospheric circulation and Mediterranean SSTs 1950-1999. Climate Dynamics, 20, 537-554.